



University
of Glasgow

<https://theses.gla.ac.uk/>

Theses Digitisation:

<https://www.gla.ac.uk/myglasgow/research/enlighten/theses/digitisation/>

This is a digitised version of the original print thesis.

Copyright and moral rights for this work are retained by the author

A copy can be downloaded for personal non-commercial research or study,
without prior permission or charge

This work cannot be reproduced or quoted extensively from without first
obtaining permission in writing from the author

The content must not be changed in any way or sold commercially in any
format or medium without the formal permission of the author

When referring to this work, full bibliographic details including the author,
title, awarding institution and date of the thesis must be given

Enlighten: Theses

<https://theses.gla.ac.uk/>
research-enlighten@glasgow.ac.uk

The Prediction of Internal Flows within Industrial Centrifugal Fans

Ian Bennett, B.Eng, GradRAeS, MIMechE, C.Eng

M.Sc. Thesis

**Department of Aerospace Engineering
Glasgow University**

(c) Ian Bennett, October 1994

ProQuest Number: 10394831

All rights reserved

INFORMATION TO ALL USERS

The quality of this reproduction is dependent upon the quality of the copy submitted.

In the unlikely event that the author did not send a complete manuscript and there are missing pages, these will be noted. Also, if material had to be removed, a note will indicate the deletion.



ProQuest 10394831

Published by ProQuest LLC (2017). Copyright of the Dissertation is held by the Author.

All rights reserved.

This work is protected against unauthorized copying under Title 17, United States Code
Microform Edition © ProQuest LLC.

ProQuest LLC.
789 East Eisenhower Parkway
P.O. Box 1346
Ann Arbor, MI 48106 – 1346

Theirs

10092

Copy 2



Abstract

During the last twenty years there has been a gradual growth in the field of Computational Fluid Mechanics (CFD). Many of these techniques have been applied to a variety of fluid and thermodynamic problems. Unfortunately, many of the computer codes were written with particular applications in mind, restricting the flow physics and, occasionally, the possible problem geometry. Consequently, there are a multitude of computer codes available to a prospective user, differing not only in the equations solved but also in the user friendliness and generality of their pre- and post-processors. A small number of these CFD codes are commercially available today and claim to be suitable for solving a wide range of flow situations. It is understandable that these are treated with some suspicion by potential users, such as industrial fan manufacturers, due to the inherent difficulty traditionally found in solving such problems. This present work has been carried out to alleviate some of the fears of this particular group through a series of CFD investigations using proprietary codes. The aim of this present investigation is to test the suitability of such codes to model the flow within centrifugal fans.

The internal flow field within a centrifugal fan is described and the salient flow features that affect the gross flow are highlighted. Also included is a review of methods used for predicting flows in centrifugal and radial machines, from which it is apparent that the centrifugal fan has been relatively neglected compared with its higher pressure counterpart, the radial compressor. Use is made of these proven techniques which are adapted here for use on lower pressure centrifugal fan machines. In all, three impeller geometries are examined covering a range of specific speeds. CFD techniques were applied to each of these geometries, incorporating configuration adaptations and changes in operational conditions. In this way known techniques for radial compressors were initially utilised and latterly enhanced for application to centrifugal fans. This step-wise approach proved successful and it is shown that such codes can be used to predict the gross flow features within centrifugal fans.

Also included in this work is an experimental investigation into the effect of the fan discharge configuration on flow stability. It is shown that the discharge has little influence over the flow at duties near stall for low pressure centrifugal fans.

This present work addresses many of the problems associated with the simulation of centrifugal fan internal flow and will allow potential investigators to quickly implement codes. This will reduce the number of confidence checks necessary prior to application. Suitable boundary conditions and modelling generalisations are discussed.

Acknowledgement

I would like to express my gratitude to my supervisor, Dr Marco Vezza of Glasgow University. His guidance, over the long and somewhat difficult years needed to complete this study, was of immense support. His continual encouragement and caring attitude helped to ease the burden of taking a part-time degree.

Thanks must also go to the staff at James Howden Group Technology, namely Mr Hugh Watson, Mr Michael Round and Mr James Hamilton. Their personal contributions were instrumental in the experimental phase of the investigation for without them some of the work would never have been completed within time. The sponsorship, both in material and time, of James Howden Group Technology is also acknowledged. Mr Blair McDermid was responsible for these contributions.

Thanks also to the staff at Cranfield University, my new work place, who were sympathetic to my needs during the writing-up period of the degree. In particular, thanks must go to Dr Archie McKenzie for an impartial and constructive proof read.

Finally, I must thank my fiancé, Suzanne, for the sacrifices she had to make. This includes the nights of widowdom whilst I worked, the holidays I couldn't take with her and the financial loss due to my studies. I pledge that I will never again allow my work to completely dominate our life as it has done over the last four years.

..... for mother and fether

CONTENTS

Chapter 1	Introduction	1
Chapter 2	Centrifugal Fan Experimental Review	6
2.1	Introduction	6
2.2	Inlet Flow Field	6
2.3	Inlet Clearance	8
2.4	Blade Leading Edge Flow	9
2.5	Blade Passage Flow	11
2.6	Blade Exit	12
	Summary	14
Chapter 3	Review of Numerical Methods Applied to Centrifugal Fans and Compressors	16
3.1	Methods Used for the Prediction of Flows within Centrifugal Compressors	16
3.2	Methods Used for the Prediction of Flows within Centrifugal Fans	24
	Summary	28
Chapter 4	The Mizuki High Pressure Compressor	30
4.1	Description of Model	31
4.2	Steady State Investigations	32
4.3	Unsteady Calculations	37
4.4	Conclusions	38
Chapter 5	The L3R Radial Bladed Fan	39
5.1	L3R Aerodynamic Experimental Investigations	40
5.2	L3R Fan CFD Investigations	50
5.3	Conclusions	69

Contents

Chapter 6	The ZM1 Centrifugal Fan	70
6.1	ZM1 Centrifugal Fan Sparsely Meshed Models	71
6.2	ZM1 Viscous Model Runs	78
6.3	Conclusions	97
Chapter 7	Conclusions and Further Work	98
	References	101
Appendix A Mizuki Radial Compressor CFD Model Runs		
Appendix B L3R 'Bladed' CFD Model Runs		
Appendix C L3R 'Bladeless' CFD Model Runs		
Appendix D ZM1 Centrifugal Fan CFD Model Runs		

CHAPTER ONE

Introduction

Centrifugal Fans have been designed and manufactured by James Howden and Company since 1854. During this time the product has developed to operate over a wide range of duties from force draughting power station boilers to circulating air for heating and ventilating buildings. The design emphasis has been on geometric simplicity, in order to allow the basic product to be scaled and customised for individual client requirements. Invariably this has meant compromising the aerodynamic ideal with designers constrained by the need to limit construction to using plate steel as the main building-block material. Any additional bending, casting or machining has had to be carefully considered to prevent costly manufacture in a very competitive market. The design environment created within these constraints has not given rise to the ideal breeding ground for new and innovative aerodynamic theory: many companies still rely on empirical 1-D flow equations for fundamental design, following up with extensive model testing, and it is at this relatively primitive level that practical centrifugal fan aerodynamics has been left. This relatively safe approach of simple calculation and experiment is slow but, with a relatively large database of previous designs, has been shown to be fairly robust and dependable. As a consequence the detailed internal flow pattern has been largely ignored, replaced by empirical relations, and indeed takes no role in the design process.

As the world fan market becomes increasingly more sensitive to high operational efficiencies, any additional understanding of the internal flow physics must be a bonus. However, the empirical aerodynamic relations developed over the years are inadequate for predicting internal flows. Limited by their 1-D nature, they are unable to model the complex internal flows within fans and we must turn to more general equation sets that include 3 or even 4 dimensions. It may be argued by groups reluctant to investigate detailed flow patterns that current designs, given the simple construction techniques, will not be bettered at peak efficiency. This is probably true, as many companies have fan designs with polytropic efficiencies of over 90%. It is at off-peak conditions that many customers are becoming aware of decreased efficiencies, particularly when the fan selected is required to operate at several duties. It is an unfortunate consequence of the flow nature within centrifugal machines that

they operate at peak efficiency at the envelope extreme rather than at the centre like low pressure axials. This is demonstrated in Figure 1.1(a) and 1.1(b) below.

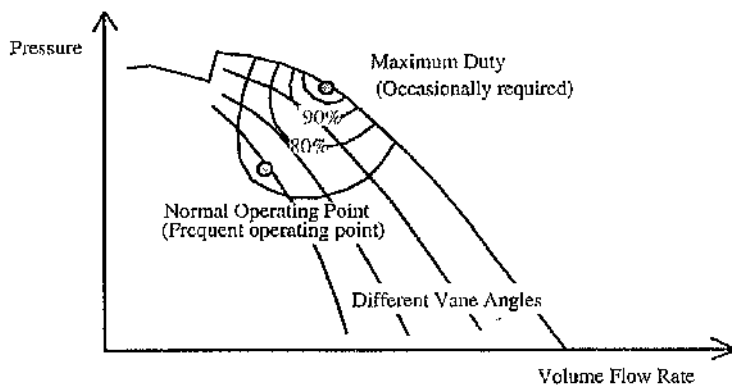


Figure 1.1 (a) Sketch Showing Efficiency Contours for a Typical Centrifugal Fan for a Variety of Vane Control Angles

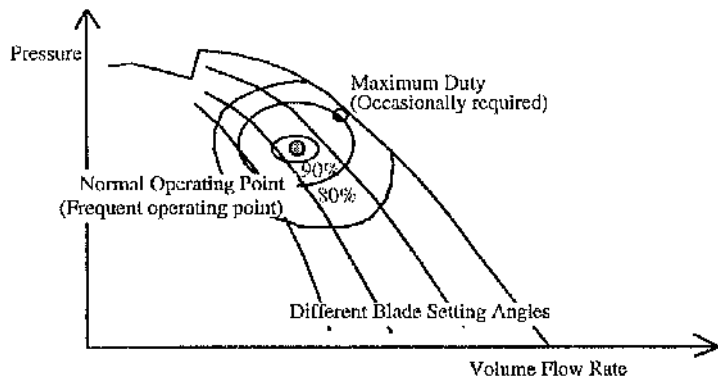


Figure 1.1(b) Sketch of Efficiency Contours for a Typical Low Pressure Axial Fan at a Variety of Blade Setting Angles

Normally the extreme operating point represents some form of emergency condition which in many cases will never be demanded in the fan's lifetime. As demonstrated, this duty corresponds to the optimum fan performance: the other 'normal' operational points lying within regions of comparatively low efficiency. With the power requirement of large power station fans being of the order of 5MW, any changes to centrifugal fan designs that could increase off-design performance would create significant savings for the operator and create opportunities for a manufacturer if retrofitting the enhancements were possible. As will become clear in Chapter 2, where an experimental review is carried out, centrifugal fans are very sensitive to small geometric changes. With more information about the internal flow field aerodynamicists will be better equipped to optimise these changes. With relatively

simplistic design methods used to date and disappointing off-design efficiency characteristics we must conclude that centrifugal fans may still be further improved and that the potential gains could easily recover research costs.

One technique that has been relatively neglected by fan manufacturers is Computational Fluid Dynamics (CFD). These techniques may be used to solve the general equations of fluid motion and thermodynamics and are particularly useful for 3-D flow as these cannot normally be solved using traditional analytic techniques. Many user-friendly CFD packages are now commercially available and the fan designer has found himself an alternative to supplement the traditional design approach. Now , in principle, aerodynamicists have the tools to predict detailed maps of internal fan flows which would be very difficult, time consuming and costly to measure by experiment. However with very few published reports incorporating their product, fan manufacturers have been naturally cautious to invest in expensive CFD codes and the application has lagged behind that of the compressor and gas turbine fields for which there is a large amount of recorded studies. This current work hopes to dispel some of these fears and show how useful CFD could be within an industrial fan research environment.

General Approach

In Chapter 2 the reader is guided through a review of published experimental papers on centrifugal fan flow. Most obvious is the lack of a complete data set suitable for CFD code verification (this is probably the main reason why CFD investigators have avoided modelling centrifugal fans as they ideally require some reference data set from which to compare their predictions). A description is given of the main flow areas within a centrifugal fan with the salient flow features identified. The findings are later used to verify a CFD model.

A computational review of the methods used to predict internal flows within centrifugal fans would have ideally followed but unfortunately very few CFD practitioners have tackled this particular flow problem. Instead, the scope of the review was extended to include centrifugal compressors, as they may be regarded aerodynamically as very high pressure radial bladed fans. Chapter 3 therefore consists of two reviews: CFD applied to Centrifugal Compressors and CFD applied to Centrifugal Fans. With such a rich and sound background in compressors, it was decided to start the CFD investigations in this report using a compressor geometry . Once satisfied with the results, this work was extended to include a centrifugal fan with radial blades. Despite the geometric similarity, this fan was designed to operate

at much lower pressures. It served well to bridge the gap between the compressor and fan CFD investigations. Finally CFD was applied to a geometry synonymous with centrifugal fans, that of a backward curved aerofoil machine. Reference is made in detail to an experimental investigation used to validate the CFD model.

The models were created in order of increasing specific speed, ensuring confidence in the results. The impellers examined are sketched below each with two views.

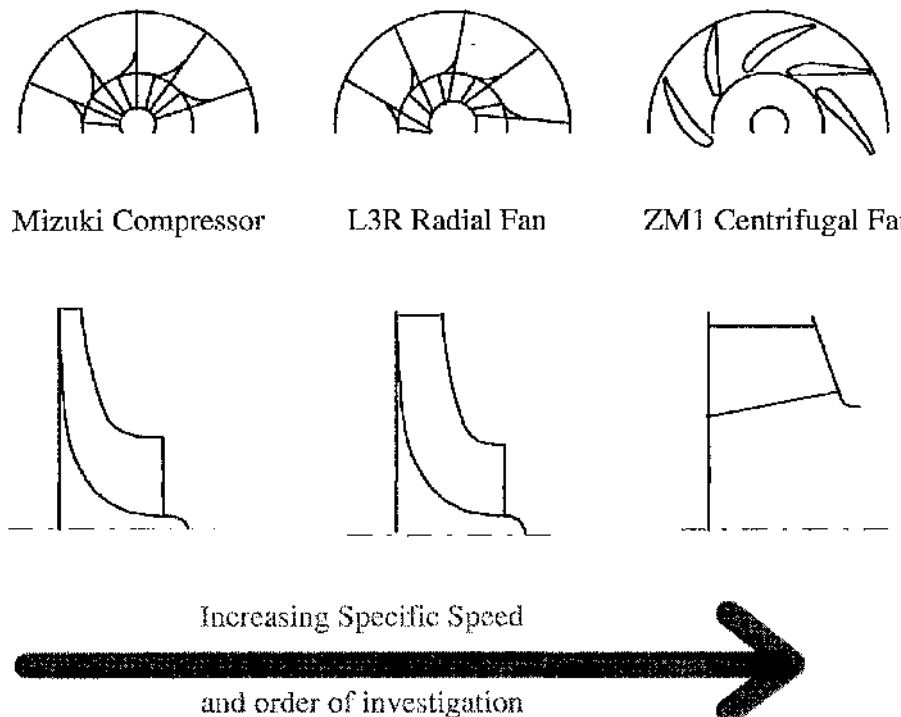


Figure 1.2 Impellers Modelled in this Report and the Order of Investigation

Each fan geometry is examined in the order given above with the results reported in Chapters 4, 5 and 6 respectively.

The combination of numerical and experimental work documented within this report will enable manufacturers to get dependable results when using CFD and save them a great deal of the time normally associated with the familiarisation and confidence building needed before adopting a new technique. The problems of mesh construction, geometric simplification, choice of equation set and the application of boundary conditions are all addressed in this document. A particular bias to the

prediction of off-design flow runs through the work as it is here that the author feels CFD will make its impact on the industrial fan industry.

CHAPTER TWO

Centrifugal Fan Experimental Review

2.1 Introduction

Centrifugal fan experimental papers are reviewed here. Each particular part of the fan is examined in turn, starting at the inlet and ending at the discharge. In this way the reader is logically drawn through the predominant gross flow features and pointed towards references should further investigation be merited. For quick reference, a summary of findings is tabulated at the end of the chapter.

2.2 Inlet Flow Field

Poor inlet ducting, whether caused by installation constraints or poor design, results in reduced performance. Wright et al [1984] demonstrated, by artificially producing distorted inlet box flows, that drops in efficiency of 10-12% could result from bad inlet design. Despite a lack of detailed flow probing the work clearly indicated that the fan performance was very sensitive to the inlet configuration and we therefore conclude that it should be carefully considered when modelling.

Computationally easier to model is cylindrical inlet ducting, due the geometric axisymmetry which enables it to be modelled in the rotating frame by the application of a tangential velocity at the duct periphery. Kubo and Murata [1976] measured the flow within such ducting whilst the fan was in rotating stall. Using a hot wire probe sensitive only to 2-D flow, they managed to capture the unsteady flow regime. Most prominent was the rotation of the unsteady velocity field regions about the duct centreline, clearly demonstrating that the rotating stall flow associated with flow about the blades was so prominent as to strongly influence the upstream inlet flow. The effects could be easily detected at distances over 1.5 times the inlet diameter upstream. It is of interest that when using a pitot tube no signs of unsteady asymmetry were detected, even in the highly stalled

condition: the manometers were insensitive to the periodic fluctuations. Unfortunately no hot wire measurements were reported at design flow rates by Kubo and Murata [1976] and hence guidelines for modelling fan configurations with cylindrical inlet ducting cannot be made for this condition. The reader is left to judge this for himself through the balancing of the following two points. Firstly, a large length of duct could be modelled so as to render the upstream boundary too far away to influence the impeller flow. This safe approach can be prohibitively expensive, even doubling the size of the computational mesh. On the other hand, a insufficient duct length with an incorrect inlet boundary condition, could restrain the flow in such a way as to render the model inaccurate; recall that Wright et al [1984]¹ have already demonstrated how sensitive the centrifugal fan flow is to inflow.

A further discussion of the inlet flow field was made by Madhaven and Wright [1985]. Whilst investigating the phenomenon called pressure side rotating stall they noticed that the amplitude of pressure fluctuations reduced with the inclusion of a dummy shaft placed at inlet. This was presented as evidence of an unstable precessional vortex at inlet. This instability has been detected by fan manufacturers for years, particularly when inlet guide vanes are fitted. These naturally induce a swirl in the flow. See Figure 2.1. Chen [1993] presents a methodology for detecting this phenomenon and distinguishing it from rotating stall.

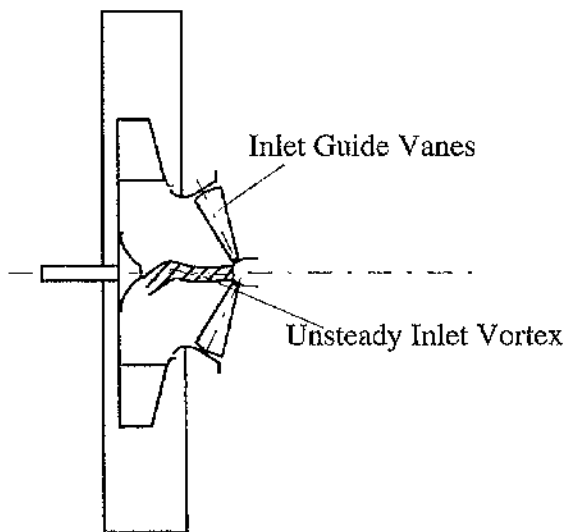


Figure 2.1 Unsteady Inlet Vortex . Chen [1993]

2.3 Inlet Clearance

At the gap between the stationary inlet duct and the impeller there exists an additional inflow as shown in Figure 2.2 below.

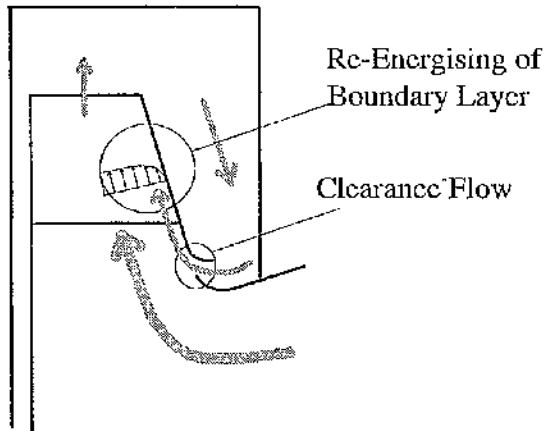


Figure 2.2 Inlet Clearance Flow

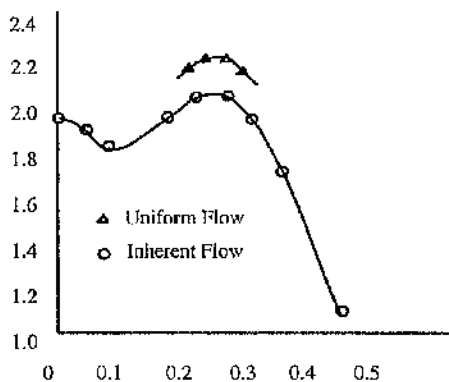
Wright et al [1982] examined this inlet flow using a series of static pressure tappings. These were placed along the inlet cone and impeller shroud. The inlet clearance was varied and pressure measurements noted. Results showed that reduced clearance resulted in a wider scatter of measurements in the region of the inlet clearance gap, suggesting an unsteady nature. Unfortunately, instead of investigating this effect in further detail, Wright [1984] concentrated on the subsequent change in overall fan performance due to different clearances as the work was primarily carried out to investigate the optimum clearance gap. Unexpectedly the best results were gained when the gap was a minimum. Interpolating the results showed that the gap should be reduced to zero for best performance. Wright [1984] himself expressed disbelief of these results and hypothesised that this may not be generally true. Subsequent work by Bennett and Watson [1993] demonstrated the performance enhancements that could be gained from fixing small stationary vanes onto the exterior surface of an inlet cone. These vanes were designed to convert the swirling internal casing flow into additional static pressure, enhancing the 'blowing' coanda effect.

Bard [1982] used a hot wire probe to examine the flow just after the inlet shroud radius. Using a series of slip rings he was able to traverse the flow with a hot wire probe rotating with the impeller. Like Wright [1982], tests were carried

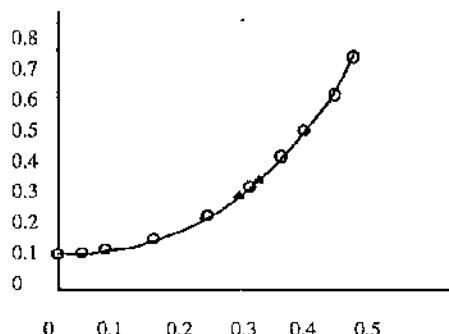
out for different inlet ring clearances. The main feature detected was a highly turbulent flow near the shroud: large amplitude and small mean velocities were measured in this area, even at peak efficiency. Note that the actual position of the probe was within the blade passage and the reference is included here as an addition to the shroud flow discussion.

2.4 Blade Leading Edge Flow

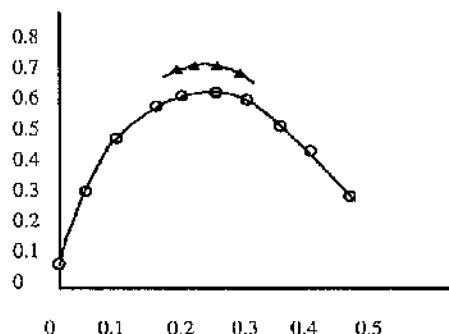
Incorrect incidence to blades is intuitively expected to be the most important factor in fan aerodynamics. Detailed work by Gessner [1967] investigated this and showed that the distribution as well as the mean incidence was of primary importance. The experiments demonstrated that an artificially produced uniform incidence gave the optimum efficiency. A comparative study is graphically represented below in Figure 2.3.



(a) Total Pressure Characteristics



(b) Power Characteristic



(c) Efficiency Characteristics

Figure 2.3 Performance Characteristics for Inherent Inlet Flow and for Artificially Produced Uniform Flow at Blade Entrance

Cau et al [1987] also published data on blade leading edge flow. However instead of predicting separation and low radial velocities at the hub like Gessner, Cau et al [1987] predicted low flow near the shroud. See Figure 2.4. These results do not uphold the observations of Gessner [1967]. One should note that Cau used a fan of 0.462m diameter and Gessner one of 0.25m. It is expected that scale

effects may be present in the small model which could effect the usefulness of the results when applied to industrial sized fans.

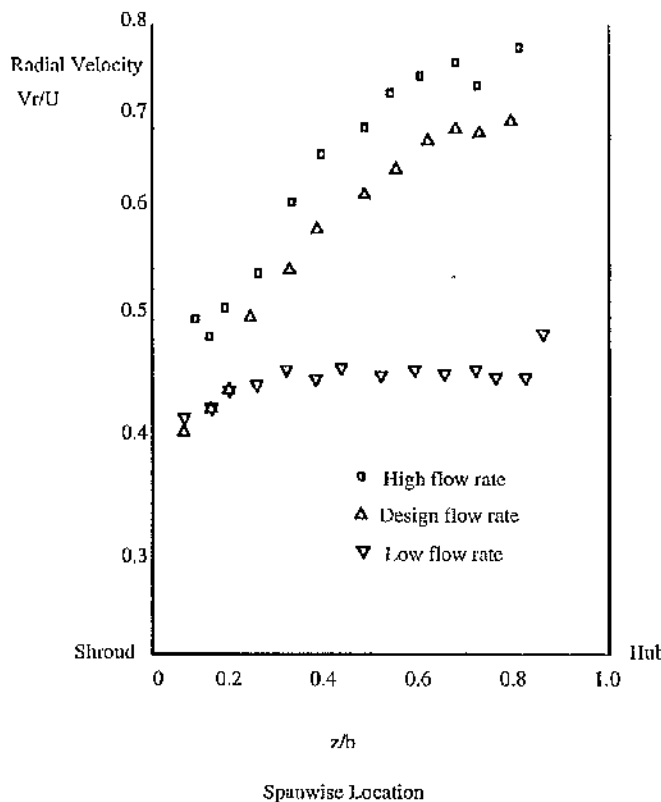


Figure 2.4 Radial Velocity Profile at Impeller Inlet Cau et al [1987]

A use for such measurements lies with the computer modelling of impeller passage flow (many researchers have restricted their calculation domain to this region when modelling turbomachinery). The success of these models depends on the specification of accurate boundary conditions to avoid the propagation of erroneous solutions into the computational domain.

2.5 Blade Passage Flow

The blade passage is an area that is common in virtually all computational domains used to investigate the internal flow regime within centrifugal fans. It is by far the most critical region of flow for it is here that the transfer of work from the rotor to the fluid takes place. Various experiments have been documented.

Wright et al [1984]¹ compared blade surface static pressure tappings with his numerical model. This analysis was clearly limited as no flow measurements between the blades were taken. No unexpected results were documented, with predicted pressure distributions correlating well with experiment.

With hot wire probes Kjörk and Löfdahl [1989] were able to measure the mean and unsteady turbulent velocities within a centrifugal fan blade passage. Five of the six Reynolds stresses which characterise turbulent viscous forces were quantified. Kjörk and Löfdahl showed that for their backward curved blade fan there existed a definite trend of increasing velocities from the pressure to the suction sides of the channel. The most dominant Reynolds stress was the normal stress component in the direction of the flow, with a minimal value located midway between the blades. The near-shroud highly turbulent flow detected by Bard [1982] was also apparent in the results.

2.6 Blade Exit

Goulas and Mealing [1984] completed laser Doppler measurements at blade discharge. Comparing their tangential and radial plots with those of Cau et al [1987] qualitatively similar trends can be spotted, namely reverse flow at the hub with high velocities at the shroud. Cau et al averaged their results and presented them pictorially as below (Figures 2.5(a) and (b))

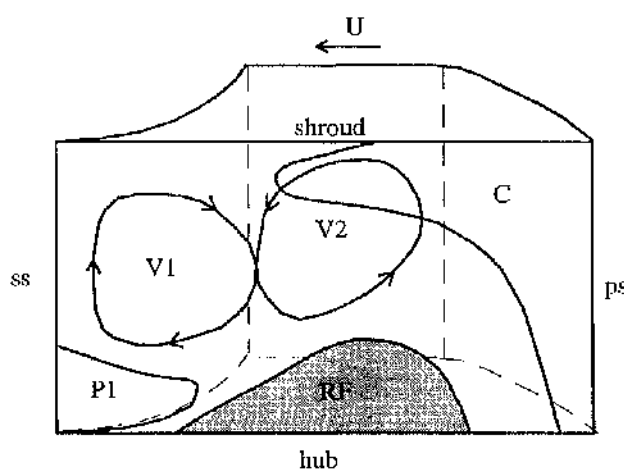


Figure 2.5(a) Design and Low Flow Rate Velocity Distribution at Discharge of a Forward Curved Blade Fan (Cau et al [1987])

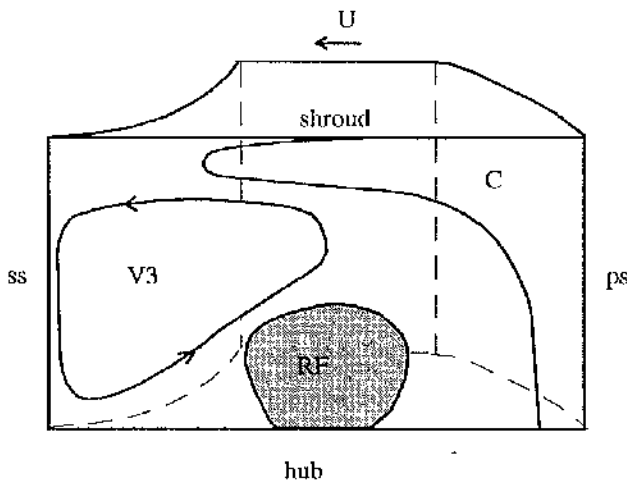


Figure 2.5(b) High Flow Rate Velocity Distribution at Discharge of a Forward Curved Blade Fan (Cau et al [1987])

Most noticeable from the above is the core flow in the shroud pressure surface corner. However this form is not generally true for all impellers. Contrasting flows were shown by Raj and Swim [1981], and Kjörk and Löfdahl [1989]. The most prominent deviation for the flow within the Raj and Swim impeller was the presence of low velocities at the shroud. Clearly this is not the case for the figure above. The measurements taken by Kjörk and Löfdahl [1989] present the highest velocities at the hub suction area of the blade passage. Again this contrasts with the above. The obvious feature that a novice would examine is the blade type. Are the blades forward or backward sloping? The quest would yield no correlation to the vast difference in gross flow features. It is expected that a dimensionless group which takes into account the acceleration forces could give a predictive quality. Such a figure is the Rossby number. It represents the ratio of centrifugal to the coriolis forces and as such gives some indication of where the core flow dominates.

The pictorial presentation by Cau et al [1987], Fig 2.5, shows up the other main gross flow features. These are the core flow C, vortex due to interaction between inclined flow and suction side boundary layer V1, vortex due to rotation of impeller V2, recirculating flow RF and a small region of core flow P1. Again, this map of characteristic flow regions is not expected to be generally the same for all fans.

The experimental papers reviewed here are summarised in table 2.1.

Table 2.1 Summary of Centrifugal Fan Experimental Papers Cited

Author(s)	Blade Type	No. of Blades	RPM	Impeller dia. (m)	Flow measurements taken at the following locations					General Comments
					Inlet Ring	Blade 1.e. Surface	Blade t.e.	Blade	Scroll/ Diffuser	
Gessner [1967]	Forward curved plate	40	1530	0.25	✓	✓	✗	✗	✗	A small fan. Some experimental work which leads to improvement of performance by ensuring uniform inlet conditions
Kubo & Murata [1976]	Forward curved plate (but backward facing)	12	1220	0.48	Inlet duct ✓	✗	✗	✗	✗	Capped hot wire probe within a fan exhibiting rotating stall. Some pitot measurements. An inlet duct investigation.
Phelan et al [1979]	Selection of fans operating at different conditions					Performance testing only				
Kubo [1980]	Forward curved plate (but backward facing)	12	1220	0.48	Just before impeller	✗	✗	✗	✗	Detailed unsteady flow measurements on a plane just before the impeller. The influence of diffuser vanes is also examined.
Raj and Swim [1981]	Forward curved plate	48	900	0.23	✗	✗	✓	✓	✓	Hot wire measurements at different duties. Static tappings on scroll casing. Smoke and tufts used to see the flow via Plexiglas housing.
Bard [1982]	Backward curved plate	9			✗	✓	✓/✗	✗	✗	Two impellers tested of different widths. Hot wire probe measurements.
Wright et al [1982]	Backward sloped aerofoil	10	1220	0.762	Pressure static tappings on inlet cone and sideplate	✓	✓	✓	No qualitative results given	Prediction and experimentation of general flow

Table 2.1 Summary of Centrifugal Fan Experimental Papers Cited (continued)

Author(s)	Blade Type	No. of Blades	RPM	Impeller Dia. (m)	Flow measurements taken at the following locations					General Comments
					Inlet Ring	Blade i.e. Surface	Blade t.e.	Scroll/ Diffuser		
Gonias and Mealing [1984]	Forward curved	27	1500 2000 2500	0.69	✗	✗	✓	✗		Laser doppler measurements at different duties
Wright et al [1984] ¹	Aerofoil backward sloped	10	1200	0.76					Performance testing only	Experimental investigation into the degradation of fan performance due to distorted inflows
Wright et al [1984] ²	Aerofoil backward sloped	10	1200	0.76	✗	✗	✗	✗	Performance testing only	Off-design work with comparisons with numerical simulations
Wright [1984]	Aerofoil backward sloped	10	1200	0.76	✗	✗	✗	✗	Velocities, pressure and performance	Inlet clearance optimisation
Madhaven and Wright [1985]	Aerofoil backward sloped	10	1200	0.76					Performance testing only	Performance with some unsteady flow investigations at trailing edge (virtually qualitative)
Can et al [1987]	Plate forward sloped	18	1300	0.462	✗	✗	✓	✗		Experimental investigation into pressure surface stalling and its rotating action
Kjörk and Löffdahl [1989]	Plate backward sloped	9	890	0.8	✗				Measurement in blade channels	Hot wire measurements at design flow rate

CHAPTER THREE

Review of Numerical Methods Applied to Centrifugal Fans and Compressors

From reading Turbomachinery reviews it is apparent that there is a lack of published numerical investigations into the internal flow field within centrifugal fans. Very few references exist. Those which do lack the sophistication of those methods already in use for axial and radial turbomachinery. It is not the purpose of this chapter to give a detailed review of computational methods for axial and radial turbomachinery; this has been recently completed by Lakshminarayana [1991], McNally and Sockol [1985], Japikse [1976] and Whitfield and Baines [1990]. The author only wishes to identify the relative position of centrifugal fan analysis with that of radial turbomachinery in general, and hence highlight methods that could possibly be utilised for centrifugal fans. In this way research steps can be made on the modelling of the internal flow field within centrifugal fans using numerical methods that have already proved successful for radial turbomachines. The first portion of this chapter is dedicated to centrifugal compressors, the latter to centrifugal fans.

3.1 Methods used for the Prediction of flows within Centrifugal Compressors

To classify the models used is somewhat arbitrary as the dimensions of the flow domain (2-D or 3-D), the system equations, boundary conditions and solution methods would all be valid. Their definitions are not mutually exclusive and overlaps will always occur. To segregate we shall use the partitions used by Whitfield and Baines [1990].

3.1.1 2-Dimensional Solutions

Initially, with the advent of the computer, researchers developed models which were by today's standards computationally undemanding. The main assumptions were that the flow was both inviscid and restricted to predetermined 2-D planes. The basic theory for such calculation procedures was presented by Wu [1952]. The blade passage was split into blade-to-blade (S1) surfaces and hub to shroud (S2) surfaces.

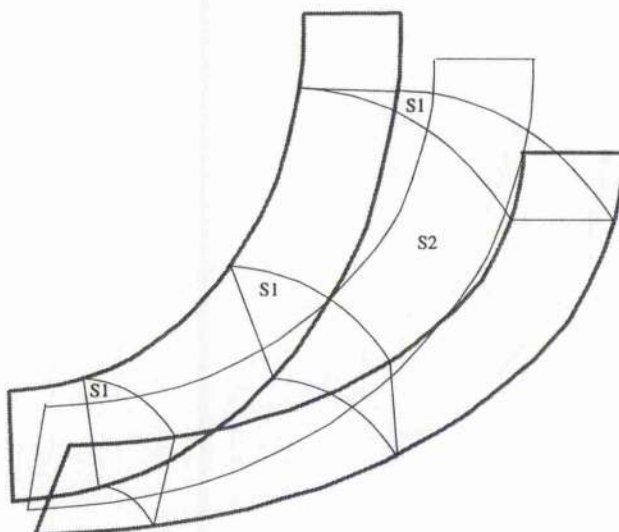


Figure 3.1 A Sample of Blade-to-Blade (S1) and Hub-to-Shroud (S2) Surfaces

Wu solved the flow on both these surfaces systematically to gain an approximation of the 3-D flow regime. As the flow was assumed to follow 2-D stream sheets it could therefore be treated with the use of a stream function. Marsh [1966] and Bosman and Marsh [1974] both used Wu's formulation for a mean stream surface. The latter work incorporated an empirical loss model in an attempt to account for recirculation and viscosity .

An alternative formulation was completed by Katsanis [1964] in which the equations of motion were described and solved for in terms of velocity gradients rather than as a stream function. This form of solution algorithm was termed a quasi-orthogonal or q-O method. Quasi-orthogonals were reference lines placed at

approximately right angles to the expected through flow direction. With their position fixed throughout the computation, the streamlines were iterated into position using a velocity gradient form of the momentum equation. The solution procedure was fundamentally parabolic; the solution stepped from inlet to outlet. Ellipticity of the flow was accounted for by the use of a curve fit equation. The method of Katsanis [1964] was applied to the meridional (S2) surface with an approximation of blade surface pressures and velocities made from the mean surface solution.

Katsanis [1965] produced an equivalent program which allowed the solution of the blade-to-blade velocities using a q-O method. This program could use the streamlines from the S2 surface equation for which a fully combined solution was written by Katsanis [1966]. The main assumptions were steady (relative to the rotating frame) and inviscid flow with rotational flow conditions allowed at inlet. The meridional part of the procedure required prescribed inlet conditions and a loss distribution, from which exit conditions and flow streamlines were calculated. The blade passage flow information was then calculated by the blade-to-blade program using the inlet, discharge and streamline information as inputs.

3.1.2 Quasi 3-Dimensional Solutions

Quasi-3D solutions developed naturally from the earlier 2D flow methods. The methods that evolved differed in the assumed stream surface geometry. Bosman et al [1977] and Novak et al [1977] both prescribed that the S1 (blade-to-blade) surface was a surface of revolution and that the S2 (meridional) surface was allowed to deviate from the mean. Krimerman and Alder [1978] used a superior four step solution algorithm with the S1 (blade-to-blade) surface and the S2 (hub to shroud) surfaces latterly unrestrained. Based on Wu's [1952] original stream function theory, the model assumed inviscid, compressible, rotational and steady (relative to impeller) flow. It is interesting to note that, in a comparison between a quasi-3D and a full 3-D method, Krimerman and Alder [1978] judged that the 3-D solution differed sufficiently from that of the 2-D solution by enough to justify the extra computational work.

3.1.3 3-D Inviscid Calculations

These methods may be separated into 4 main groups. In decreasing order of generality: the full Euler (steady and unsteady), the stream function, the potential function and the potential flow formulations.

Using an unsteady Euler solver, Bosman and Ahrabian [1984] modelled "stalled flow" within a centrifugal compressor impeller. They predicted unsteady regions of recirculation when modelling flows with high blade incidence i.e. at low volume flows. As the distinctive recirculation only occurred in regions of extreme duty it was concluded that the phenomenon predicted was that characteristic of stalled impeller flow.

Although stall is thought of as a classically viscous phenomenon, another similar inviscid prediction was made much earlier by Stanitz [1948]. Stanitz demonstrated streamlines that showed pressure side separation using a stream function formulation. This work, by nature of the stream function, was limited to a 2-D domain, namely a blade-to-blade surface. More recently however some hybrid stream functions have been developed that are fully 3-D e.g. Hafez et al [1983].

The solution of the full Euler equations, the most general inviscid flow equation set, may normally only be achieved by solving for the primitive variables directly i.e. in the terms of velocity components, pressure and density. Clearly this requires a large amount of computer power given five unknowns per node. Savings may be achieved by reduction in the number of dependent variables by substituting two or more variables with a single unknown. Such substitutions may be made using the potential function or the stream function. The introduction of these causes a loss of generality. The stream function has the penalty of reducing the flow to 2 dimensions (as above with Stanitz [1948]), with a potential function implying irrotationality. Deconinck and Hirsh [1981] used a finite element formulation to solve the full potential formulation, predicting transonic flows through axial turbomachinery cascades. This code was later used by Prince and Bryans [1984] in a comparison between an Euler, a full potential and a q-3D formulation. The Euler code was a time marching finite volume formulation developed by Denton and Singh [1979]. The full potential algorithm, as would be expected, was shown to be more economical, with only some minor differences observed between it and the Euler solution. In comparison with the actual Eckhart [1980] radial compressor impeller, neither formulation gave distinctly better predictions. Final comparison with the q-3D method showed that the 3D methods were better at predicting the loadings near the hub and shroud.

As already mentioned, the simplified Euler Equations may be solved with the introduction of an incompressible Potential Flow function. This is far more restrictive in its use, in that the flow is assumed to be both isentropic and irrotational, however the simple Laplacian form may be rapidly solved and is quite thrifty on computer space (only one dependent variable). A wide range of solution methods exist for this common equation set.

3.1.4 Viscous Fluid Flow

The inclusion of viscosity into the momentum equation requires increased computational work which in some situations is arguably unnecessary. Adler and Krimerman [1980] discussed the relevance of an inviscid 3-D compressible calculation solution and indicated, that for regions outside the classical jet wake structure, that an inviscid computation yielded adequate results. Clearly these regions were outside the areas of viscous domination, the boundary layers. A logical response was the development of coupled inviscid/viscous methods which only account for viscosity within boundary layers. A blading design method by Stow and Newman [1990] examined the use of these coupled viscous methods. They concluded that the main limitations are due to the boundary layer calculations, and they predict scope for improvement especially for separation treatment. However this work was based on axial fan blade design and it is expected that axial compressors are relatively free from the complex 3-D mixing and interaction of viscous jet-wake flow present within centrifugal machines. In addition centrifugal machines operate at much higher pressure ratios and are consequently more susceptible to boundary layer separation, even at design flow rates. Therefore if we are able to adequately predict detailed centrifugal turbomachinery flows we need methods of incorporating the effect of turbulence into the flow equations. This is normally achieved by inclusion of a 'turbulent viscosity' term into the Navier Stokes equations. The value of turbulent viscosity is calculated using turbulence models. These are classified into groups corresponding to the number of additional transport equations required for closure. The simplest is the Zero-equation group, which requires only algebraic calculation and no additional differential equations. There are also one and two equation groups, normally calculating values for turbulent kinetic energy, K , and for the two equation case a value for dissipation rate, ϵ . From these values an expression for turbulent viscosity is calculated. Unfortunately this approach only yields an

isotropic approximation for turbulence. One alternative involves solving directly for the primitive variables of the time-averaged Navier-Stokes equations. The Reynolds Stress Model (RSM) does this via seven additional transport equations, one for each of the six paired fluctuation velocities and one for the dissipation term. It is expected that the swirling and adverse pressure gradient flow regime within centrifugal turbomachinery may only be properly modelled using the RSM formulation. Unfortunately due to the additional unknowns, the RSM model is computationally expensive.

The extra computational effort needed for viscous flow calculations has predictably encouraged researchers to make broad flow simplifications. These are classified here, using the divisions of Baines[1990], as parabolic, partially parabolic and elliptic. As the name mathematically suggests, the fully parabolic solutions assume a predominant flow direction in which the influence of the flux downstream is not felt. This allows a solution to be found by a single sweep through the domain. The next section deals with partially parabolic solutions. These are less restrictive to the flow, with some ellipticity introduced via the continuity equation. Finally, classified here as fully elliptic solutions, attempts at using the full Navier Stokes equations to model centrifugal impeller flow are documented.

3.1.4(a) Parabolic Approximations

With some simplifications, the Navier Stokes equations may be solved using parabolic solution schemes. These schemes are fully explicit with flow upstream used to explicitly calculate the flow downstream. In this way the solution is found with a single sweep, from inlet to discharge, through the computational domain. The method is very frugal on computational effort.

The trade-offs due to the flow simplifications (from Bains [1990])are:

- a) A predominant flow direction is assumed.
- b) In this direction diffused quantities are negligible.
- c) The downstream pressure field has little effect on the upstream.

A criterion for the use of parabolic solutions was given by Majumdar et al [1977] who stated that the parabolic solutions were only useful for low values of the Richardson number , R_n .

$$R_n = \frac{\omega b}{\bar{w}}$$

where ω = angular velocity

b = duct width in the circumferential direction

\bar{w} = is the mean relative velocity.

3.1.4(b) Partially Parabolic Viscous Approximations

Partially parabolic methods allow a relaxation of the stringent parabolic assumptions by introducing an elliptic pressure correction scheme. This scheme updates the pressure field in an iterative fashion: using momentum, the velocities are calculated assuming predetermined pressures; continuity is then used to make pressure corrections. Despite the neglect of velocity gradients in the bulk flow direction (as above for partially parabolic problems), Moore et al [1981] were able to adequately predict wake growth within a radial impeller. This was achieved using a simple algebraic (zero equation) turbulence model. Unfortunately, this model was unable to predict blade leading edge flow.

3.1.4(c) Elliptic/Navier Stokes Solutions

Elliptic flow regimes do not have zones of influence as do hyperbolic and parabolic flows, with both upstream and downstream conditions effecting the flow field. Although in the first instance an implicit method would intuitively be chosen due to the ellipticity, explicit marching methods, particularly for unsteady flows, have proven computationally efficient (Fletcher [1988])

In this section the predominant difference between the references cited are due to the turbulence models utilised. As already discussed, the methods may be classified by the number of additional transport equations required for closure. We shall deal with the references in increasing order of differential equations required for closure.

Edwards et al [1985] used a high constant value of viscosity to model the turbulent flow within two radial compressors. Good agreement with predicted performance and blade loading were achieved although there were some noticeable discrepancies for the lowest pressure impeller at off-design flows. The equations were solved using a commercial CFD package with the SIMPLE (Semi-Implicit-Pressure-Linked-Equations) algorithm. This algorithm is reminiscent of

that used for the partially parabolic formulation due to the method of coupling continuity with the momentum equations via pressure, but in this case no velocity gradient terms were omitted. Particularly coarse meshes were used in this investigation with the emphasis on rapid turnover for integration into a design process.

A solution procedure for the 2-D laminar viscous Navier-Stokes equation set was published by Khalil et al [1980]. This method used a meridional solution as a basis for a blade-to-blade laminar calculation. Khalil and Tabakoff [1981] then enhanced the formulation by using a standard K- ϵ model for turbulent stresses. This was applied to a radial turbine with no modifications made to the standard K- ϵ model to account for curvature effects.

Dawes [1987] used a time marching finite volume method to model 3-D viscous compressible flow to gain a steady state solution. A zero equation algebraic model was used for turbulence. The work predominately investigated the entropy generation within a centrifugal impeller. Main losses are shown to be at the shroud region.

Rahmatalla and Bosman [1980] used a 3-D turbulent K- ϵ model for a centrifugal impeller. They concluded that the predictions were improved with the addition of viscosity but noted that the inviscid forces were instrumental in the primary and some secondary flow. Tourlidakis and Elder [1991] give a calculation procedure based on a finite volume formulation incorporating a K- ϵ eddy viscosity model. The main investigation was into the effects of tip leakage on the flow. The use of the loss prediction ability of viscous flow solution methods is demonstrated to good effect.

Hah et al [1988] applied a full 3D elliptic solver to the Eckhart impeller operating at off-design. They were able to qualitatively predict the changing flow structure for duties near both stall and choke. A similar investigation was completed by Lapworth and Elder [1988], who used an incompressible SIMPLE calculation procedure to predict the internal flow and exit structure of a centrifugal impeller. The wake was adequately modelled at an off design condition and showed good correlation with reality. Both of these methods used modified K- ϵ eddy viscosity models.

Casey (1990) completed a comparison between two codes incorporating different turbulence models; the first was a zero equation type and the second a two equation variety. Both methods predict similar flow fields despite their differences and accurately model the separated flows.

3.2 CFD applied to Centrifugal Fans

As already stated in the introduction, centrifugal fans have been relatively neglected by CFD investigators. Many more techniques have been applied to centrifugal compressors using techniques of increased accuracy (and required computational power). To highlight the gap, a review follows of methods that are attempts at using CFD to model internal centrifugal fan flows. Instead of the detailed partitions used in the preceding review, the works are simply separated into inviscid and viscous investigations.

3.2.1 Inviscid Methods: Centrifugal Fans

A Potential flow solution of flow within a centrifugal fan was completed by Whirlow et al [1981]. The boundary conditions incorporated the Kutta condition in order to prescribe the necessary circulation to make the flow about the blade realistic. This was achieved by the superposition of a number of program runs. The blade pressure distributions were compared with experiment and showed excellent correlation. See Figure 3.2 below

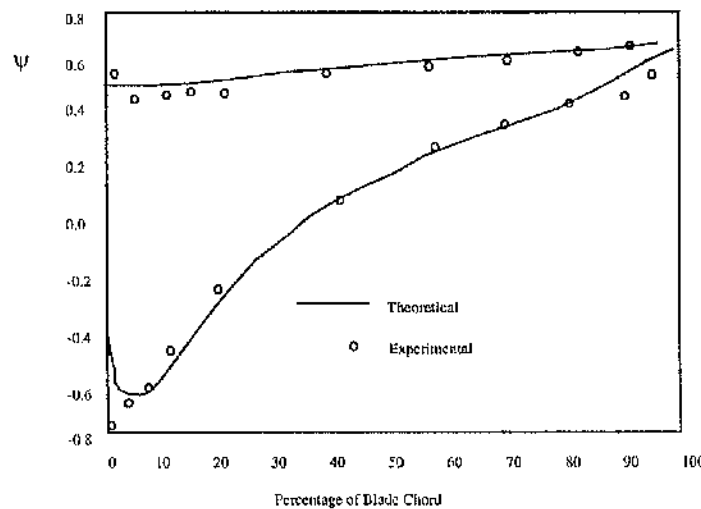


Figure 3.2 Comparison of Theoretical and Experimental Pressure Distribution Along Blade Surfaces at Mid Span (Whirlow et al [1981])

Despite the simplicity of the formulation the method was able to predict some suction surface separation towards the trailing edge of the blades, as would intuitively be expected when operating at flows below design. In parallel with the detailed blade examinations, the overall performance predictions were scrutinised. Without a loss mechanism the predicted fan pressure rises were high. However by multiplication with the fan overall efficiency, better correlation was achieved. See Figure 3.3 below.

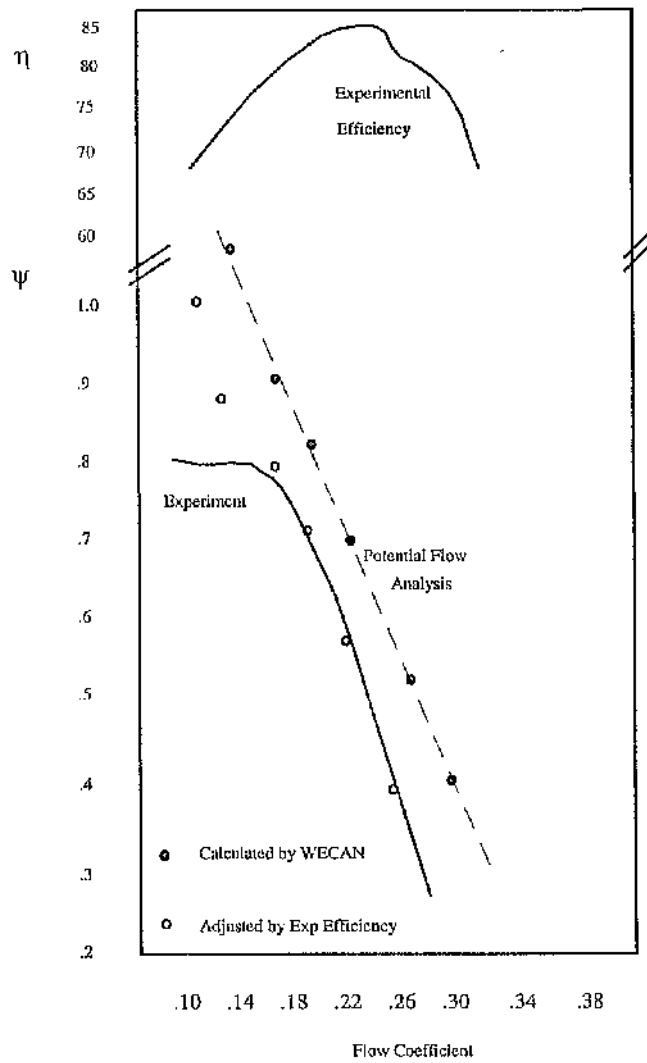


Figure 3.3 Fan Pressure Rise and Efficiency Curves (Whirlow et al [1981])

Further enhancements to fully automate the performance estimation were completed by Wright et al [1984]². The efficiency multiplier was replaced by a momentum deficiency calculation based on boundary layer theory, the details of which are not fully explained. However these adjustments did improve predictions and more importantly did not require the input of an experimentally derived efficiency. Some additional work was included in this to account for the differences in discharge conditions between the CFD model, with a vaneless annular discharge, and the tested fan, which discharged into a scroll casing. Additional performance manipulations were introduced in the light of this work. Finally Wright et al [1984]¹ compared a q-3D method and their 3-D method for a centrifugal fan operating between 80% and 125% of design flow. Results were compared against experimental casing and blade static tappings. Some minor differences were noted but the report did not detail these. It was disappointing that the author was not clear, or did not indicate, which method he thought was best at predicting the internal flow. The main concern seemed the additional computational power required for the 3-D method and how it should be used as a final analysis due to its additional computational penalty. Compared to the full 3-D viscous codes reviewed for compressors, the power requirement for the inviscid 3-D code is several orders of magnitude less and it is therefore not an issue today.

3.2.2 Viscous Methods: Centrifugal Fans

The only methods to date that have accounted for the losses within centrifugal fans have used total pressure losses or resistive force vectors. These approaches are limited in that they do not predict the gross flow features (see figures 2.5(a) and 2.5(b)) that occur within the blade passage. They are only able at best, given a loss calculation algorithm, to predict the overall performance of the impeller. To model the gross regions as already indicated by the aforementioned figures, it is expected that viscous influences must be numerically accounted for as an integral part of the solution. Unfortunately the references in which viscosity has been incorporated are restricted to radial turbomachinery. As these methods are general solvers, there is no reason why centrifugal fan geometries may not be tackled. Therefore it is expected that further steps in the numerical experimentation of centrifugal fan flow will take advantage of these already established methods.

Tables 3.1 and 3.2 summarise the computational methods reviewed in this chapter and gives an indication of the applicability of each method for predicting the flow within centrifugal fans.

Table 3.1 Applicability of Various Inviscid Methods for the Prediction of Flows within Centrifugal Fans

Solution Type	Reference	Applied to centrifugal fan?	Inlet box	Inlet ring gap	Unsteady inlet vortex	Blade passage core	Blade passage reverse flow	Blade passage vorticity	Exit jet wake	Scroll Casing	Comments
Quasi-3D	Wright et al [1984] ^I	Yes	0	0	1	0	0	0	0	0	This quasi-3D method suppresses the full 3D flow and requires influential empirical assumptions
Potential Flow ($\nabla^2=0$)	Whirlow et al [1981]	Yes	0	1	0	1	0	0	0	0	Simple equation set requiring little storage and computer power. Limited as it assumes incompressible, irrotational, inviscid flow.
Potential Function	Laskaris [1978]	No	0	1	0	1	1	1	1	0	Irrotational, inviscid, compressible formulation
Steady Euler	Prince and Bryans [1984]	No	0	1	0	Π	1	1	1	0	Full steady inviscid equations of motion. Some of these solvers time step the unsteady equations.
Unsteady Euler	Bosman and Ahrabian [1984]	No	0	1	1	Π	Π	Π	Π	0	Unsteady, large regions of recirculating flow were documented-could be possible for fans to exhibit the same characteristics.

Key: 0 Not suitable

I Some indications of promise

II Theory/Experiments show that this may be suitable

III Some work already completed but needs developed

IV Good Modelling

Table 3.2 Applicability of Various Viscous Methods for the Prediction of Flows within Centrifugal Fans

Solution Type	Reference	Applied to centrifugal fan?	Inlet box	Inlet ring gap	Unsteady inlet vortex	Blade passage core	Blade passage reverse flow	Blade passage vorticity	Exit jet wake	Scroll Casing	Comments
Partially Parabolic, Viscous, incompressible	Moore and Moore [1981]	No	0	I	0	I	I	I	0	0	Despite the parabolic flow assumptions the formulation offers good modelling capabilities
Viscous (Laminar) Elliptic	Khalil [1980]	No	0	0	0	I	I	I	0	0	2-D blade to blade laminar solution
Viscous (Turbulent). Elliptic	Khalil and Tabakoff [1981]	No	0	0	0	II	II	I	I	0	A turbulent version of the above
Viscous (Turbulent)	Dawes [1987]	No	0	I	0	II	II	II	III	0	A fully 3-D viscous turbulent solver

Key:

0 Not suitable

I Some indications of promise

II Theory/Experiments show that this may be suitable
III Some work already completed but needs developed
IV Good Modelling

CHAPTER FOUR

The Mizuki High Pressure Compressor

The Mizuki [1974] impeller is the first of the impellers to be examined. The geometry is classical for a high speed radial impeller consisting of blades which are curved at inlet and subsequently extend and straighten to discharge radially. Unlike the lower pressure machines examined in this dissertation the design did not have a shroud. See Figure 4.1 below.

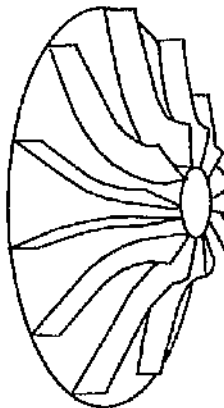


Figure 4.1 Sketch of the Mizuki Impeller

The geometry and initial boundary conditions for this impeller were available as a PHOENICS standard test case [PHOENICS Library No. 524] and thus little preprocessing was required before obtaining a first series of verified results. The associated mesh was very coarse, with dimensions of $5 \times 5 \times 12$, essentially limiting its use to inviscid simulations (although the original work Edwards [1985] included a constant high value of molecular viscosity in order to crudely simulate the effects of turbulence). Consequently, it was decided to concentrate on modelling inviscid flow, for which there had been identified a selection of relevant published works worth investigating. Of particular interest were those claiming to predict off-design flows. Traditionally it had not been considered possible for an inviscid model to predict and properly simulate flow separation, an inherently viscous phenomenon. However the results from a 2-D scheme by Stanitz[1948] first indicated some doubt in this philosophy, when he correctly predicted fully separated stalled zones using an

inviscid formulation. More recently, Bosman and Ahrabian [1984], using a fully 3-D Euler code demonstrated not only separated zones but also some of the unsteadiness associated with highly stalled turbulent flow. These stall zones were also correctly predicted at the low flow rates characteristic of stalled flow. This work was carried out with an impeller similar to that of the Mizuki [1974] and encouraged the present attempt to predict such highly stalled cells.

4.1 Description of Model

The computational library casc model for the 12 bladed MIZUKI impeller was fully 3D and the equations solved were steady state, with laminar viscosity (set to an insignificant value when simulating inviscid flow) and incompressible. Momentum source terms modelled the additional body forces needed for working within a rotating frame of reference. An inlet velocity condition prescribed the impeller mass flow and the air discharged through a constant pressure outlet positioned downstream of the impeller exit on a surface representative of the vaneless diffuser discharge.

Due to changes in available hardware and software resources, the first series of steady state runs were completed using PHOENICS software and the latter runs using FLUENT. A small FORTRAN utility called CONVERT.F77 was written to translate the original PHOENICS BFC (Body Fitted Co-ordinate) geometry file of the Mizuki impeller for import into FLUENT. The computational mesh is shown in Figure 4.2.

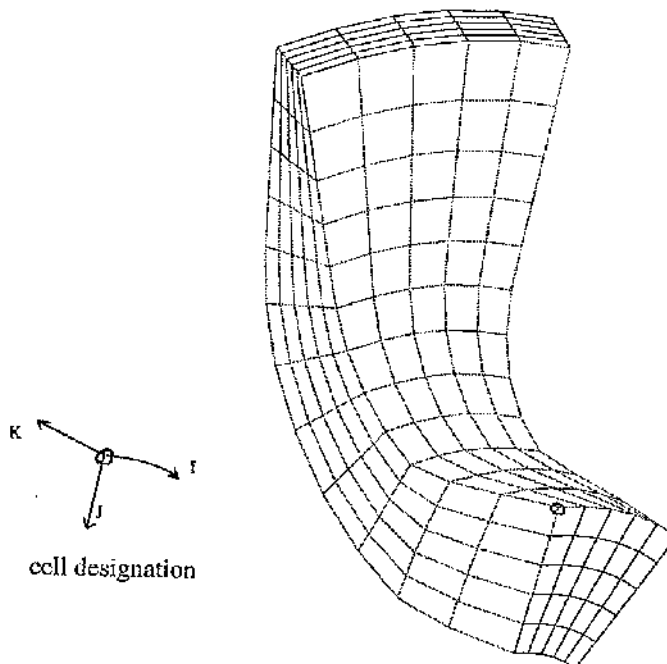


Figure 4.2 Computational Mesh of the Mizuki Impeller

4.2 Steady State Computational Investigations

All runs were carried out at the impeller design speed of 6000 rpm (\equiv tip speed of 84 ms^{-1}) at flow coefficients of 0.4, 0.2 and 0.1, the former representing design flow and the latter a highly stalled condition. The standard PHOENICS library case, together with a high laminar viscosity to compensate for the lack of a proper turbulence model, was run first. The results were as expected for design flow ($\varphi=0.4$), with velocity vectors following surface contours and without any areas of recirculation detected. In order to mimic inviscid flow, the value of viscosity was set to zero and the run repeated. No differences were noted, as would be expected when performing viscous calculations on such a coarse mesh. Reductions of flow-rates down to $\varphi=0.2$ and 0.1 proved most interesting with an emergence and subsequent growth of recirculating eddies. Figure 4.3 shows this development using relative (to the impeller rotation) velocity vectors of the flow on a plane adjacent to the blade pressure surface. Most prominent is the reverse flow at the impeller inducer. This flow is similar to that predicted by Bosman and Ahrabian[1984] (see Figure 4.4) but with the exception that they showed maximum recirculation on the suction rather than pressure surface.

The three meridional planes of velocity vectors that are shown in Figure 4.5 are from a run with $\varphi=0.1$, and reveal the extent and three dimensional nature characteristic of such highly stalled flows.

It is not only the velocity distribution that is effected by low volume flow rates; significant qualitative variations in pressure also occur as may be seen in Figure 4.6. For the design flow case the pressure contours are almost normal to the velocity vectors; however for the low volume flow case the pressure contours stratify so that the maximum pressure gradient is in the radial direction. This is particularly apparent just after the impeller inlet, near the shroud.

It was at this stage that the author started to use FLUENT instead of PHOENICS, with the emphasis now on unsteady simulations. As the unsteady calculation procedure required a converged steady-state solution from which to iterate, some of the earlier PHOENICS runs were duplicated, using FLUENT, but with a slightly different wall treatment. Instead of using non-slip conditions for the inviscid simulations, it was decided to fully uncouple the influence of the wall by using more appropriate slip boundary conditions. These fixed wall normal velocities to zero. Despite this subtle change, no differences were noticed in the solution with the inlet boundaries set to flow coefficients of 0.4 to 0.1 as before. The runs are documented in Appendix A.

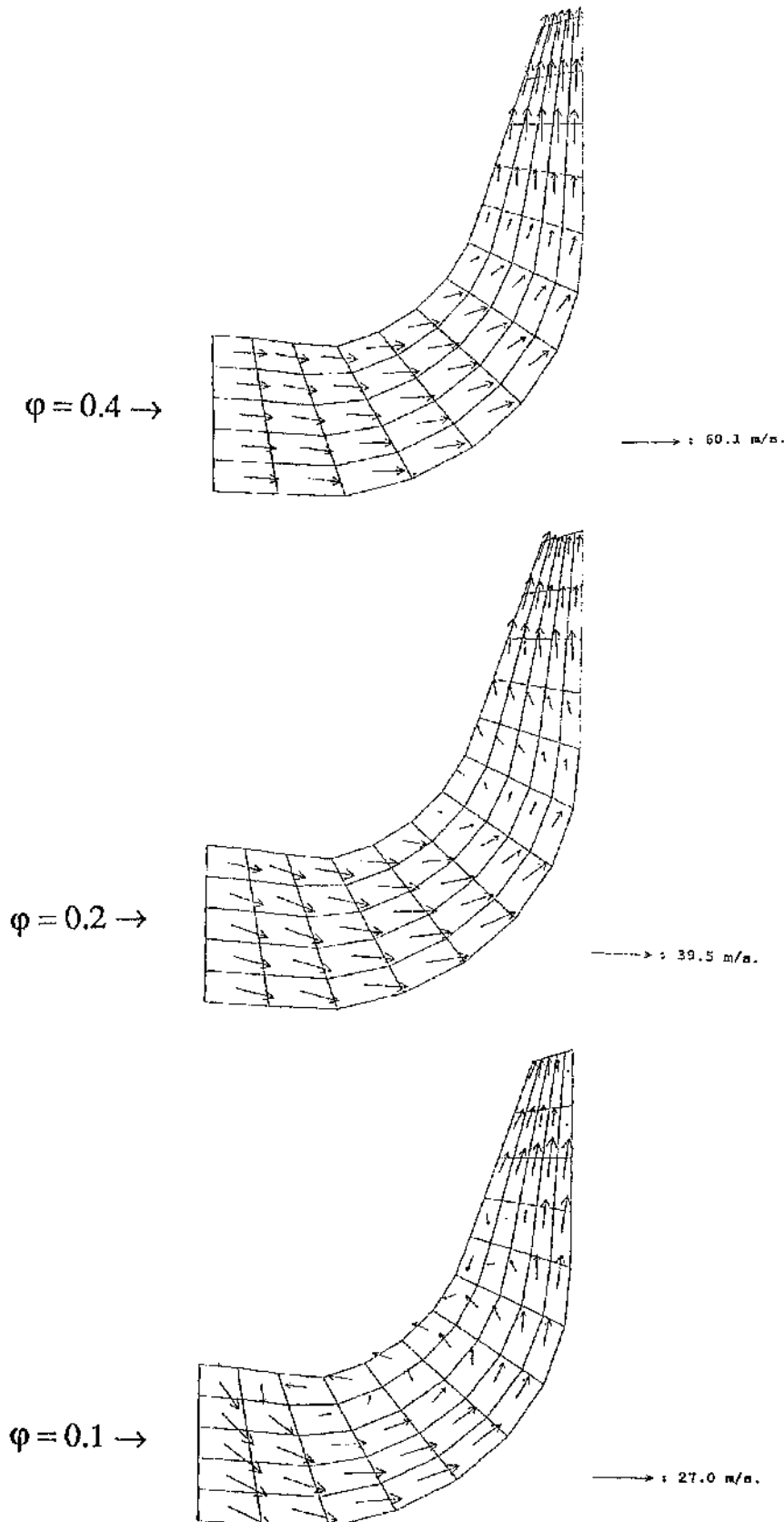


Figure 4.3 Development and Growth of Recirculation at Progressively Lower Flow Rates

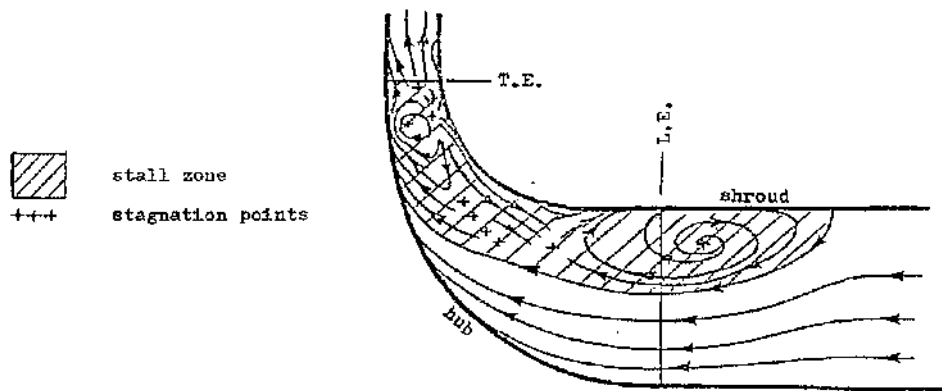


Figure 4.4 Recirculation On The Suction Surface As Predicted By Bosman and Ahrabian [1984]

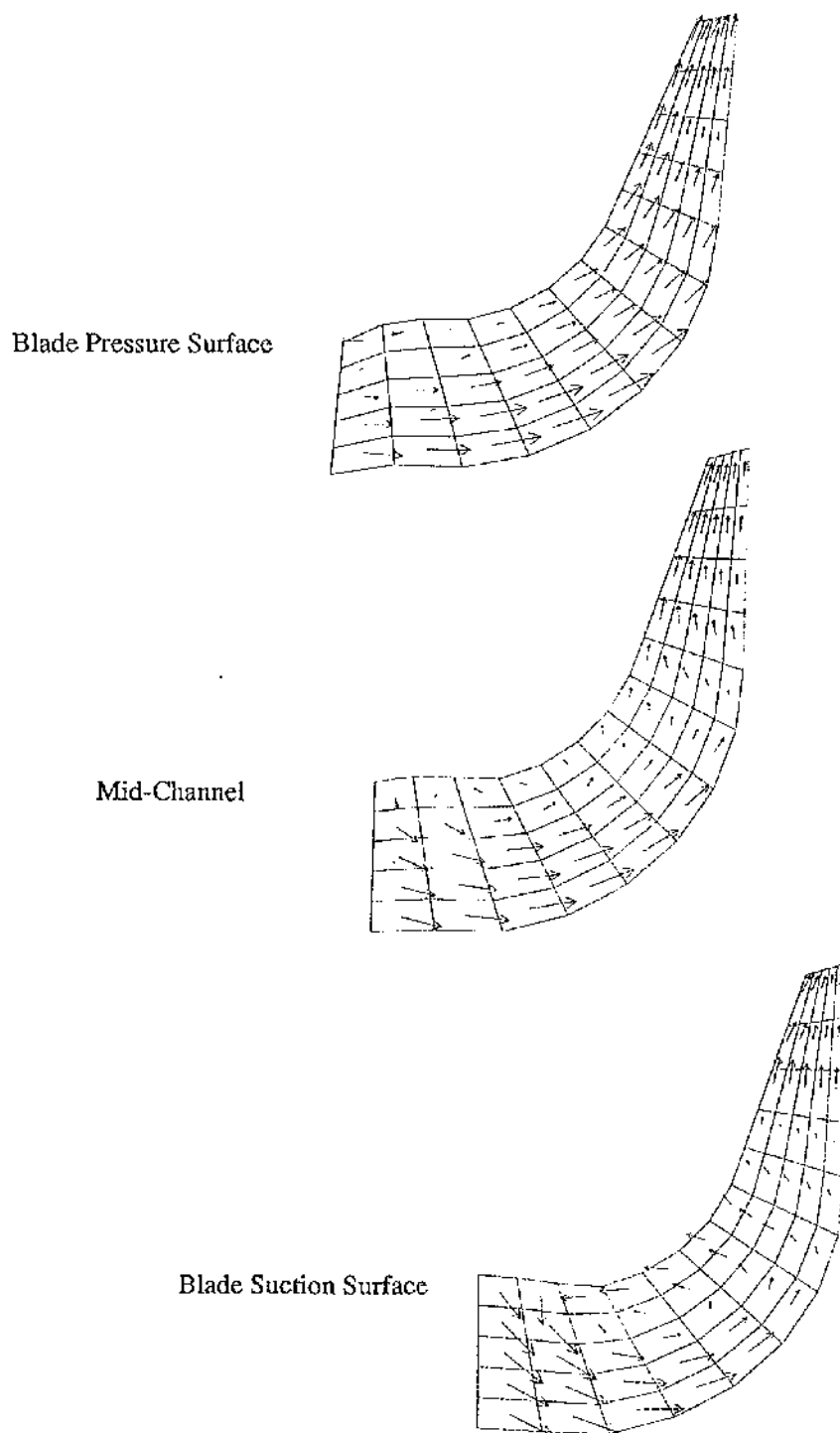


Figure 4.5 The Three-Dimensional Nature of Highly Stalled Impeller Blade Passage Flow: Velocity Vectors

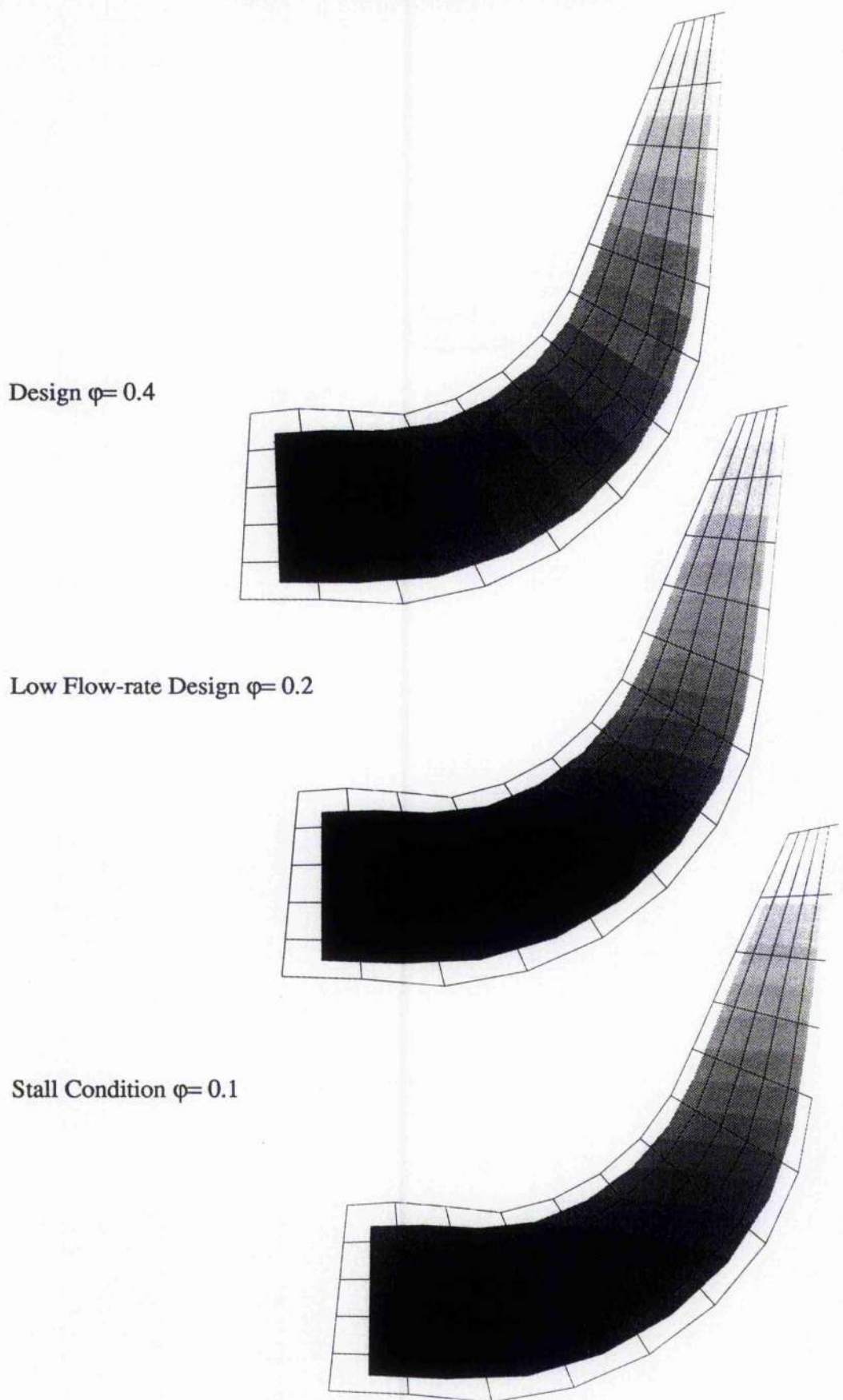


Figure 4.6 Variation in Pressure Distribution with Changes in Flow Rates

4.3 Unsteady Calculations

Bosman [1984] used a time-stepping Euler code to calculate the converged steady state flow within a radial compressor and was seemingly surprised by the detection of unsteady perturbations. As the SIMPLE algorithm within FLUENT does not use such a pseudo-time stepping procedure it was necessary to invoke time dependence separately. Once invoked no unsteady perturbations were noted even for the most highly stalled condition of $\varphi=0.1$ for which a variety of time steps ranging from 4×10^{-2} to 4×10^{-8} seconds were used. Figures 4.7(a) and (b) demonstrate the smoothness of the output in the form of pressure history plots. On the X-axis, every 100 iterations represents a time step for which there were twenty completed during this particular batch run. The length of the time step was 2×10^{-4} , representing a tenth of the approximate time for a stall cell to pass from one blade passage to the next. This cell movement obviously cannot happen in a single blade passage model due to the flow asymmetry, but this work does show the solver is stable and would be suitable for the multiple passage work necessary to simulate rotating stall.

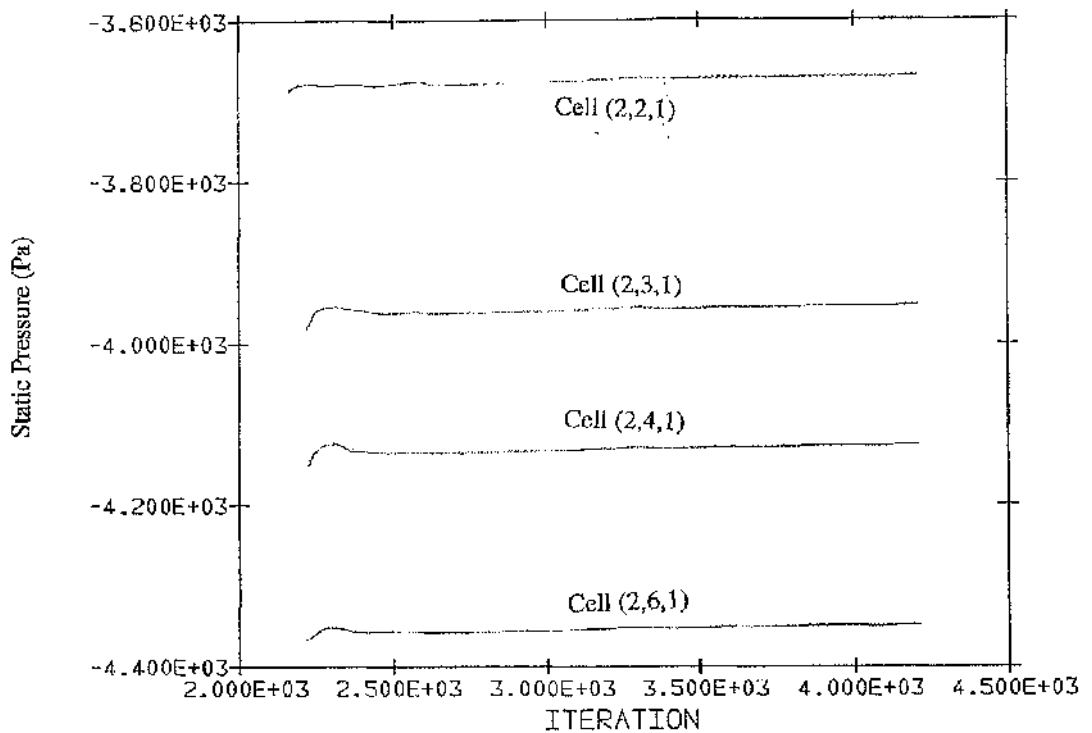


Figure 4.7(a) Pressure History Plot of Flow at Inlet of the Mizuki Impeller

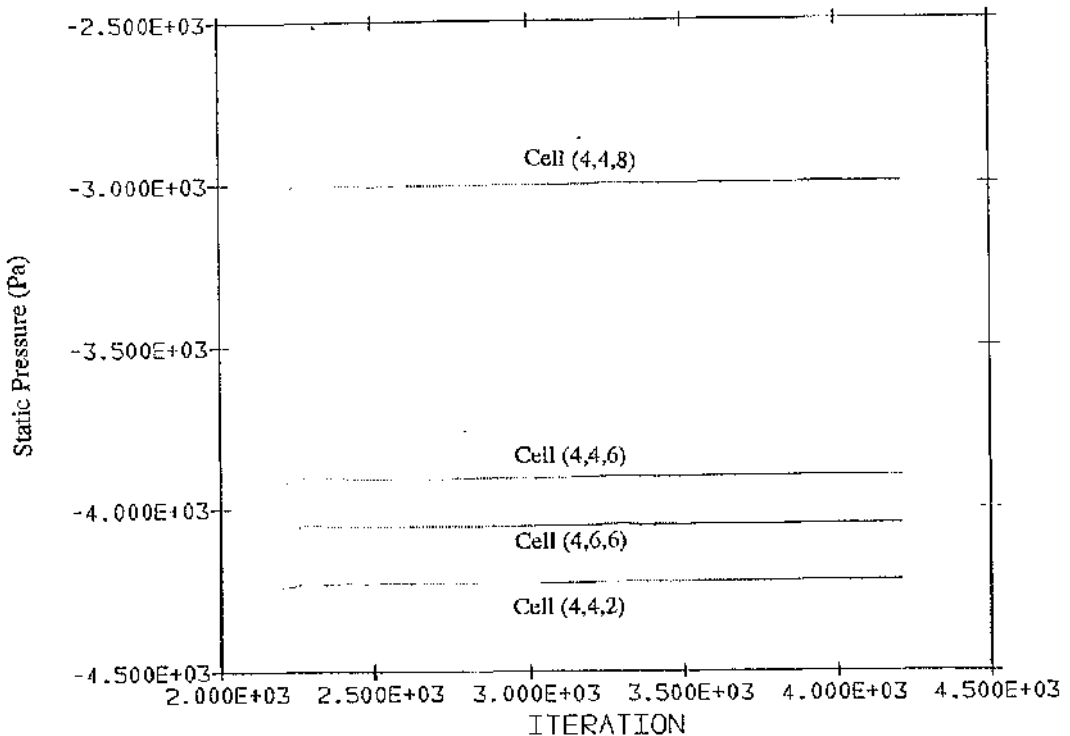


Figure 4.7(b) Pressure History for Flow within Highly Stalled Region

4.4 Conclusions

1. The SIMPLE (Semi- Implicit- Pressure- Linked- Equation) algorithm has been shown to be suitable for solving the flow within turbomachinery radial blade passages.
2. The coarse mesh given in the PHOENICS Library [No. 524] does not have the grid resolution needed to properly model viscous flow.
3. The radial blade passage model was able to predict the large flow recirculating regions presented by Bosman and Ahrabian [1984]. However, the model did not show any of the reported unsteadiness.

With the author satisfied with the applicability of the software and method, the investigation then proceeded with the next model, that of the L3R radial fan.

CHAPTER FIVE

The L3R Radial Bladed Fan

The L3R fan was initially designed for an extreme variable speed duty. The corresponding mechanical requirements imposed were outwith the normal material and construction methods used for traditional centrifugal fans and therefore the design included several departures from the norm. Most significantly, the aerofoil blades, normally mounted onto the impeller periphery, were replaced by plate steel blades positioned radially resulting in a geometry similar to that of a radial compressor. Together with a small 5° backsweep this gave the design the high strength and torsional rigidity needed to operate over the demanded wide speed range.

With its novel construction, the L3R provided herein an important bridge between our existing knowledge of radial compressors, for which there is a great deal of published data, and centrifugal fans, which have been comparably neglected. A sketch of the impeller is given below.

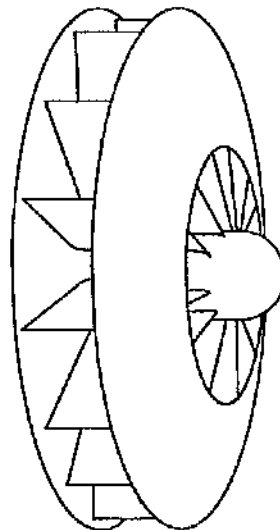


Figure 5.1 Sketch of the L3R Impeller

Any CFD investigation is incomplete without some experimental comparison. As no previous performance data was available for the L3R, and with the design incorporating features that overextended existing fan aerodynamic rules for performance prediction, a nominal 1m tip diameter model was constructed and tested. The subsequent aerodynamic testing also included an investigation into the destabilising effect of diffusers, an important factor in the overall fan system stability and which in many instances has been neglected by the CFD investigators due to the inherent modelling difficulties. The implications of not modelling the diffuser are highlighted later in this chapter together with the possible consequences of this, often necessary, modelling simplification.

This experimental work was followed up by several CFD models of the L3R fan incorporating a vaneless diffuser. These models are classified here into two categories. Models of the first category are denoted 'bladed' as the blade thickness was represented in the computational mesh. These runs were infested with stability problems as the domain contained far too many skew cells with high aspect ratios. Subsequently the number of poorly shaped cells was reduced by neglecting the blade thickness. This second category of CFD runs are denoted 'unbladed' model runs. Not modelling the blade thickness allowed the domain to be constructed as a solid of revolution. The associated simplifications gave rise to a far more suitable grid, curing the stability problems experienced earlier. Finally within this chapter, the L3R CFD performance predictions are compared directly with experiment and the detail flow patterns, particularly at stall, compared with the predictions of Bosman and Alrabian [1984].

5.1 L3R Aerodynamic Experimental Investigations

The test arrangement was generally in accordance with BS848:1980:Part 1 utilising the 'C' layout comprising of inlet ducting for flow metering and a free fan discharge expelling into atmosphere. Together with a vaneless diffuser, the arrangement had axisymmetric inlet and discharge flow boundaries which made the setup particularly amenable for CFD modelling and it is to this basis that comparisons are made. See Figure 5.2

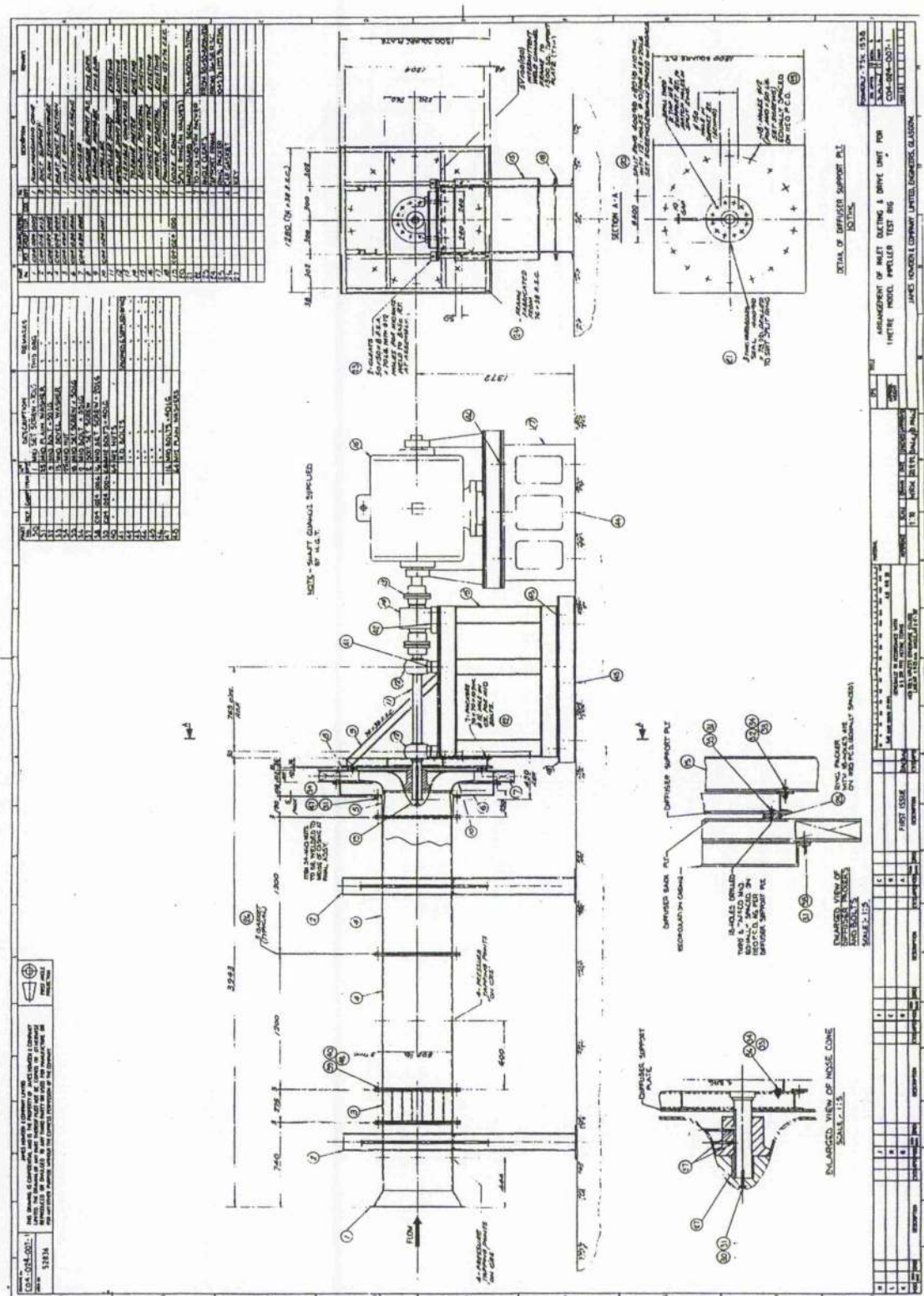


Figure 5.2 L3R fan test arrangement

However in the majority of applications, industrial fans are required to operate within scroll casings. To adequately model such scrolls requires either some iterative matching between the impeller mesh and the scroll mesh and/or some kind of averaging to cope with the necessary complicated boundary conditions. Such work is beyond the scope of the present study, requiring much larger computational power and a computer code capable of handling rotating and stationary planes simultaneously. Here we concentrate on using single blade passage computational domains. This simplification dramatically reduces the required computational power but introduces several possible inaccuracies into the solution. For example the inlet domain is assumed to be of uniform flow- a reasonable assumption for ducted arrangements as tested here. The assumption breaks down however when an inlet box is incorporated and/or where Inlet Guide Vanes or Inlet Louver Dampers introduce flow asymmetries. These, apart from introducing swirl to the flow and changing the blade incidence for regulation, introduce an unsteady precessional vortex. However, despite affecting the fan efficiency by a few points, little effect on the gross mean impeller flow features is thought to occur when the guide vanes are fully open and omission avoids the need to model the complete impeller. At the discharge modelling assumptions also have to be made. It has been well documented that the discharge has a destabilising effect on the flow within turbomachines (c.g. Pampreen 1993) and for fans this has been experimentally demonstrated for various vaned annular diffuser configurations by Kubo[1980]. This has particularly important implications when modelling fans encased within scrolls as there must be some estimate of how much the solution is effected by using simplified exit boundary conditions.

The remainder of section 5.1 details investigations undertaken to address these unknowns with the L3R impeller, tested with a variety of scroll and vaned diffuser designs.

5.1.1 Experimental Apparatus and Instrumentation

Static pressure tappings were attached to the inlet metering cone (used to measure flow rate) and at three diameters upstream of the fan inlet (to measure the inlet static pressure). In both cases a series of four tappings were joined together in order to gain a good average plane pressure. These were connected to precision calibrated manometers. Shaft speed and power were both measured using a calibrated torquemeter (Type: Torquemeters Ltd. Model. ET60). The air temperature was measured at inlet and discharge using mercury in glass thermometers with the system

resistance varied using a combination of expanded mesh and coarse cotton weave material.

Unsteady pressure measurements were carried out using a piezo electric pressure transducer (Type: Birchall M01/F/A) amplified using a Brüel & Kjaer charge amplifier (Type: 2635) and connected to a Hewlett-Packard Analyser (Model 3582).

5.1.2 Vaneless Diffuser Results

The performance of the fan with vaneless diffuser is shown in Figure 5.3 and the performance curve is denoted 'Test 29- corrected for discharge area'. This curve includes a correction to account for the swirl at fan discharge with the flow angle calculated from the fan power. For comparison the equivalent curve, which is based on the discharge angle at design flow and does not account for variation of swirl with flow rate, is shown.

5.1.3 Vaned Diffuser Designs

A flat plate and curved plate diffuser design were also tested and may be compared, together with the vaneless diffuser results, in Figure 5.3. It is evident that all designs stall at approximately $5 \text{ m}^3/\text{sec}$. Changes in blade angle were also made (See Figure 5.4 for a sketch of vanes tested). These had no effect on the unstalled minimum flow either but did make changes to the size of the hysteresis loop. After reducing the system resistance from deep stall, the 20° design recovers far more quickly than the 27° counterpart. This is probably due to the lower incidence created by the 20° blades, intuitively expected to operate better at low flow-rates. This small blade angle helps recovery but strangely was unable to help delay stall in the first place.

This difference in hysteresis is not of concern here as it is only possible to model flow just prior to rotating stall with a single blade representation. Therefore if attention is concentrated on the results for the tests with 'increasing system resistance' it can be concluded that vane angle and design has little influence on stable operation. This result does not contradict the findings of Kubo [1980] who showed that the onset of stall was only sensitive when 6 or less vanes were used. A minimum number of 23 were used here.

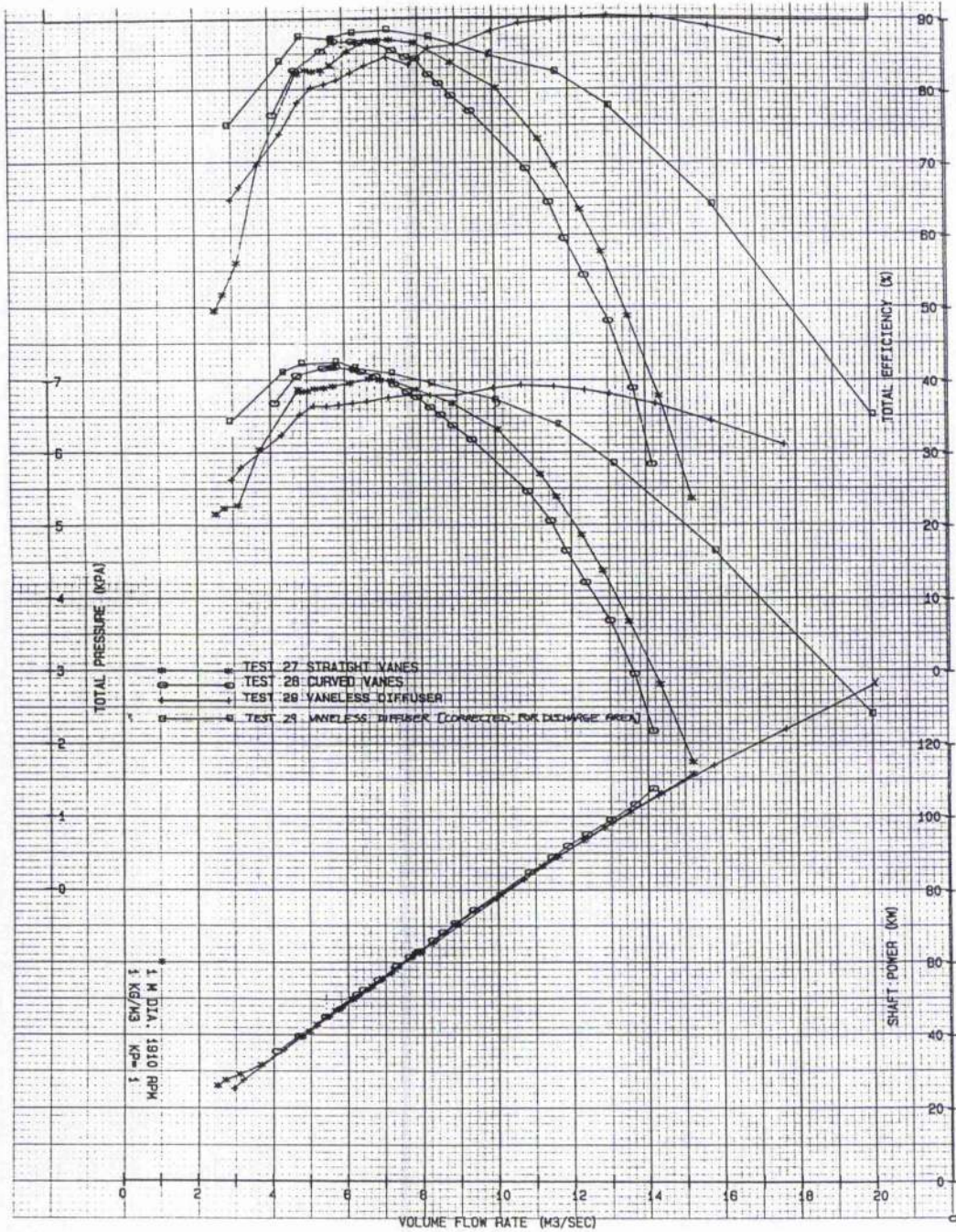
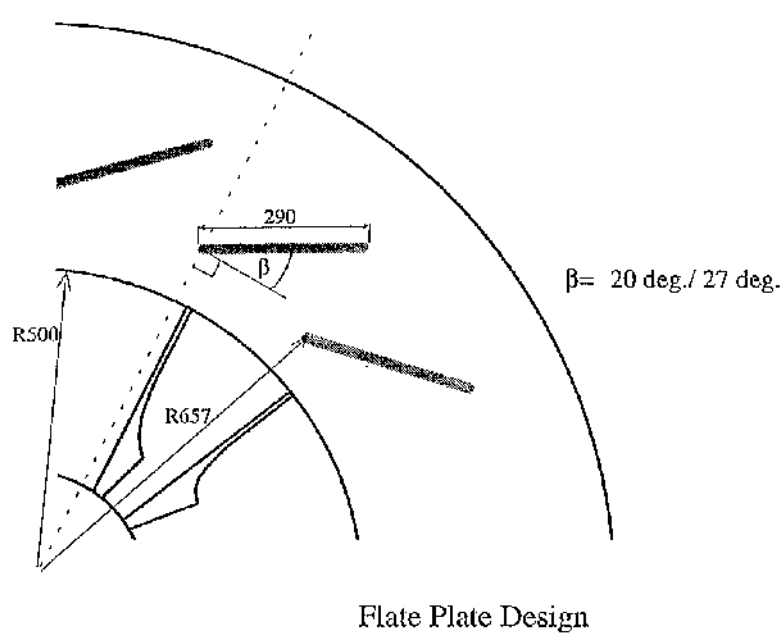
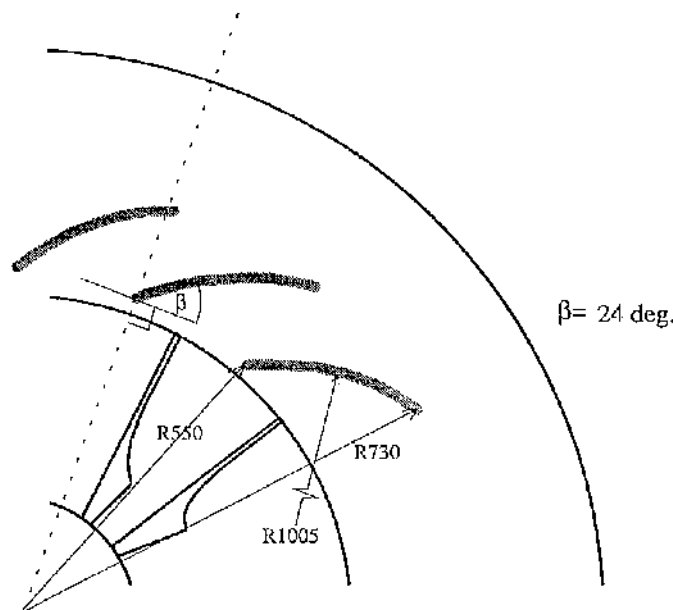


Figure 5.3 Performance Characteristic of the L3R with Different Annular Diffuser Configurations



Flat Plate Design



Curved Plate Design

Figure 5.4 Sketch of Vane Designs Tested

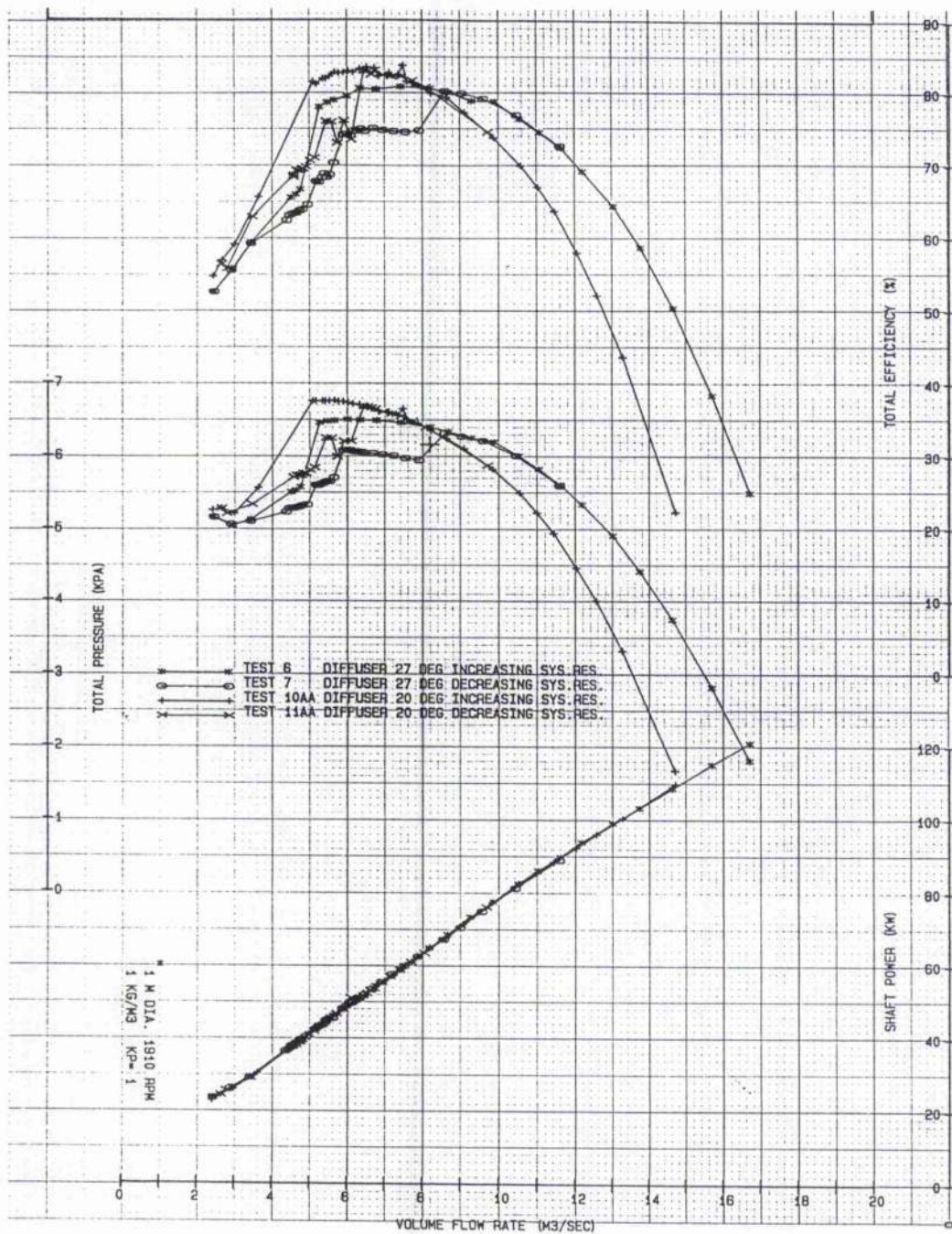


Figure 5.5 Performance Characteristic of the L3R with Different Vane Designs

5.1.4 Scroll Casing Designs and Experiments

The designs were based on the design rules given in Eck [1973] using a logarithmic spiral but with a small distortion of increased clearance at the scroll cut-off to reduce noise. This distortion was optimised by perturbing from the initial design position. The resulting aerodynamic performance results were similar to those of the vaned diffuser arrangements and we would therefore expect matching internal flows. See Figure 5.6.

5.1.5 Stall Detection

As the system resistance is steadily decreased there are several noticeable indications that the fan is in rotating stall. Firstly, a periodic aerodynamic noise can be heard together with a large increased step in rig vibration. Then, on examining manometers the readings may be seen to oscillate at high frequency, with the inlet static pressure readings having fallen by a disproportionate amount.

With a fan of thirteen blades it was decided to check the speed of the rotating stall cell(s) within the vaneless diffuser configuration. The transducer was placed 20cm from impeller discharge on the backplate side of the diffuser casing. A sample frequency domain plot for the L3R operating in rotating stall is shown in Figure 5.7. This shows a distinct pressure pulsation at 9.75Hz, representing $\frac{1}{2}$ of the impeller rotational speed. This is not in line with the experimental results of Bolton [1975], who measured the frequency of the flow unsteadiness within centrifugal fans exhibiting rotating stall. See Figure 5.8. However, Pampreen [1993] surmised that for radial turbomachines, there was presently no reliable method to either predict the number of stall cells or their frequency of rotation.

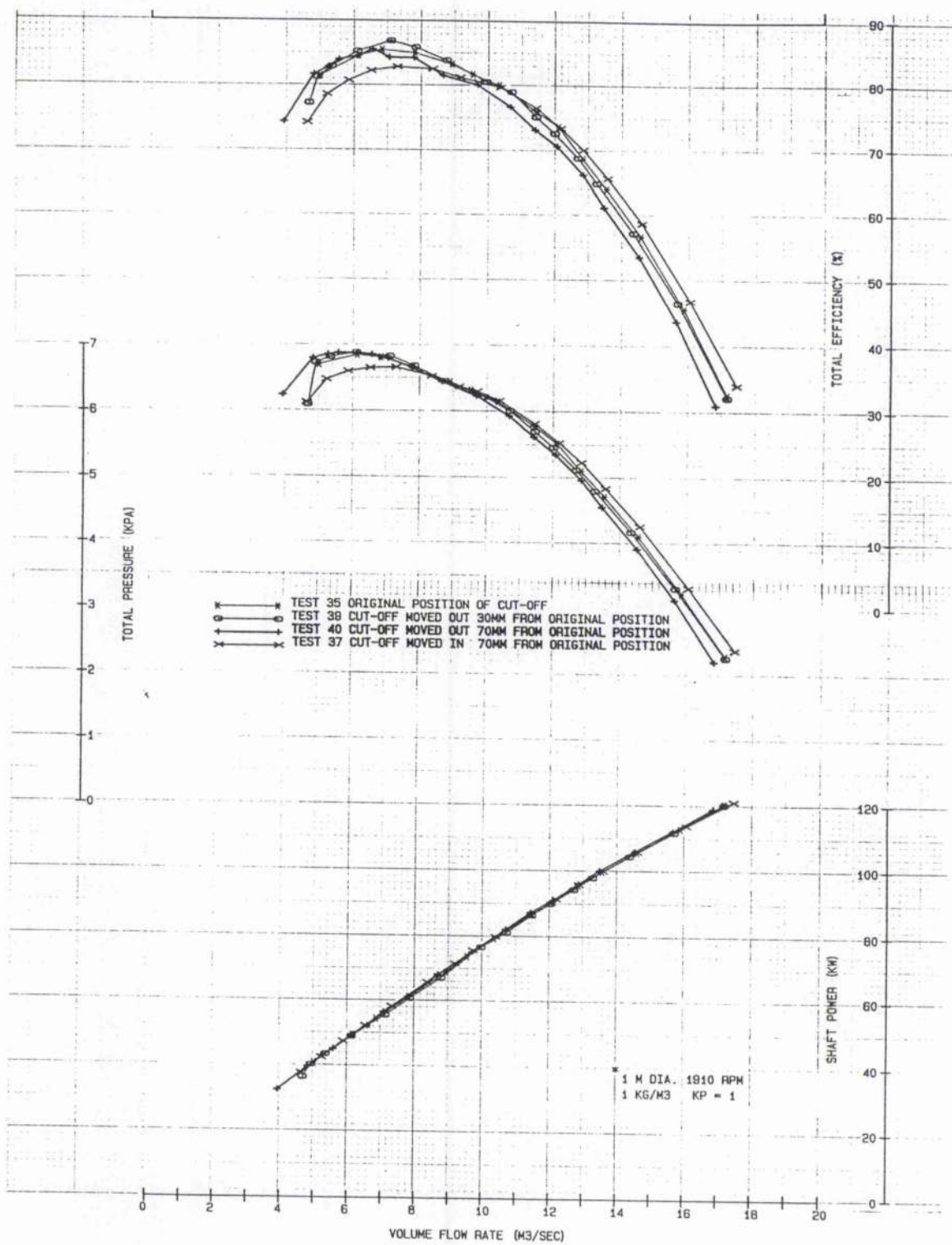


Figure 5.6 Effect of Different Scroll Designs

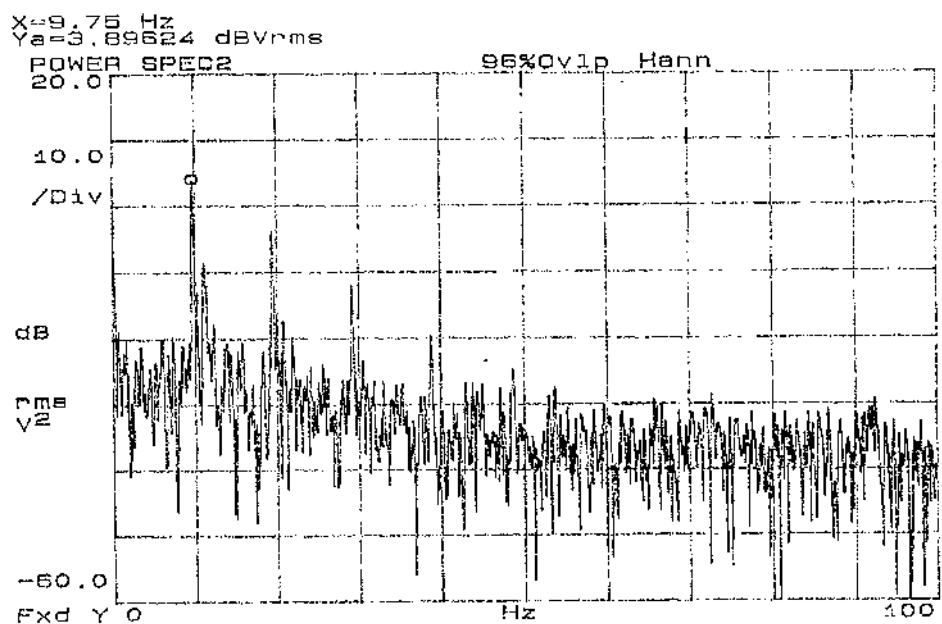


Figure 5.7 Frequency Domain Plot of Pressure Pulsations within the L3R Vaneless Diffuser whilst Operating in Rotating Stall

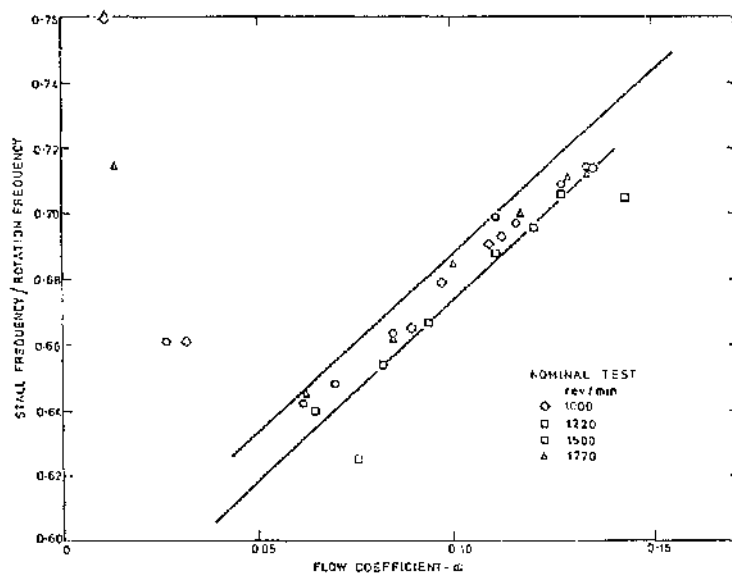


Figure 5.8 Frequency of Rotating Stall Pressure Fluctuations (Bolton [1975])

5.2 L3R Fan CFD investigations

Two models of the L3R centrifugal fan impeller were constructed, the main features of which are shown below in Table 1.

Table 5.1 L3R Model Differences

Model	Number of Computational cells	Blade Thickness Modelled?
'bladed'	$12 \times 10 \times 41 = 4920$	Yes
'bladeless'	$5 \times 5 \times 30 = 750$	No

These models will be subsequently referred to as the '*bladed*' and '*bladeless*' cases, for which the computational grids are shown in Figure 5.9.

Choice of computational domain

When constructing a computational mesh the engineer must decide whether to model the blade thickness or not. The choice is primarily dependant on whether the model is to be subsequently cyclically replicated to form a multi-blade channel domain and/or whether the blade blockage effect is expected to be significant. Large savings in mesh construction time are possible if the user decides to neglect the blade thickness. Construction is then based on an axisymmetric meridional plane which is then rotated to form a volume of revolution. This avoids difficult 3-D modelling. However this is not the only saving: when using FLUENT walls must be modelled 2 cells thick for the correct treatment of boundary conditions. The addition of these cells needed to model blade thickness can increase the total number in the mesh by over 20% causing an estimated 50% increase in computer time required for solution.

Despite the expected extension in computer run times due to the increased number of computational cells, a bladed model was built first. This model would allow progression to a multi-channel domain for which the modelling of blade thickness would be necessary. It is referred to as the *bladed* L3R model in the remaining text. This configuration is shown at the top of Figure 5.9. The other computational mesh shown in Figure 5.9 is the *bladeless* model. The '*bladeless*' simplification was justified here as the impeller blade plate thickness caused little blockage within the L3R fan. A significant saving in computation cells was made, with the blade passage bounded cyclically by wall boundaries.

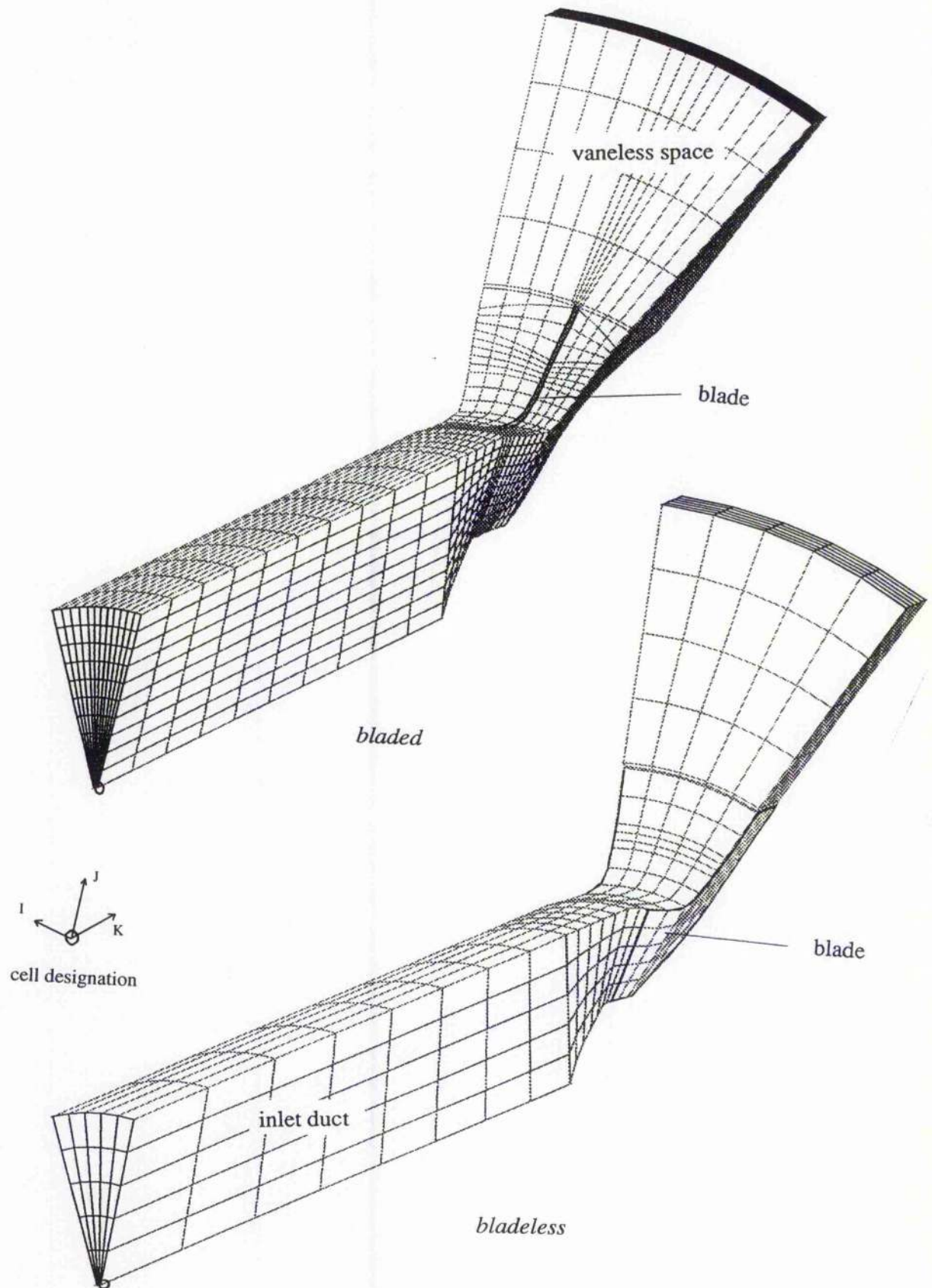


Figure 5.9 L3R Impeller Computational Meshes

The other choices that the CFD modeller is faced with concern the inlet and discharge boundaries -that is the extent of the flow upstream and downstream of the impeller to be modelled. At the inlet, as the unsteady disturbances at stall influence the flow several duct diameters away from the impeller (Kubo 1976), the choice of modelled duct length is really dependent on the operational duty to be modelled. In the series of runs included in this chapter, the part of the inlet duct from inlet static pressure tappings to the impeller was modelled. The choice of discharge conditions, for this particular model, was straightforward as results were available for a configuration which included a vaneless diffuser. The diffuser and impeller were completely modelled in both the bladed and unbladed meshes.

Boundary Conditions

A uniform inlet velocity was prescribed at inlet and zero static pressure set at discharge. This pressure boundary included a feature that allowed reverse flow at discharge i.e. allowed fluid to enter the domain via the vaneless diffuser. When reverse flow was detected, locally the boundary condition changed from zero static to zero total pressure. With this facility it was hoped to model highly stalled cells when using multi-blade domains.

For the runs involving the energy equation (i.e. for compressible flow calculations), temperature was additionally prescribed at the fan inlet and discharge. The switch to time dependency did not necessitate any change in boundary conditions.

Convergence Criteria

Although FLUENT by default reports the complete field residual errors, the most useful and indicative means found to gauge convergence was to examine the calculated pressure field at inlet. These values were recorded against iterations to see if they settled: once constant, the solution was deemed converged. The two L3R computer models are now discussed in turn.

5.2.1 Single Passage L3R *Bladed* Model Runs

This section describes the runs completed using the L3R bladed model.

Solution strategy

The FLUENT documentation warns that the program's SIMPLE (Semi-Implicit-Pressure-Linked-Equations) solver employed is not entirely suitable for solving highly swirling flows or flows with non-linear pressure gradients. Unfortunately it is in the nature of centrifugal compressors to operate within both of these regimes and it was therefore anticipated that some stability problems would occur.

The adopted strategy was to run the model at a duty that would minimise the adverse pressure gradients that were expected to be detrimental to stability. It involved the application of flow boundaries representative of the high-flow/low-pressure operating regime of the fan, and hence making the convective momentum terms outweigh the diminished pressure-gradient terms. In this way the model would initially be of a fan operating without any system resistance, then with prescribed step decrements in inlet flow velocity, the fan would develop higher and higher pressures finally reaching the stall condition sought. It was thought that this approach of steadily increasing the pressure gradient would have a beneficial effect on stability. In practice however, this approach did not overcome the numerical instabilities and after a series of exploratory runs the model was abandoned. Despite these disappointing results, the attempts are documented here for completeness.

5.2.1a Model Set-up

Maximum flow conditions were prescribed to the preliminary CFD model runs i.e. zero fan static pressure rise. The coriolis and centrifugal body forces were set to model the impeller rotating at 1118 rpm, for it was at this velocity that the experimental flow measurements were taken.

Non-slip boundaries, rather than slip boundaries that are normally prescribed for inviscid flow, were used on the blade, hub and shroud surfaces. This seemingly ill-prescribed boundary set was acceptable as the influence of these boundaries on the inviscid flow field was uncoupled by a prescribed low (negligible) constant laminar viscosity of 1×10^{-15} kg/msec. Checks carried out, before impeller model implementation, on parallel wall test cases confirmed that this uncoupling did indeed occur.

5.2.1(b) Results

After a long series of attempts to gain an inviscid flow solution, the model was abandoned. A variety of solution parameters were used together with different flow solutions, but in all cases the model failed to properly converge. These runs are tabulated and described in Appendix B.

5.2.2 Single Passage Bladeless Model Runs

The results of the bladeless model computer runs of the L3R impeller are reported and analysed here.

FLUENT allows the user some control over the solution algorithm with options that include changing the iterative 'relaxation' factors and adjusting the number of computational 'sweeps'. However, even after optimising these parameters the solver became unstable when attempting to model at impeller design conditions. To overcome this it was decided to solve the equations using a series of steps in impeller rotational speeds (this was not tried on the first model due to the expected large computational effort needed for the densely meshed domain). At first the fan rotational speed was set to 10% of the experimental value. Once a stable solution was found, the speed was increased by a small increment and the process repeated until the full test speed of 1118 rpm was attained. Each preceding solution acted as the iterative starting point for the next step with further increments in rotational speeds only applied after the user was convinced that the equations had fully converged. In this way the iterative solver did not encounter any of the large incremental changes in variables found when starting from the initial guessed field and then attempting to solve the problem in one large step. In physical terms this approach was equivalent to moving the fan operating point gently up a system resistance line. Rotational speeds of 10%, 30%, 50%, 75% and 100% of the impeller test speed were used.

5.2.2(a) No Rotation

Having already encountered stability problems with the preceding L3R bladed model, it was decided that some preliminary investigations into stability should be completed. Of particular interest was the solver performance in the absence of the destabilising effects of high pressure gradients and swirl. Consequently this model was run without rotation and the residuals noted for future reference. As the problem

had neither the swirl or the pressure gradients found in turbomachines, it was relatively easy to solve with no convergence problems encountered. The recorded residuals were used for reference in further runs to help define convergence. Instead of zero inlet flow corresponding to no rotation, a flow rate representing 10% of design was prescribed. The model yielded a stable solution with the following error residuals after only 500 iterations.

Table 5.2 Residual Values for Runs with no Rotation

Model Name(s)	Pressure Residual	U-Velocity Residual	V-Velocity Residual	W-Velocity Residual
NAB9-NAB11	3×10^{-3}	1×10^{-2}	3×10^{-3}	7×10^{-4}

5.2.2(b) Steps towards a full speed solution of the impeller flow at design conditions

The inlet volume flow rate and the body forces corresponding to 10% rotation were applied to the model. With a small number of computational cells, the program could run interactively at reasonable speeds. A numerically stable solution strategy was quickly found: a series of batch runs were completed with the results regularly examined for signs of convergence. Six batch runs were required before the problem was deemed converged for the 10% flow rate. Corresponding filenames for these runs, and the others that follow, are all prefixed with NAB and detailed in Appendix C.

Similar batch runs, as above, were completed with further increases in rotation speed. Again, for every few thousand iterations, the program output was examined. Interestingly all of the computer runs showed similar error residual and variable history characteristics, apart from a small increase in pressure residual. Examination of Table 5.3 shows the recorded residual values and how they responded to steps in speed.

Table 5.3 Final Residuals of different speed runs

% Of Test Speed	Pressure Residual	U-Velocity Residual	V-Velocity Residual	W-Velocity Residual	Number of Iterations
10%	0.8×10^{-2}	5×10^{-4}	1.5×10^{-3}	5×10^{-4}	6400
30%	2.0×10^{-2}	4×10^{-4}	1.3×10^{-3}	5×10^{-4}	3200
50%	3.3×10^{-2}	4×10^{-4}	1.4×10^{-3}	5×10^{-4}	3300
75%	5.0×10^{-2}	4×10^{-4}	1.3×10^{-3}	5×10^{-4}	4000
100%	6.3×10^{-2}	4×10^{-4}	1.0×10^{-3}	4×10^{-4}	4000

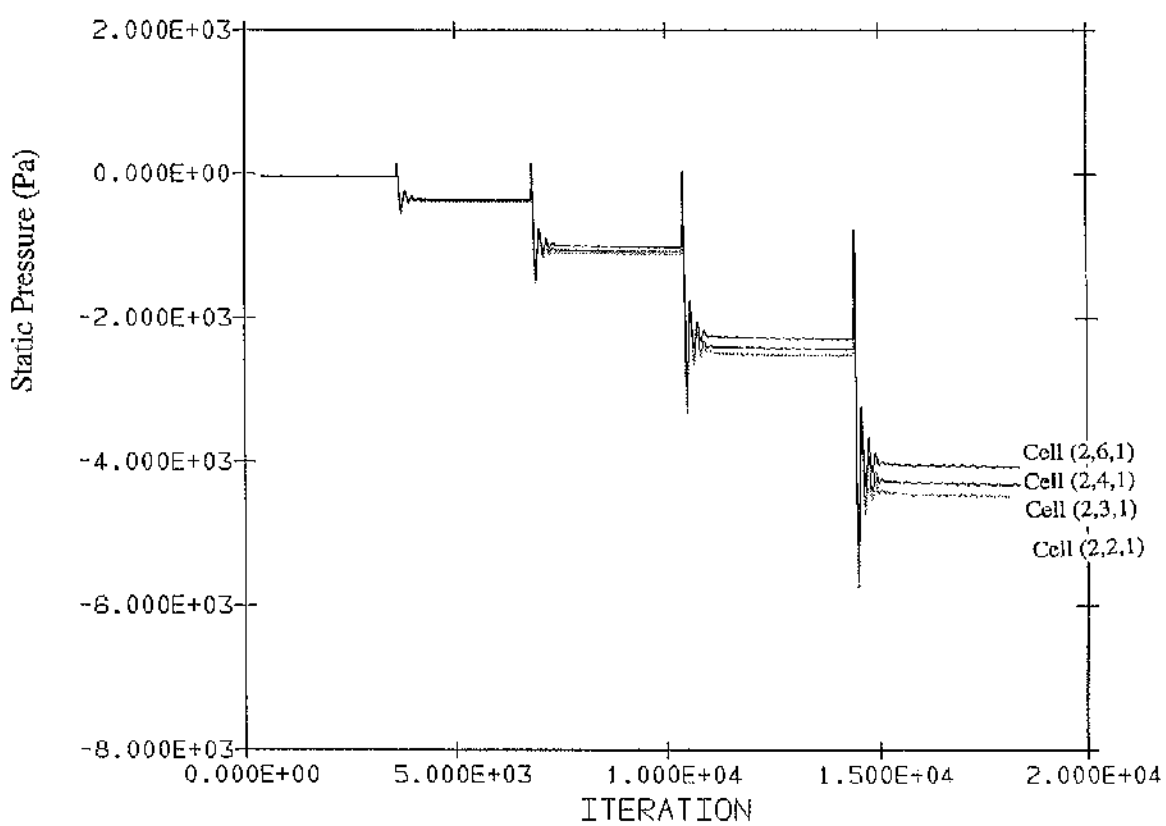


Figure 5.10 Variation of inlet pressure with steps in fan speed

Likewise the recorded pressures at the inlet duct shown in Figure 5.10 demonstrate how the solver seemed unaffected by the fan rotational speed. Together with the experience gained from the previous L3R 'bladed' and the PHOENICS Mizuki investigations, one may conclude that the solution parameters may need tuning for modelling different fan system resistances, but are best kept constant for changes in speed.

5.2.2(c) Prediction of fan performance

The CFD boundary conditions chosen corresponded to the measuring planes used in experiment and therefore allow the calculation of fan performance.

Firstly we must define what is meant here by the term 'fan pressure rise'.

The following definitions are inherent within BS848:Part 1:1980

$$\begin{aligned}\text{Fan Total Pressure, } P_{tF} &= P_{t2} - P_{t1} \\ &= P_{v2} - P_{t1} \text{ (as zero discharge gauge static pressure)}\end{aligned}$$

$$\begin{aligned}\text{Fan Static Pressure, } P_{sF} &= P_{tF} - P_{v2} \\ &= P_{v2} - P_{t1} - P_{v2} \\ &= -P_{t1}\end{aligned}$$

where $()_2$ denotes the conditions at impeller discharge
 $()_1$ denotes the conditions at impeller inlet
 $()_v$ denotes velocity head
 $()_t$ denotes total pressure

Therefore, for the test configuration chosen, to calculate the fan static pressure only requires the measurement of the fan total pressure, $-P_{t1}$ at inlet. For the CFD model this required some special averaging as the prescribed inlet pressure was not uniform as per experiment. It is expected that this discrepancy derives from the mesh distortion near the inlet duct centreline. Here, due to the need to stick to a structured mesh, the cells nearest the duct centreline had to incorporate a small inside radius. If this was not done, the mesh would have been degenerate with these cells having 6 rather than the necessary 8 nodes. The Fluent solver would reject such a mesh.

From the mesh inlet plane an earth-frame-relative velocity head and a static pressure may be extracted. The absolute inlet velocity head, needed for calculating the fan total pressure rise, was calculated from the prescribed axial inlet velocity and density. Due to the inlet pressure field asymmetry an averaging technique was necessary to calculate a corresponding inlet static pressure. For this the 5×5 inlet computational mesh values were mass flow weighted.

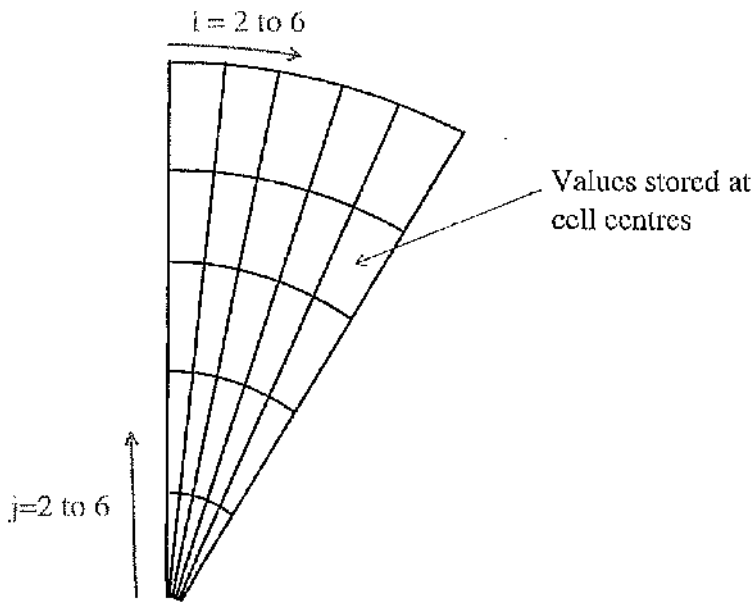


Figure 5.11 Inlet Finite Volume Cell Structure

The inlet pressure was calculated using the following expression

$$p = \sum_{j=2}^6 w_j \sum_{i=2}^6 \frac{1}{5} p_{i,j}$$

where i and j refer to the cell co-ordinates in Figure 5.11
and the weighting w_j is given by

$$w_j = \frac{r_j^2 - r_{j-1}^2}{r_6^2}$$

where r_j is the outer radius of cells with ordinate j .

i.e.

Table 5.4 Weighting Applied

radius (m)	j	weighting, w_j
0.592	6	0.36
0.4736	5	0.28
0.3552	4	0.20
0.1184	3	0.12
0.005	2	0.04
total =		<u>1.00</u>

This weighting technique was applied to the computer solutions calculated earlier. The results are given in Table 5.5 below.

Table 5.5 Predicted Fan Static Pressure Rise

% of Actual impeller test speed	Mass Weighted inlet static pressure (Pa)	Prescribed axial inlet velocity (ms ⁻¹)	Calculated Fan Static Pressure $P_{SF'}$ (Pa)	Experimental Fan Static Pressure P_{SF} (Pa)	Ratio of experimental to CFD predicted pressures $P_{SF}/P_{SF'}$
10 %	-42.3	2.104	39.6	24	0.606
30 %	-381	6.267	357	212	0.594
50 %	-1060	10.441	995	589	0.591
75 %	-2380	15.664	2233	1325	0.593
100 %	-4230	20.886	3968	2356	0.594

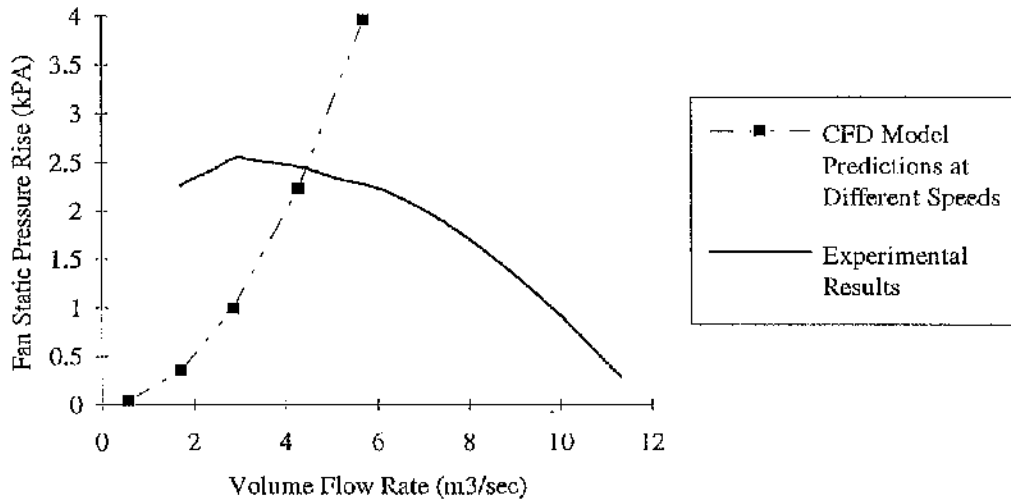


Figure 5.12 Path of CFD Model Variable Speed Runs

As can be seen from Table 5.5 the ratios of calculated fan static pressure rise to those found in experiment are remarkably consistent. This ratio may be thought of as a kind of efficiency, with the computational results representing the ideal performance. With this we can gain further assurance of the computation model accuracy, as in reality the fan speed has very little effect on fan efficiency at low Mach numbers.

It should be re-iterated here that this inviscid model was in no way expected to predict the overall fan performance. Its isothermal, incompressible and inviscid formulation make it unable to predict losses. This is apparent in Figure 5.12 where the results from the CFD model are plotted with the actual aerodynamic test results. The point of maximum pressure predicted by the CFD model should coincide with the equivalent experimental pressure at the same volume flow rate. It is expected that proper modelling of flow turbulence would reduce the discrepancy.

5.2.2(d) Steady State Pressure/Volume Excursions

The inlet flow rate was varied to model different operating points on the fan characteristic. Conditions representing peak efficiency, high flow rate, stall and deep stall were all modelled. The predicted fan static pressures rises, analysed as in the previous section, did not follow or even shadow the fan characteristic curve. Indeed the fan static pressure rise predicted was almost constant. These runs are plotted below.

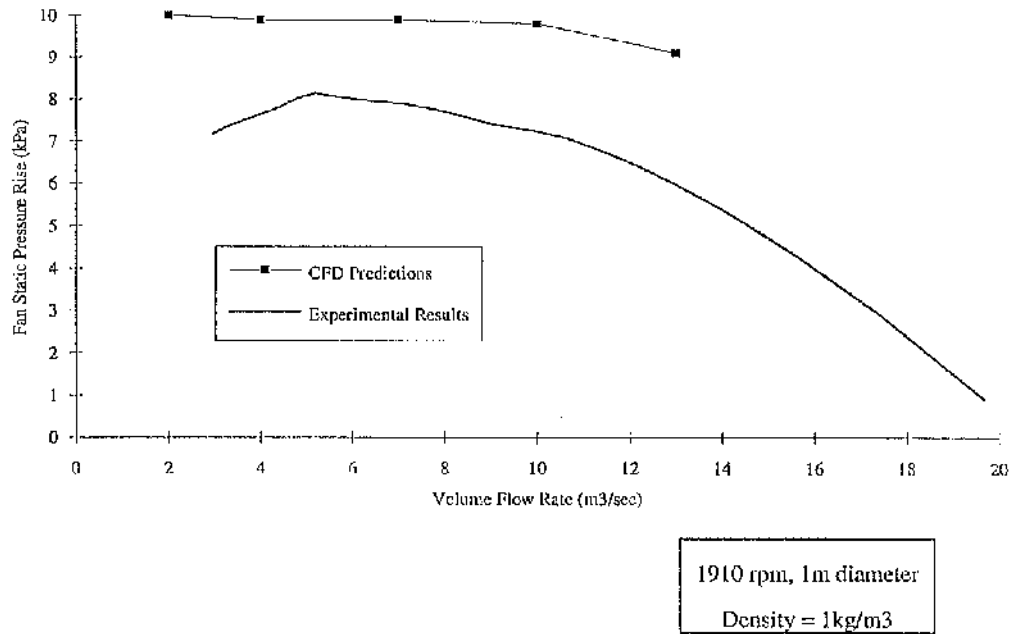


Figure 5.13 Comparison of Inviscid CFD Predictions with Experiment

The most apparent phenomena seen in the predicted velocity fields is the inception and subsequent growth of large recirculating regions at flow rates corresponding to stall. These can be seen in the velocity vector plots of Figures 5.14 to 5.18.

The nature of these stall cells is not yet fully understood but we can deduce that they were not generated by viscous forces, as the flow model was completely inviscid; or by some thermal energy transfer, as the model equations were isothermal.

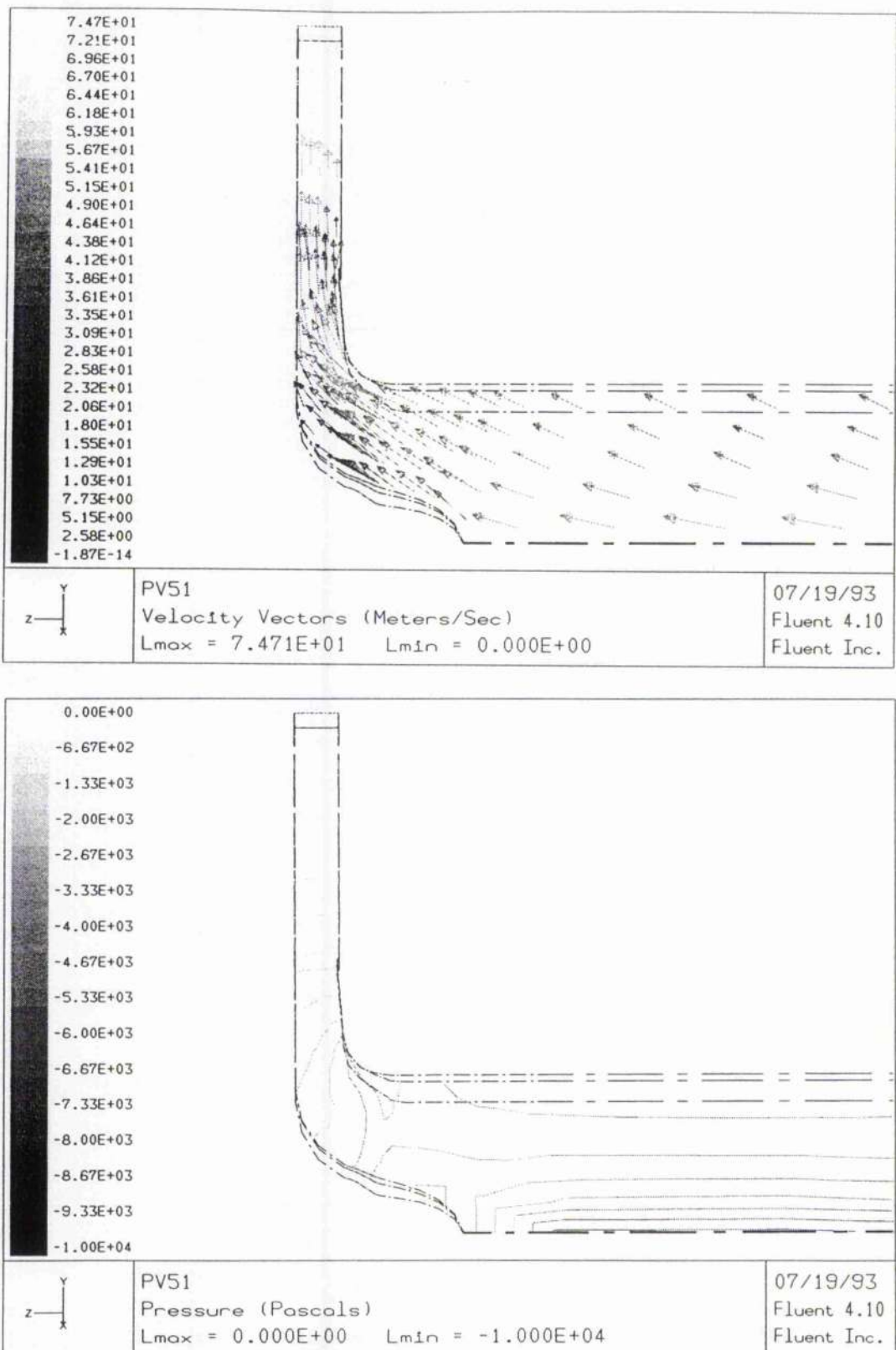


Figure 5.5 High Volume Flow

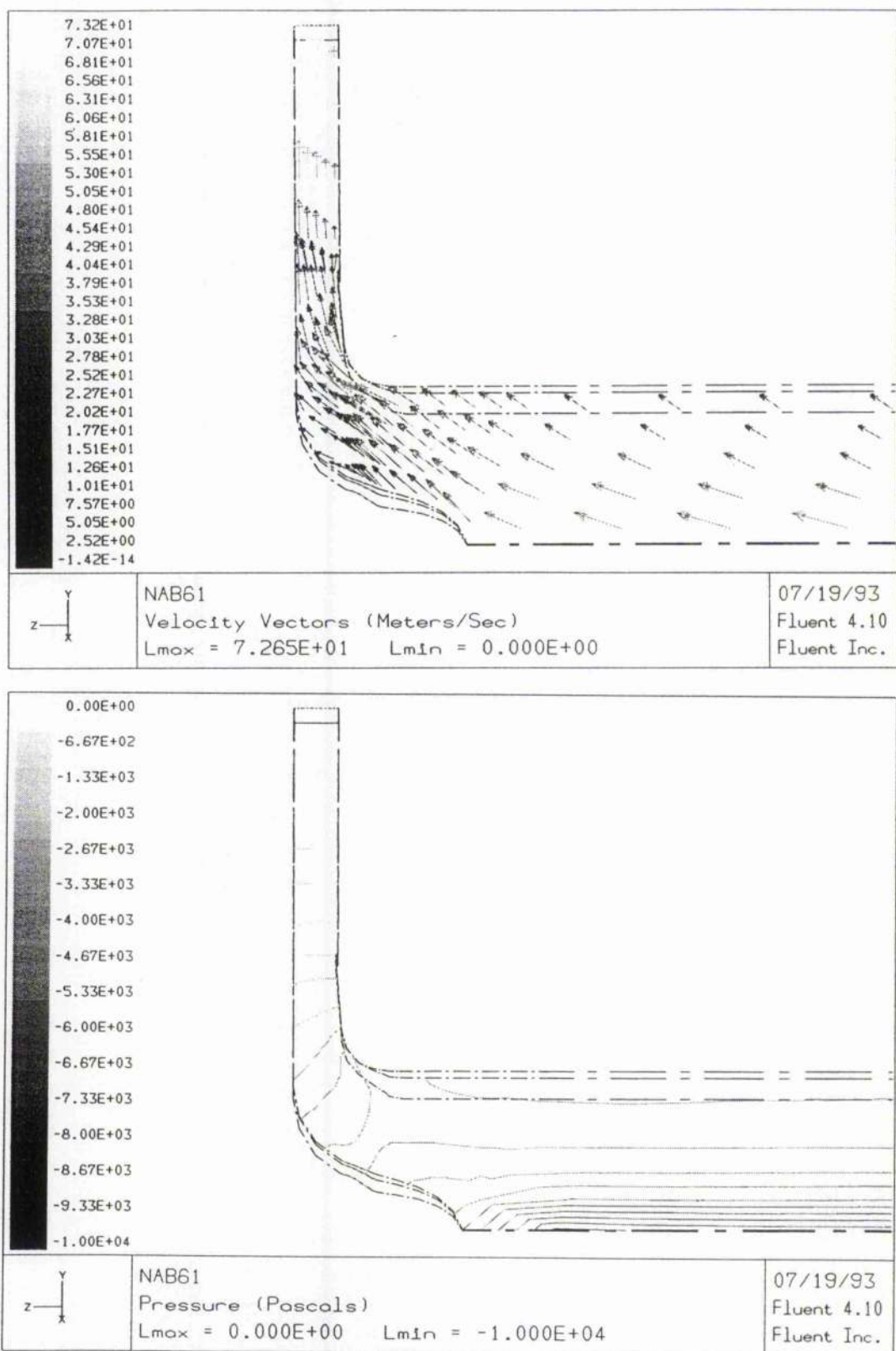


Figure 5.6 Design Flow

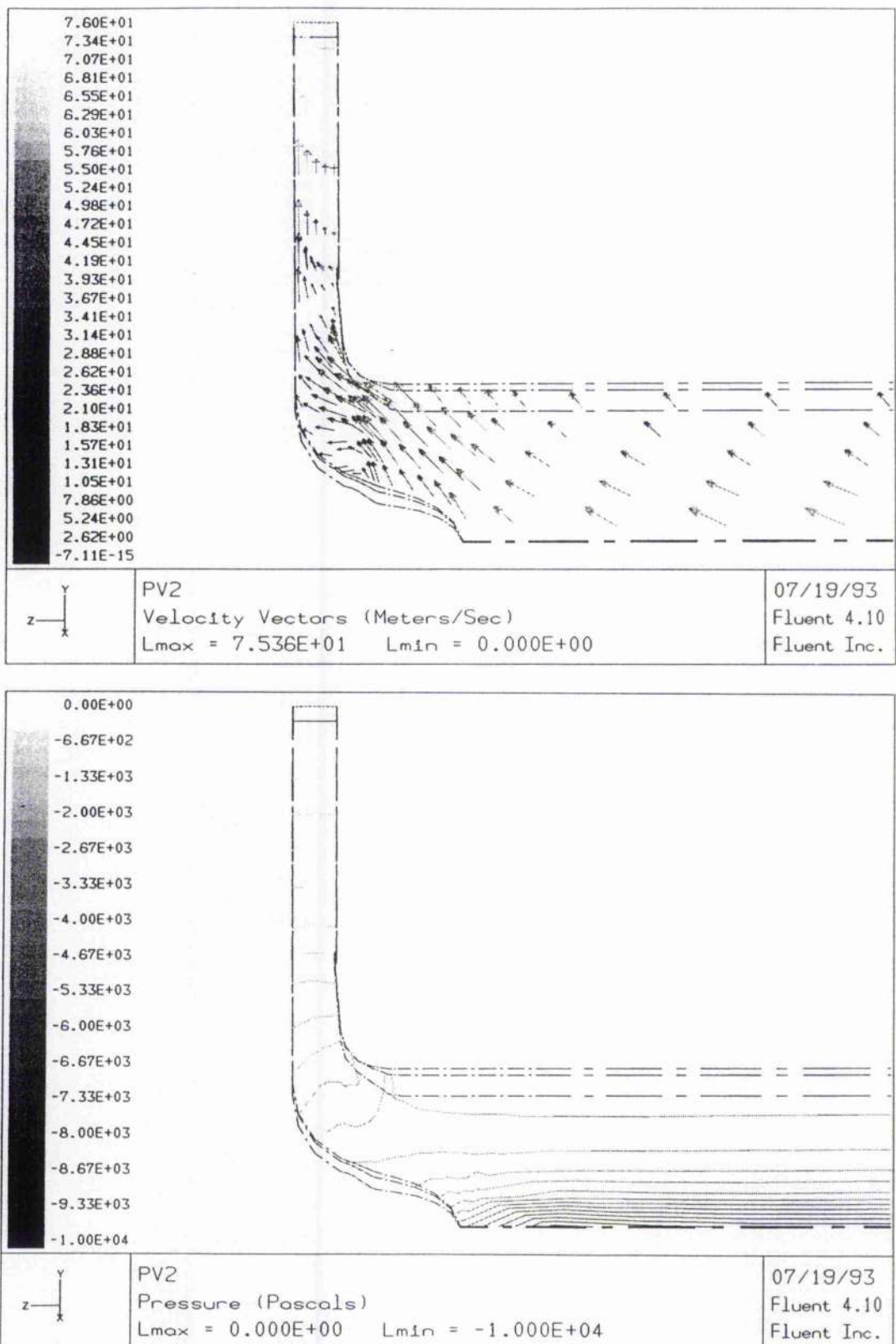


Figure 5.7 Peak Efficiency

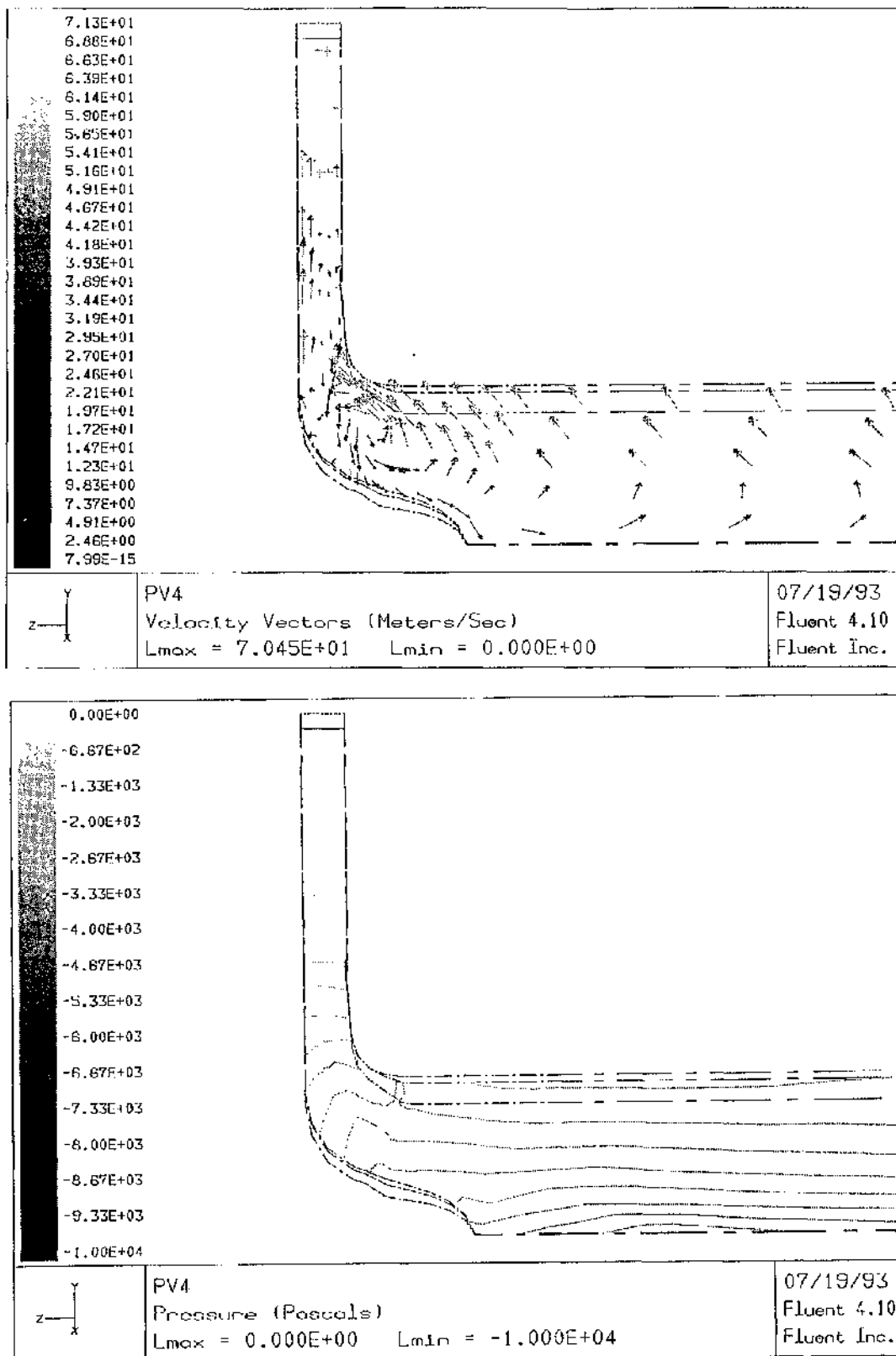


Figure 5.8 Stalled Flow

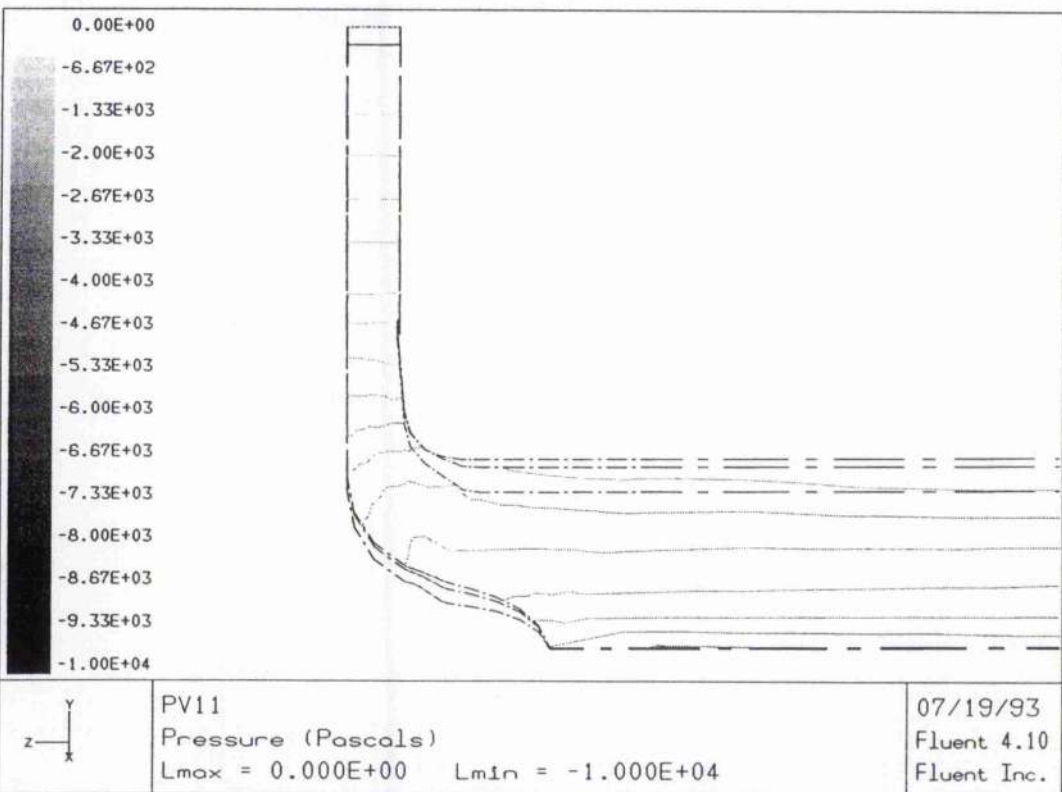
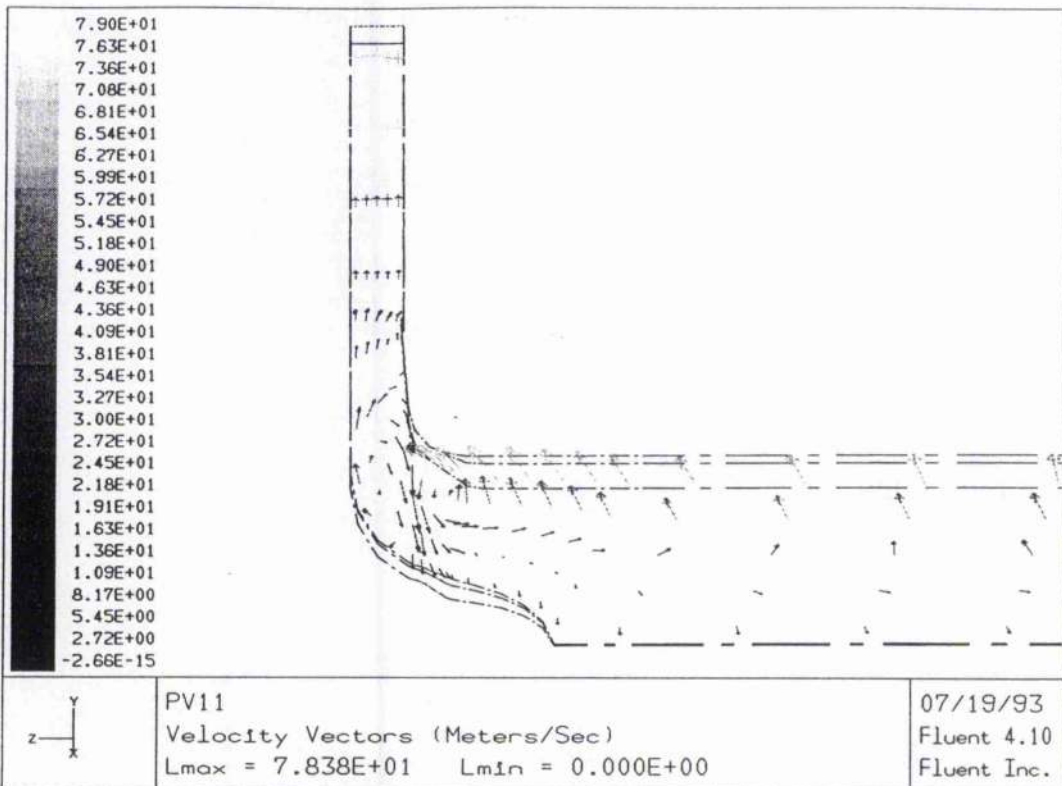


Figure 5.9 Highly Stalled Flow

5.2.2(e) Numerical Convergence

The residuals for the above runs are tabulated below, together with the number of iterations completed at each stage. For all cases the number of computational sweeps and the relaxation parameters were unchanged.

Table 5.6 Pressure/Volume Excursion Runs: Error Residuals

Run Name	Description of Flow	No. of iters	Pressure Residual	U-Velocity Residual	V-Velocity Residual	W-Velocity Residual
PV51	High	3000	1.2×10^{-1}	1.2×10^{-3}	2.6×10^{-3}	7.7×10^{-4}
NAB61	Design	4000	6.3×10^{-2}	4.2×10^{-4}	1.0×10^{-3}	3.8×10^{-4}
PV2	Peak Efficiency	3000	5.4×10^{-2}	4.6×10^{-4}	1.4×10^{-3}	4.1×10^{-4}
PV4	Stalled Flow	2000	2.1×10^{-1}	1.6×10^{-3}	5.5×10^{-3}	3.7×10^{-3}
PV11	Highly Stalled	2000	1.3×10^{-1}	8.1×10^{-4}	5.1×10^{-3}	2.2×10^{-3}

There is a noticeable trend of increased residual as we move away from the fan design conditions. This was noticed as well in the Mizuki impeller investigation.

5.2.2(f) Time-Dependent Runs

To conclude the investigations into the flow within the L3R fan, time dependent runs were completed, for both incompressible and compressible flow. The main interest centred about predicting some of the stall cell unsteadiness shown by Bosman [1984].

The series of computer simulations were troubled by numerical divergence, with time step size shown to be the main stability criterion. For incompressible runs the solver became unstable for a time step, Δt below 0.04 seconds. Alternatively, for compressible flow the solver became unstable for time steps of $0.005 > \Delta t > 1 \times 10^{-6}$. For the larger time steps, in both incompressible and compressible cases, no differences in solution were predicted. The results from each of these runs are compared below. Predictions are shown for the highly stalled condition at 20% of design flow. As may been seen, the solutions are consistent with only minor differences in pressure.

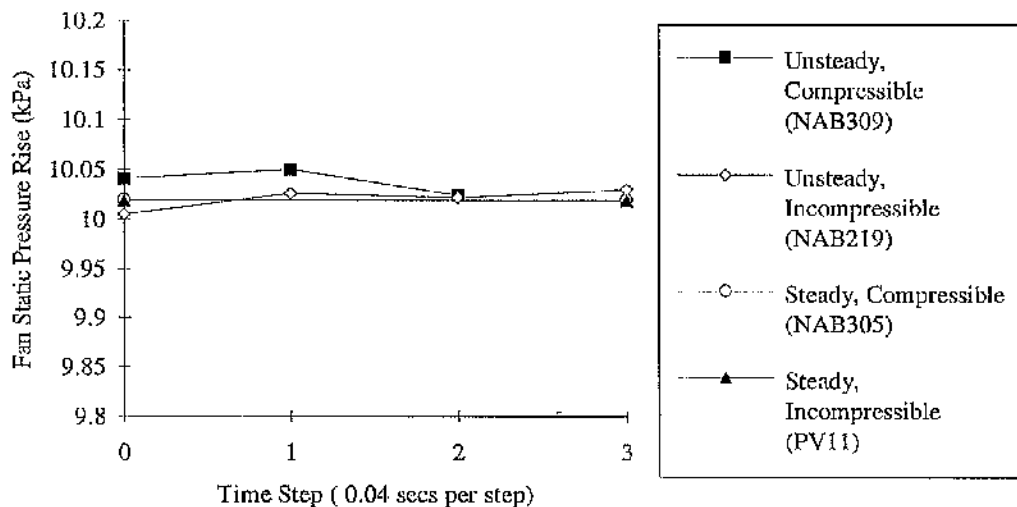


Figure 5.19 Temporal and Compressibility Effects on Solution

For very small time steps ($\Delta t = 1 \times 10^{-7}$ sec) the compressible solutions showed some fluctuations in inlet pressure (See Figure 5.20). These were too large to be attributed to numerical perturbations and are shown below in terms of fan static pressure rise. To investigate this further would have required further time steps. As only 4-5 could be completed overnight on an IBM RS6000 to continue the investigation to cover a reasonable time interval would have been impractical and is left here as an item for further work when more powerful computers become available. A detailed description of all unsteady runs is given in Appendix C.

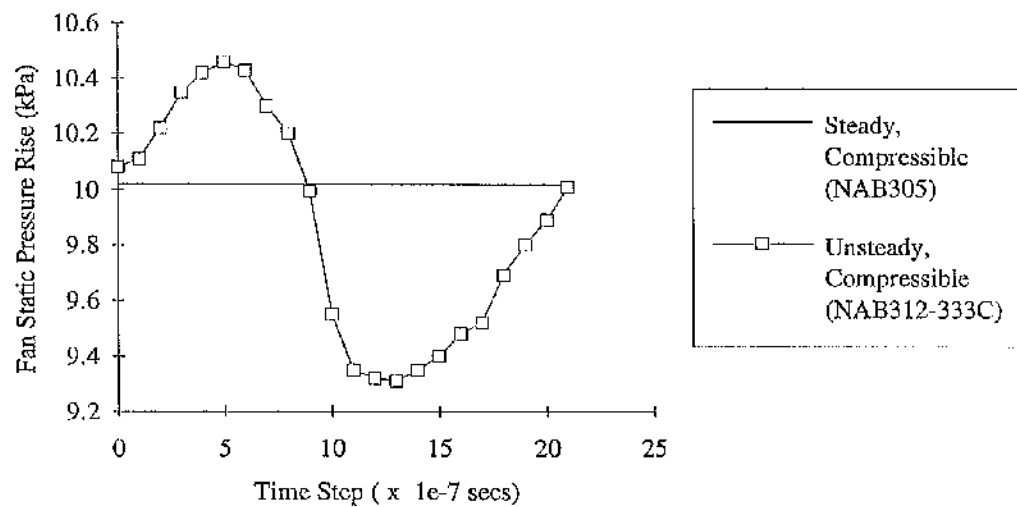


Figure 5.20 Small Time Step, Compressible Transient Performance Fluctuations

5.3 Conclusions

A radial bladed fan has been aerodynamically tested with an assortment of discharge configurations. Of these the vaneless diffuser arrangement has been modelled using FLUENT with two different computational meshes. The main conclusions from this chapter are given below:

1. The L3R impeller aerodynamic performance has been shown to be fairly insensitive to discharge configuration.
2. Some tuning of solution variables is necessary when using the SIMPLE solution algorithm for flows at different system resistances.
3. The stability of the SIMPLE algorithm employed by FLUENT is very sensitive to cell shape.
4. Consistent CFD results were obtained over a range of fan speeds.
5. Large areas of flow recirculation were predicted at operating ranges shown by experiment to be in stall. The CFD model was able to predict the onset of rotating stall.
6. No flow unsteadiness was predicted, apart from at very high frequencies, whilst operating in stall. Such oscillations were predicted using a time stepping scheme by Bosman and Ahrabian [1984] to which some parallel between the overall flow structures predicted may be drawn. However, this part of the work has been inconclusive as more computational power is required to model an elapsed time period of meaningful length.
7. Contrary to FLUENT's documentation, the solver has been shown to be sensitive to time step size.

CHAPTER SIX

The ZM1 Centrifugal Fan

The final geometry modelled was a high specific speed centrifugal fan called the ZM1. Characteristic of this particular fan are the conical side-plate and large span aerofoil blade enabling operation at high volume duties normally associated with fans of mixed flow design. For this kind of fan the impeller flow is no longer restrained to long radial blade passages, but is aerodynamically 'coaxed' by aerofoil sections operating virtually in isolation. The need to properly model the flow around the blade is highlighted with an investigation into the effect of mesh density and quality on predicted flow. The results illustrate not only a lack of resolution in, but the prediction of completely different flow states: for example the fan performing like a crude turbine even when proper compression boundary conditions were incorporated.

This chapter is split into two sections. The first is dedicated to models with 'sparsely meshed' domains. These models were built initially in the hope that once successful results were obtained, the domains could be cyclically replicated to form a model representing the complete impeller wheel. With such a mesh it was hoped to examine rotating stall and the unsteady inlet vortex. Therefore it was a prime concern to keep the number of cells on the single blade passage model to a minimum such that the full impeller mesh would be of manageable size (below 100,000 elements). These 'sparsely meshed' models were of comparable dimensions to the earlier inviscid models and it was initially thought a formality to prove the suitability of the representation, given the earlier successes. As will be shown, these representations proved disappointingly unsuitable and consequently no multi-blade channel models were attempted.

The latter half of this chapter deals with how the author overcame some of these difficulties by constructing a much more refined mesh and invoking viscosity. Reasons for the poor results with the 'sparsely meshed' models are given.

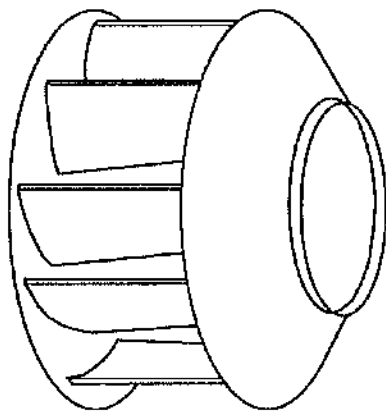


Figure 6.1 Sketch of the ZM1 Centrifugal Impeller

6.1 ZM1 Centrifugal Fan Sparsely Meshed Models

In all, four computational 'sparsely meshed' domains were constructed to examine the flow within the ZM1 impeller. As before, to simplify the applied boundary conditions, a ducted inlet configuration was adopted together with a presumed vaneless annular diffuser. The mesh density of these models , although called 'sparse' here, were similar to those used for the inviscid L3R and Mizuki impeller runs. Investigations utilising much finer meshes, capable of capturing boundary layer flow, follow in the next section.

The differences between the four 'sparsely meshed' models are given below in Table 6.1 with the corresponding computational domains shown in Figure 6.2.

Mesh Designation	Computational Cell Dimensions	Full or Short Length of Inlet Duct Modelled?
ZM1(a)	5×5×21	Full
ZM1(b)	10×10×42	Full
ZM1(c)	5×5×16	Short
ZM1(d)	10×10×32	Short

Table 6.1 ZM1 Centrifugal Fan Inviscid 'Sparsely Meshed' Computational Grids

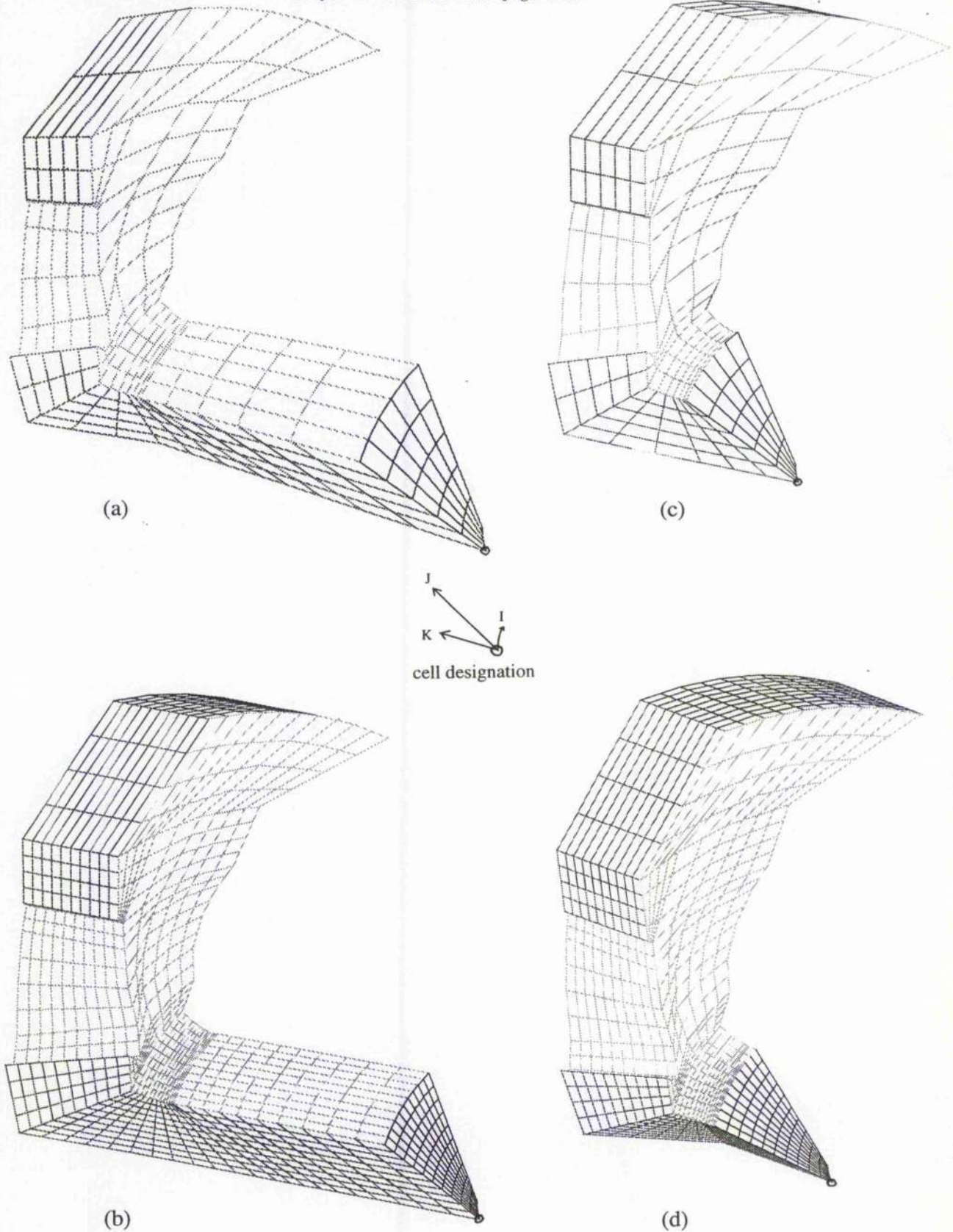


Figure 6.2 Computational 'Sparsely Meshed' Models

To these meshes either a prescribed inlet velocity or inlet total pressure, together with a static discharge pressure, were applied. In all cases an incompressible steady state form of the Euler equations were solved. These computational runs are summarised in APPENDIX D.

6.1.1 The Inviscid Results

The results were scrutinised using the following criteria:

- a. Fan Aerodynamic Performance Predictions
- b. Fan Power Via Blade Pressure Distribution
- c. Fan Power Using The Energy Equation
- d. Fan Power From Angular Momentum
- e. General Flow Distribution

6.1.1(a) Fan Aerodynamic Performance Predictions

As already seen in the previous two chapters, the CFD models formulated here were able to give a prediction of the fan overall aerodynamic performance. Given an inlet volume flow rate and a static discharge pressure an inlet static pressure is predicted. Alternatively, given an inlet total pressure and inlet flow direction with a static discharge pressure, an inlet volume flow rate is predicted. Using both of these choices of boundary conditions it became apparent that there were deficiencies in the flow simulation. These differences could not be attributed to the inability of the inviscid, isothermal, model to account for losses. The discrepancies were far greater, as may be seen in the figure below showing the predicted and actual fan characteristic.

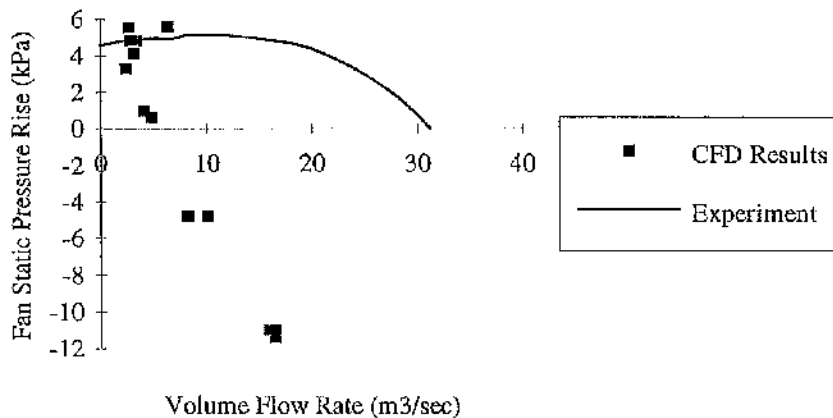
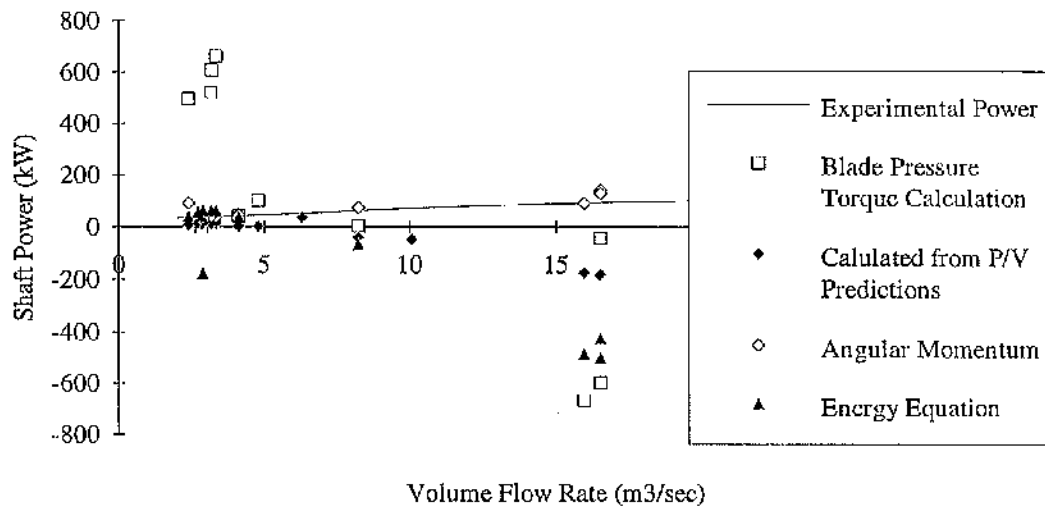


Figure 6.3 Aerodynamic CFD Predictions

At design flow rates all models predict that the fan is acting like a turbine i.e. that instead of a pressure rise there is a drop across the wheel. There is, however, some consistency in the results in that both types of boundary conditions give the same, almost linear, prediction. The CFD results and experiment only coincide at 25% of design flow-rate. Within this operational range the flow would normally exhibit rotating flow, a phenomenon that cannot be predicted with a single blade passage model. We must therefore conclude that the 'sparsely meshed' models are unable to model the flow.

6.1.1(b) Fan Power Via Blade Pressure Distribution

A FORTRAN utility program, called TORQ.FOR, was written to post-process the CFD results by reading in FLUENT 'UNIVERSAL' files. The algorithm summated the elemental cell face blade pressure contributions in order to calculate a torque, and hence evaluate a shaft power. Results are graphically displayed below in Figure 6.4.

*Graph 6.4 Post-Processed Predictions*

The values of shaft power calculated using blade pressure distribution show a negative slope, unlike those measured by experiment which follow a positive gradient. Further comparisons can be made by calculating the fan power from the CFD predicted fan pressure rise and volume flow. Multiplication of these two variables yields a power term and is also plotted on Graph 6.4. This CFD 'P/V' power prediction has also a negative slope; however the gradient is not as steep as the power characteristic calculated from blade pressure.

6.1.1(c) Fan Power Using The Energy Equation

The energy equation, neglecting viscous effects and heat transfer, may be written in the form :

$$\text{Power} = \iint_{\text{Control Surface}} \left(\frac{P}{\rho} + u + \frac{v^2}{2} + g.z \right) \rho \vec{v} \cdot d\vec{A}$$

where P = static pressure (Pa)

ρ = fluid density (kg/m^3)

v = velocity (m/sec)

g = acceleration due to gravity (m/sec^2)

u = internal energy (J/kg)

z = distance from datum level (m)

(The flow control surface was taken to enclose the fan inlet and blade discharge.)

This expression was programmed within another FORTRAN utility called ENERGY.FOR. The results from post-processing the CFD output sets are also shown in Figure 6.4. Again a negative power slope is calculated.

6.1.1(d) Fan Power From Angular Momentum

For steady flow and neglecting gravitational effects, we get the following equation for angular momentum (e.g. Jorgensen 1983).

$$\vec{T} = \iint_{C,S} (\vec{r} \times \vec{v}) \rho \vec{v} \cdot d\vec{A}$$

where \vec{T} = torque (Nm)
 \vec{r} = position vector (m)
 \vec{v} = velocity (m/sec)
 ρ = density (kg/m^3)

We can therefore calculate the shaft power viz.

$$Power = [0 \ 0 \ \omega] \cdot \vec{T}$$

where ω = fan angular speed (rad/sec)

Another FORTRAN utility was written, this time called ANG.FOR. The same CFD output data sets were examined. The resulting predictions are shown plotted on Figure 6.4. These are the closest to the measured experimental power.

6.1.1(e) General Flow Distribution

Blade to Blade velocity plots demonstrate the deficiencies in the flow model. Irrespective of whether the original or a mesh of double the density was used, the flow separated prematurely from the blades as seen in Figures 6.5(a) and 6.5(b). This occurred irrespective of whether velocity or pressure inlet boundaries were applied.

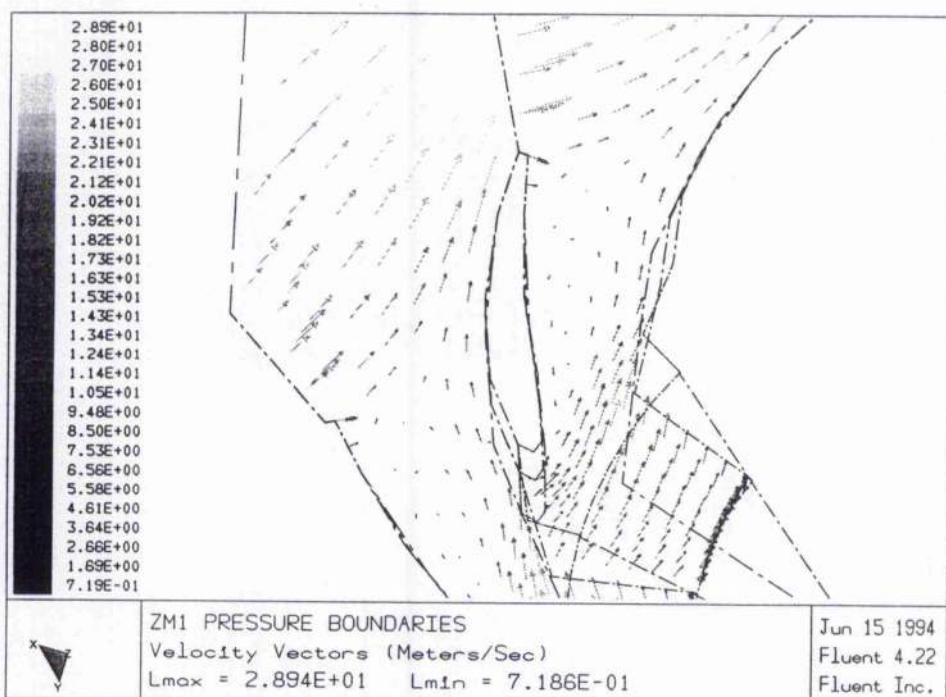


Figure 6.5 (a) Velocity Vectors of Mean Blade-Blade Surface

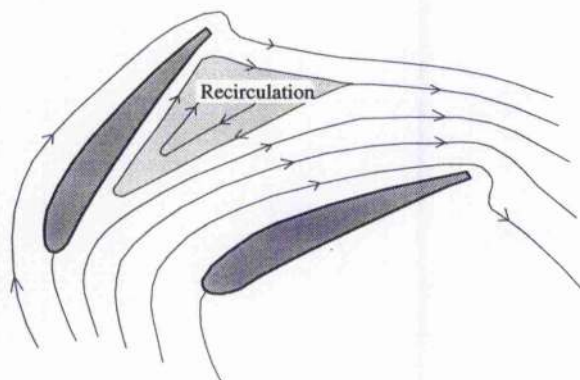


Figure 6.5 (b) Schematic of Mean Blade-Blade Surface Flow

These figures above explain how the impeller model acted like a turbine: to compress the flow the relative velocity vectors should discharge approximately tangent to the blade mean surface, much like 2-D aerofoil flow, with separation near or at the trailing edge. This did not occur in the CFD model.

It should be recalled that Whirlow et al [1981] used the Kutta condition for their similarly meshed centrifugal fan inviscid runs. The need for such application is clear if such coarse meshes are to be used, but if invoked would be very restrictive, for example prohibiting off-design flows where there are large regions of highly separated

flow. The Kutta condition would suppress these tendencies and invalidate the solution at these important extreme operational points.

6.2 ZM1 Viscous Model Runs

To help model a correct discharge angle without the empirical input of the Kutta condition, a viscous representation of the ZM1 impeller flow was constructed. This required an enhanced grid to resolve the viscous near-wall flow together with additional transport equations for the turbulence terms.

6.2.1 Grid Considerations for turbulent flow Models

The full influence of surface friction may only be properly accounted for by using a sufficiently fine grid near wall boundaries. However, several factors restrict the user from constructing the ideal cube-like computation cells with aspect ratios of almost unity and adjacent sides at right angles.

6.2.1(a) Turbulence Model

The Full Reynolds Stress Model (RSM) used here includes a separate empirical wall friction formulation, the so-called log-law, to model the mid-region of the boundary layer. This formulation, together with the addition of a wall treatment equation for wall friction, allows the user to neglect the near-wall very thin viscous dominated layer, the viscous sub-layer region, saving on computational cells. To model the flow adequately, FLUENT recommends that the first cell is placed within the log-law region of the boundary layer such that the non-dimensional distance, y^+ is at a value of

$$25 \leq y^+ \leq 300 \text{ to } 500 \quad (6.1)$$

where

$$y^+ = \frac{yU_\tau}{v} \quad (6.2)$$

$$U_\tau = \sqrt{\frac{1}{2} \gamma \bar{u}^2} \quad (6.3)$$

For a smooth pipe, Kuethe and Chow [1986] give the following empirical equation:

$$\gamma^{-\frac{1}{2}} = -0.4 + 4.00 \log_{10} \left(\text{Re} \cdot \gamma^{\frac{1}{2}} \right) \quad (6.4)$$

where: $y^+ =$ nondimensional distance from wall

$y =$ distance from wall (m)

$U_\tau =$ 'friction velocity' (m/sec)

$\gamma =$ pressure drop coefficient

$\bar{u} =$ mean freestream velocity (m/sec)

$\nu =$ kinematic viscosity (m^2/sec)

$\text{Re} =$ Reynolds Number (based on pipe diameter and \bar{u})

Choosing an 'average' value for y^+ of 200, equations (6.2), (6.3) and (6.4) were solved iteratively using a proprietary mathematics software package. Post-processing of results indicated that these equations were suitable for sizing near wall mesh spacing.

6.2.1 (b) Cell Aspect ratios

The two commercial software packages used to solve the flow equations of motion within this report were both restricted to structured meshes.

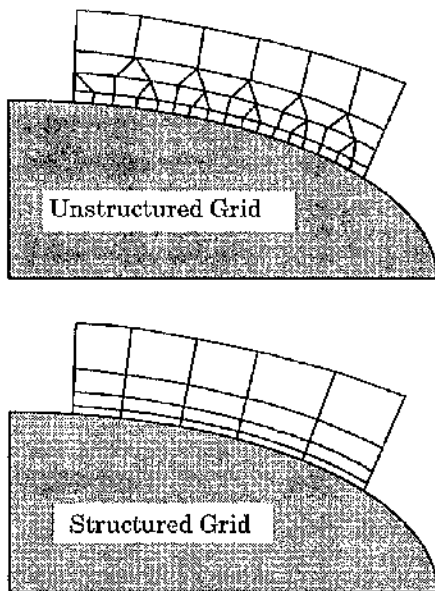


Figure 6.6 Example of a Structured and Unstructured Mesh

Structured grids naturally introduce cells of high aspect ratios, particularly near wall boundaries, as computational mesh dimensions must be conserved in all directions. See Figure 6.6.

With the near wall grid spacing in the normal direction fixed due to boundary layer considerations, the tangential cell length is governed by the individual cell aspect ratios. If they are too high then instabilities and/or inaccuracies are introduced into the solution and high aspect ratio cells are therefore to be avoided. A maximum aspect ratio of 8 was used in this present work. This was compromise between the maximum of 5 recommended by FLUENT [1993] and an effort to reduce the number of cells.

6.2.2(d) Skew cells

Like high aspect ratios, highly skew cells ($45^\circ < \text{internal angles} < 135^\circ$) must also be avoided. Again the limitations of using a structured grid, this time coupled with the required cyclic boundaries, introduces difficulties. Cyclically symmetric cells must be circumferentially matched in position as may be seen in Figure 6.7.

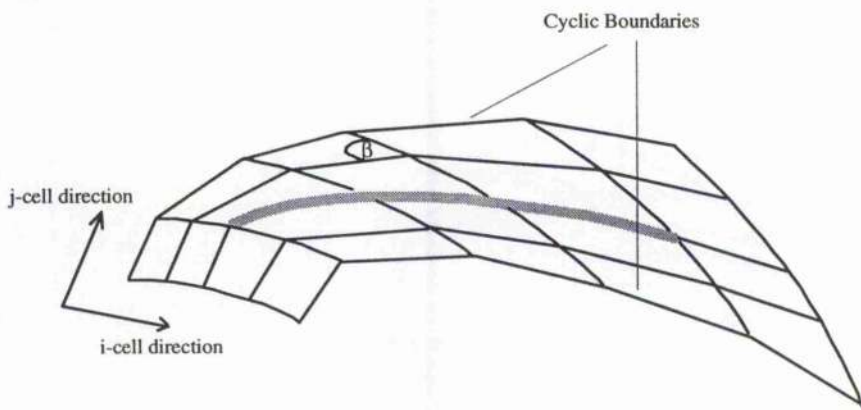


Figure 6.7 Matching Cyclic Cells for a Centrifugal Fan Model

Backward curved blades naturally induce skewed meshes. In the tangential direction, to ensure proper matching of cyclic boundaries, the i-direction cells are restrained to values of constant radius. In the j-direction, to ensure a structured mesh, the cells must generally follow the blade contour. The combination of both these restrictions results in a distorted mesh. For the ZM1 high specific speed fan average values of β were approximately 65° , even well away from additional influence of the blade. See Figure 6.8 below.

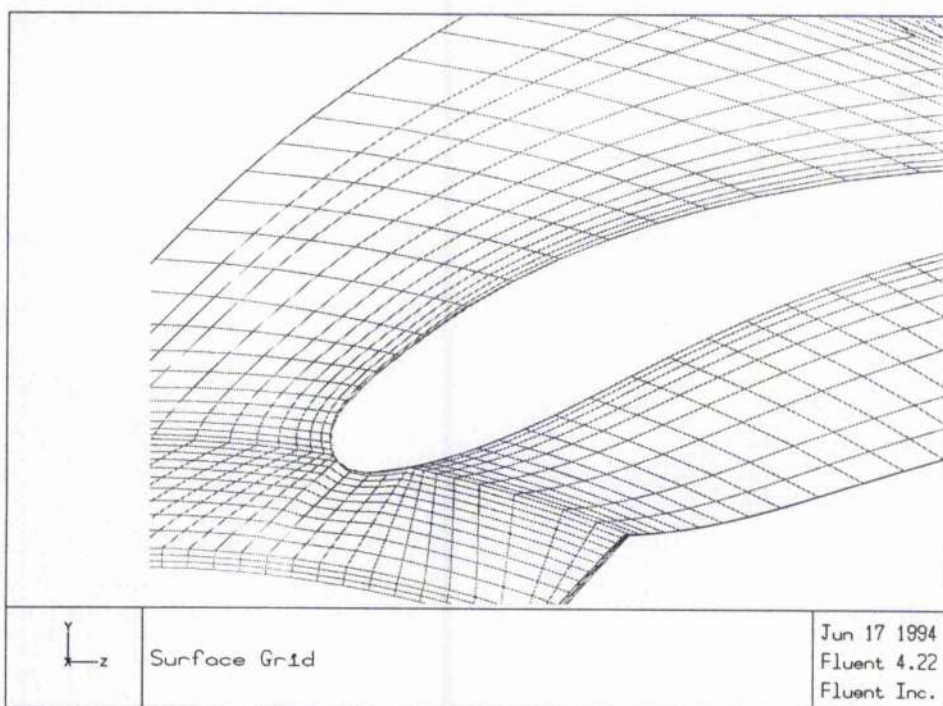


Figure 6.8 Detail of ZM1 Computational Mesh

6.2.1(e) Expansion ratio

As may been seen in Figure 6.8 adjacent cell dimensions differed gradually. This smooth transition was achieved using a geometric series algorithm for grid construction. FLUENT [1993] recommends that such adjacent cells should have expansion ratios of 0.7 to 1.3. In order to reduce the overall number of cells, a compromise upper limit of 1.5 was used.

6.2.2 ZM1 Viscous Model runs: Computational Results and Comparison with Experiment

To ensure stability, results at the full model speed of 1000 rpm were achieved via a series of speed increments together with the specification of laminar viscosity. The final solution field was then used as a iterative start data set for subsequent inviscid and turbulent model investigations. For interest, inviscid runs were completed using this refined mesh.

With such a large number of computational cells, minimising the number of iterations to convergence was a priority. Generally speaking, for most problems, the solution has converged when residuals of order 10^{-4} have been reached. In this case, however, having gained experience in dealing with similar flow models it was decided to stop the solver earlier, that is, once the inlet static pressures had settled and the residuals decreased to order 10^{-3} . This saved on valuable computational effort.

A full list of runs completed are given in Appendix D.

6.2.1 Performance Predictions

The calculated fan performances are displayed below in Figure 6.9. All values are referred to 1910 rpm and a density of 1 kg/m^3 .

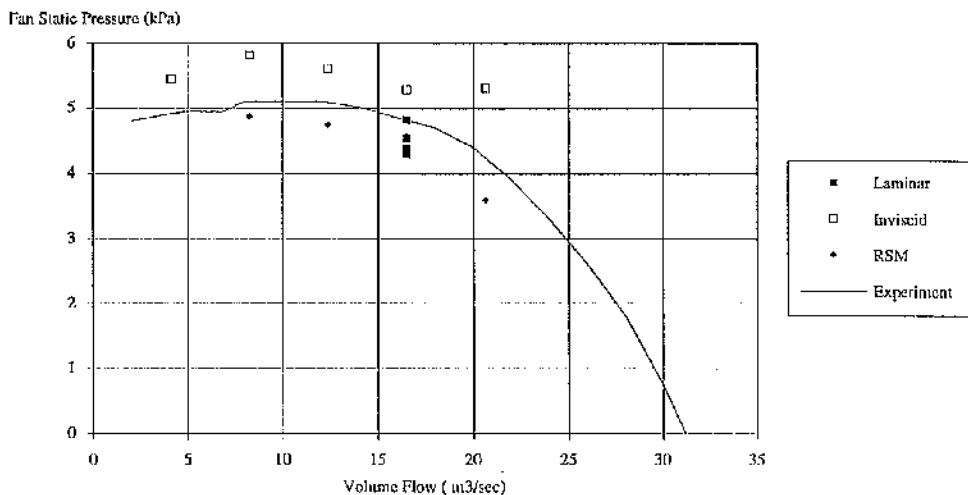


Figure 6.9 Results using a Fine Computational Mesh Suitable for Turbulence Modelling

The inviscid results over-predict pressure and show a slightly negative linear incline. This follows simple Euler Turbine Equation theory for a backward curved machine and confirms that the model is performing satisfactorily. The turbulent viscosity Reynolds Stress Model (RSM) results follow the experimental performance curve well, especially at high flow rates where the effects of friction, which cannot be picked up with an inviscid model, are apparent. However, the model under-predicts the fan pressure rise at all considered flow rates. This fault could be due to the prescribed boundary conditions. Firstly there is the discretionary application of the inlet turbulence quantities, namely the Kinetic Energy of Turbulence and Mixing Length. Tuning of these could go some way in closing the difference, but with no experimental readings any attempts at this would be simply 'tweaking' the results. Secondly, all wall surface roughness parameters were estimated from the assumption of hydraulic smoothness. The unattractive finish of centrifugal fans is far from smooth with weld runs and other surface blemishes making this assumption a little inapt. Finally the clearance between the inlet cone and impeller shroud surface, known as the inlet clearance, was not modelled. The importance of the flow near this region will be highlighted later.

6.2.2 Detailed Flow Predictions

In this section the results from a RSM turbulent model solution of the ZM1 (run MEG72) are compared with experiment. With no detailed flow measurements available for the ZM1 impeller it was decided to compare the salient flow features

with the measurements taken from within a similar impeller i.e. one with comparable specific speed and geometry. The Kjörk and Löfdahl[1989] experimental paper was chosen as it was closest available in terms of fan operational performance and geometry. See Table 6.2.

Kjörk and Löfdahl [1989] Impeller (Experimental)		ZM1 (CFD Model)
No. of Blades	9	12
Type of Blade	Backward curved plate	Backward curved aerofoil
Specific Speed	1780	2375

Table 6.2 Impeller Comparison

where the fan specific speed is defined here as

$$N_s = \frac{N \cdot Q^{\frac{1}{3}}}{\left(\frac{P_{tF}}{\rho}\right)^{\frac{2}{3}}} \quad (6.5)$$

where N_s = Specific Speed (RPM)
 Q = Volume Flow Rate (m^3/sec)
 P_{tF} = Fan Total Pressure Rise (kPa)
 ρ = Inlet Density (kg/m^3)
 N = Fan Speed (RPM)

The Kjörk and Löfdahl[1989] hot wire measurements were unfortunately restricted to the blade passage area and it is to this region that the following discussion is restricted. Reference measuring planes were based on a series of arc plane generations as shown below in Figure 6.9.

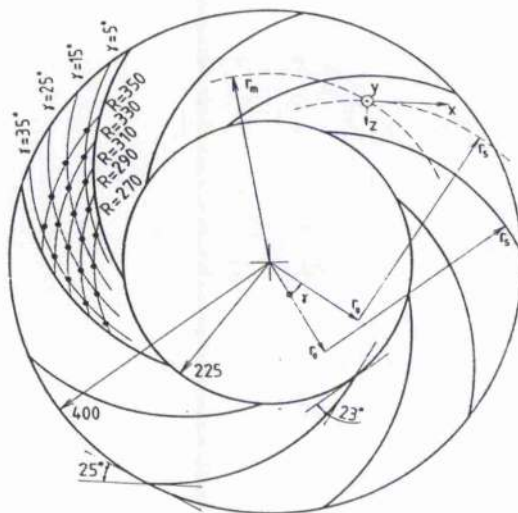


Figure 6.9 Designation of Measuring Planes Used By Kjörk and Löfdahl[1989]

Comparison is directed towards the inner and outer measurement cylindrical surfaces, designated R270 and R350 respectively.

All results are non-dimensionalised as follows:

- Velocities by division of blade tip peripheral speed
- Turbulent Kinetic Energy by division of blade tip peripheral speed squared

6.2.2(a) Comparison of RSM CFD results (Run MEG72) and Kjörk and Löfdahl[1989] experimental measurements

Inlet Velocity Field

Both experimental and measured radial velocity fields may be seen in Figures 6.10(a) and (b).

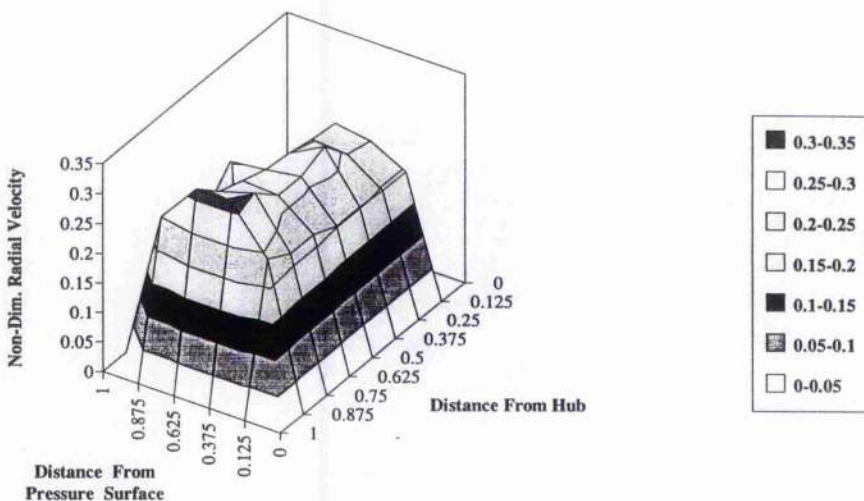


Figure 6.10 (a) Radial Velocity Field Measured by Kjörk and Löfdahl[1989]

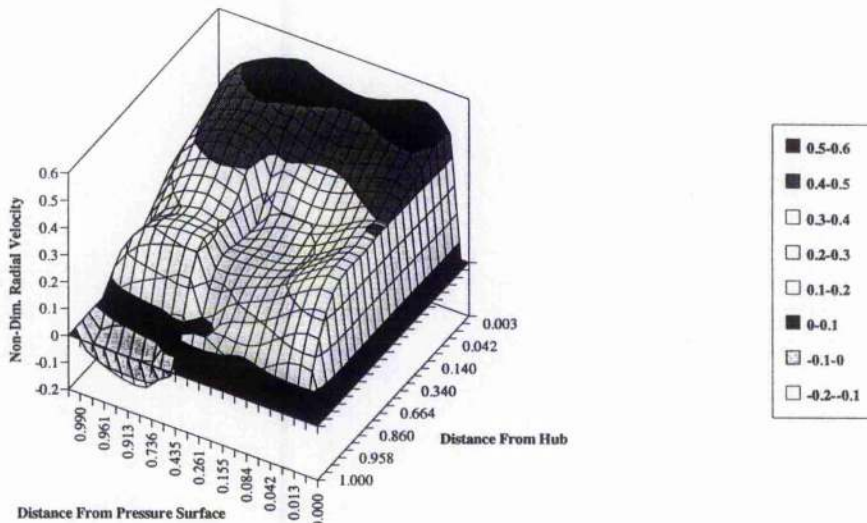


Figure 6.10(b) CFD Reynolds Stress Model Predictions of Radial Velocity for the ZM1 Impeller

The CFD results predict a larger radial velocity near the hub with little bladewise variation. The Kjörk and Löfdahl[1989] measurements however show much larger shroud radial velocities. These may be attributed to the inlet clearance flow 'blowing' into the mainstream together with the generally high velocities associated with the flow, due to rotation and curvature effects, in this region. The latter effect is apparent in the CFD meridional plots where, unaided by the additional clearance flow, there are larger velocities near the inlet ring. Within this region, without the re-energising of the shroud boundary layer, the flow separates resulting in

a drop in local radial velocity. This separation is reflected by the, locally predicted, increased level of Kinetic Energy of Turbulence.

The tangential velocities predicted also suffer because of not modelling the inlet ring clearance flow. See Figure 6.11.

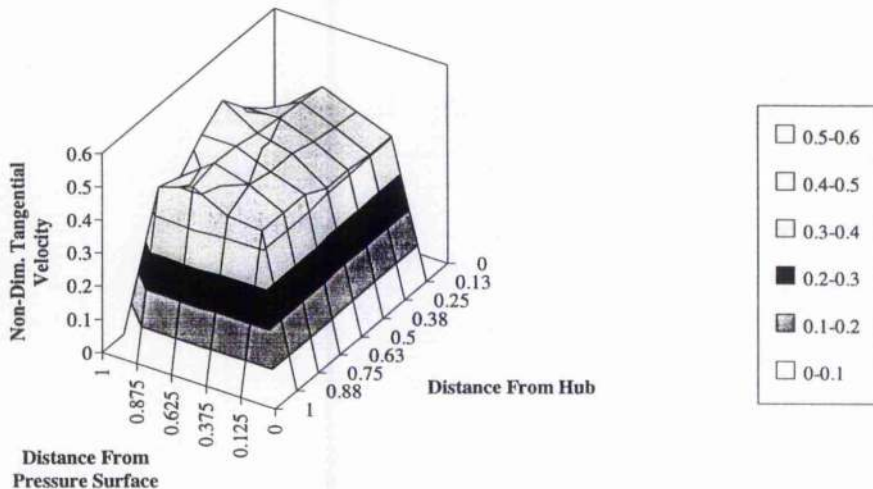


Figure 6.11(a) Tangential Velocity Field Blade Passage Inlet Measured by Kjörk and Löfdahl [1989]

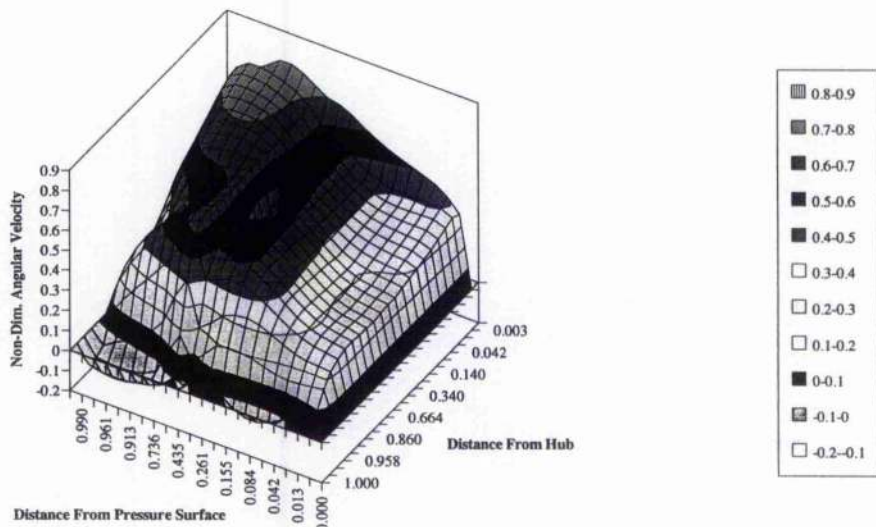


Figure 6.11(b) CFD Reynolds Stress Model Predictions of Angular Velocity at Inlet to the ZM1 Impeller

The CFD model again shows stagnant flow near the shroud with the Kjörk and Löfdahl [1989] measurements showing full flow. In this case, however, this difference may be due to the coarse measurement grid resolution used by Kjörk and Löfdahl

[1989] with the nearest measuring points lying, perhaps, just outside this stagnant region.

The comparative axial velocity fields are very similar, see Figure 6.12(a) and (b)

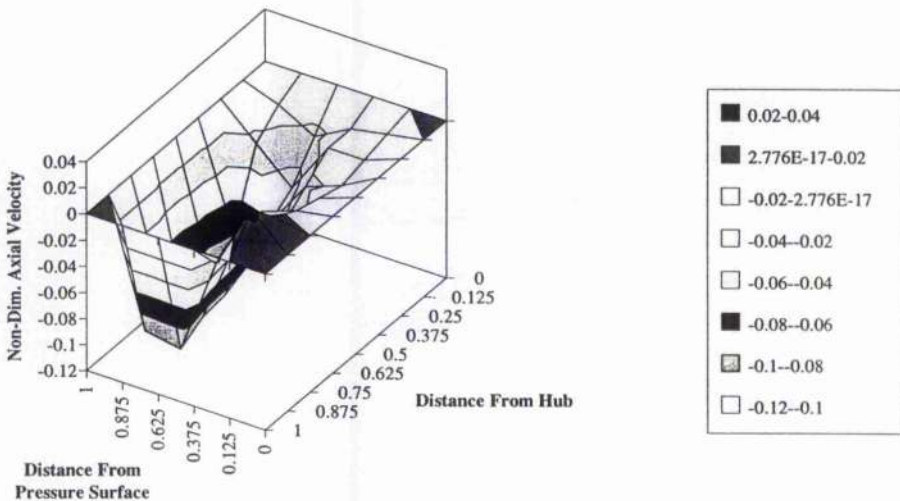


Figure 6.12(a) Axial Velocity Field Blade Passage Inlet Measured by Kjörk and Löfdahl [1989]

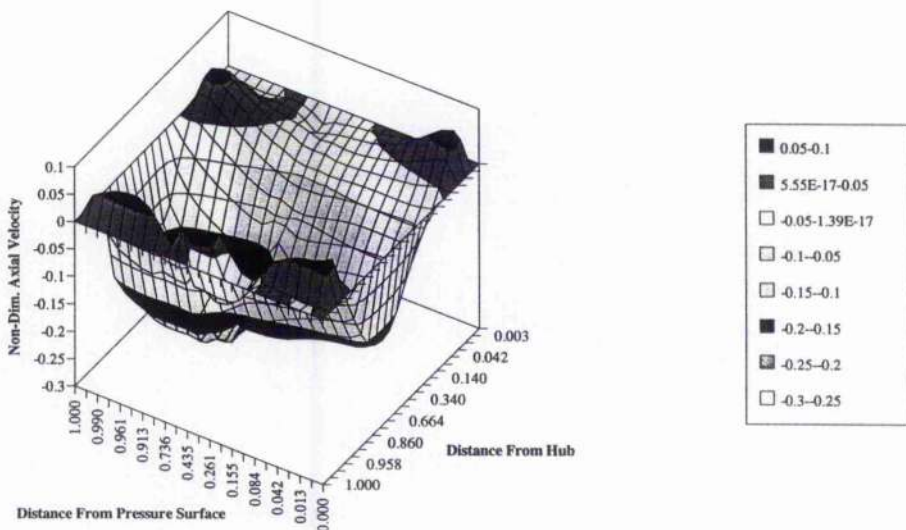


Figure 6.12(b) CFD Reynolds Stress Model Predictions of Axial Velocity at Inlet to the ZM1 Impeller

In addition, both experiment and CFD prediction demonstrate higher suction surface velocities together with some rotation, which appears in the sense as to keep the flow irrotational. See Figure 6.13 below.

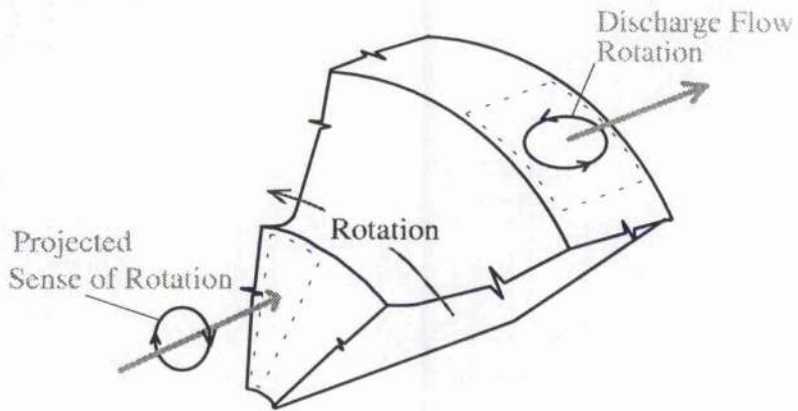


Figure 6.13 Schematic of the Irrotational Nature of Blade Passage Flow.

Inlet Turbulence Quantities

Comparison of the KE values shows that there are some differences between experiment and prediction. See Figures 6.14(a) and (b).

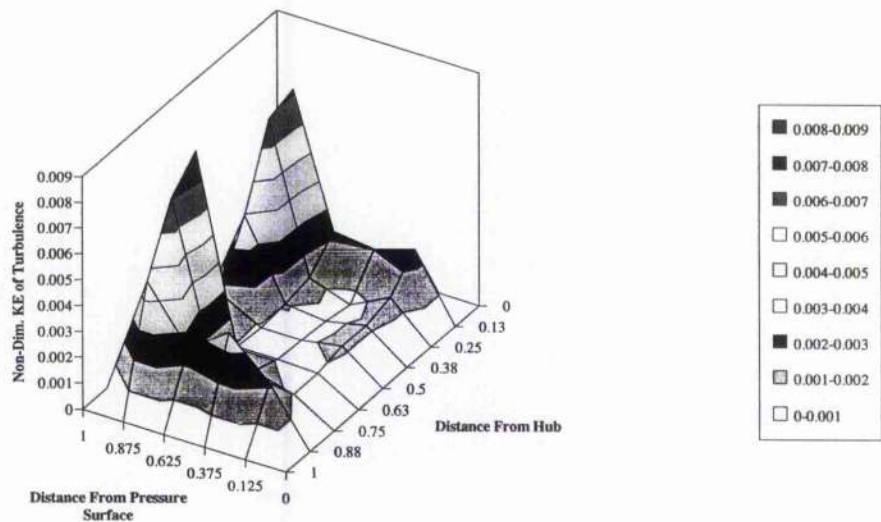


Figure 6.14(a) Kinetic Energy of Turbulence Measured by Kjörk and Löfdahl[1989] at Inlet

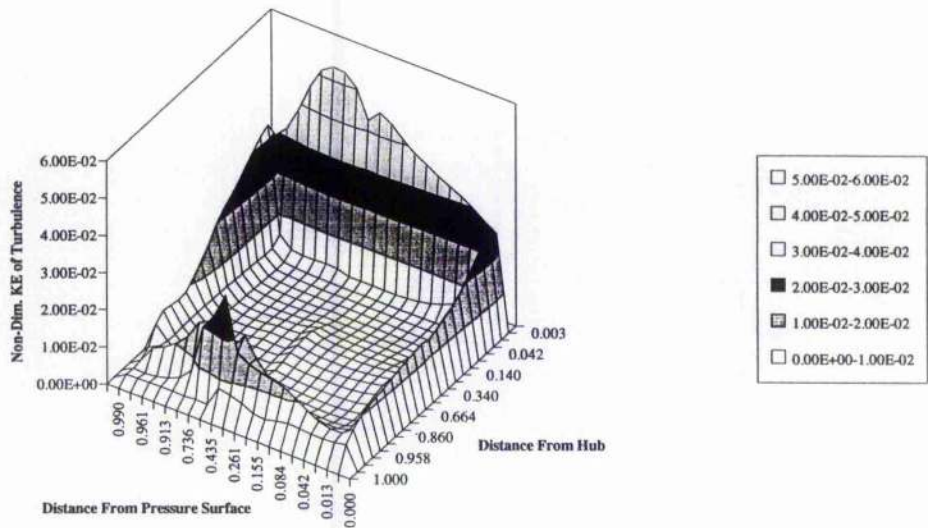


Figure 6.14(b) CFD Prediction of Kinetic Energy of Turbulence for the ZM1 at Blade Inlet

The most striking of these is that the turbulent pressure side fluctuations are not predicted by the CFD model. It is thought however that this is due to the differing blade geometries; a simple plate blade construction impeller was used by Kjörk and Löfdahl [1989] as apposed to the aerofoil section blades modelled. The high wall turbulence values predicted at wall surfaces by the CFD model are not reflected in the measured results. As before, Kjörk and Löfdahl [1989] did not measure sufficiently close to the wall surface to pick up these effects.

Near-discharge Velocity Flow Comparison

Most prominent is the CFD prediction of reverse flow at the shroud suction surface . The radial velocity measurements by Kjörk and Löfdahl [1989] only indicate a slight depression in this region, see Figures 6.15(a) and (b).

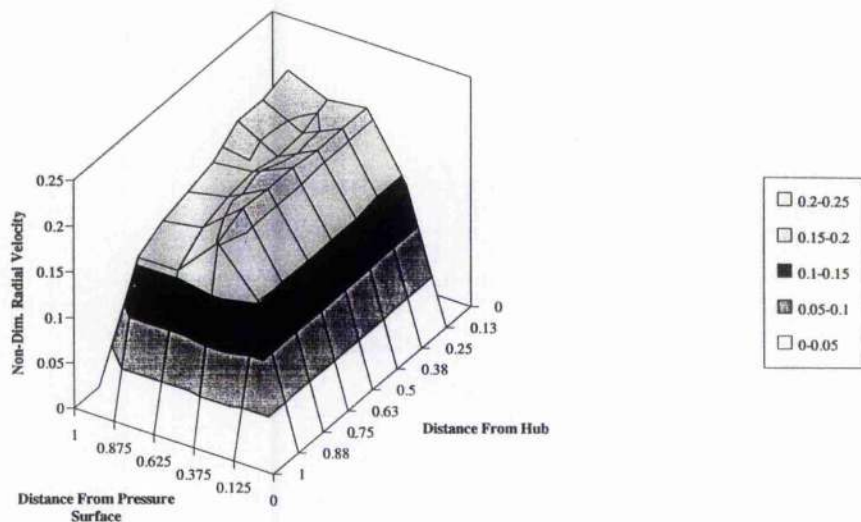


Figure 6.15(a) Near Blade Discharge Radial Velocity Measurements Made by Kjörk and Löfdahl [1989]

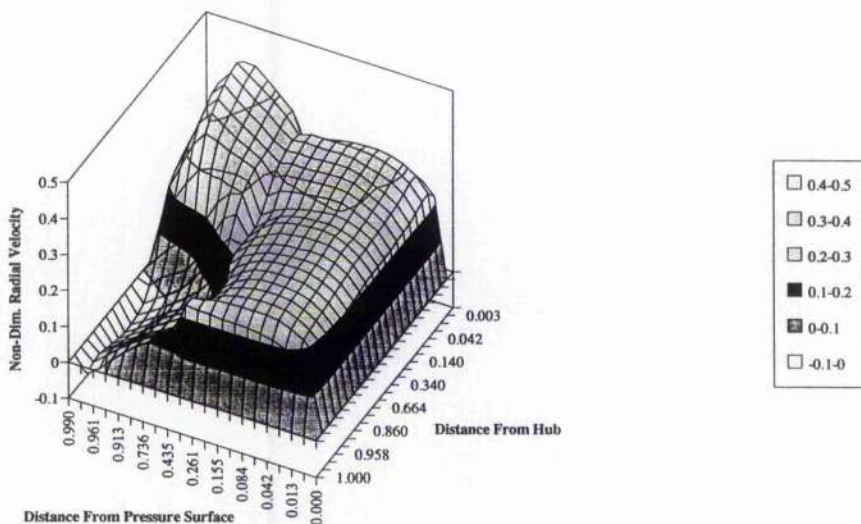


Figure 6.15(b) Near Blade Discharge Radial Velocity of the ZM1 Predicted by CFD

Further discrepancies are apparent in the tangential velocity plots where Kjörk and Löfdahl [1989] show a measured increase in the tangential velocity field from the pressure to suction surface. This is not mimicked in the CFD predictions where the remaining $\frac{3}{4}$ of the non-reverse flow is uniform. See Figures 6.16(a) and (b)

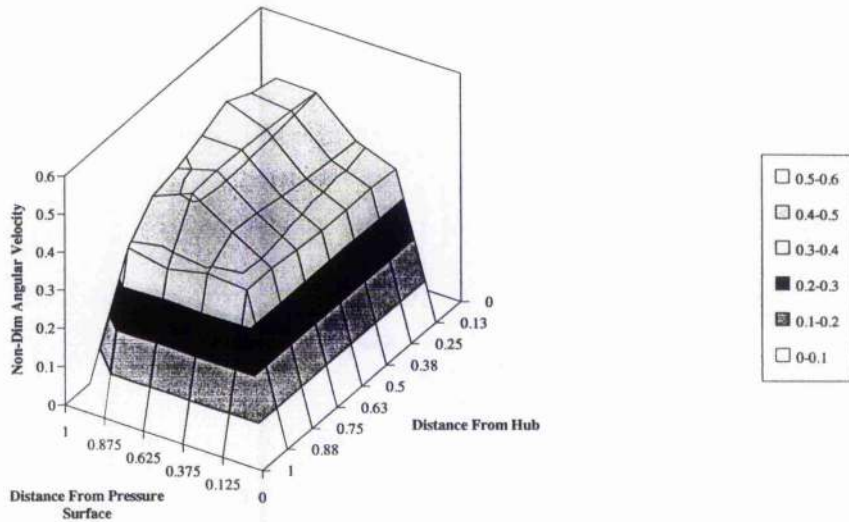


Figure 6.16(a) Measured Angular Velocity Near Blade Discharge (Kjörk and Löfdahl [1989])

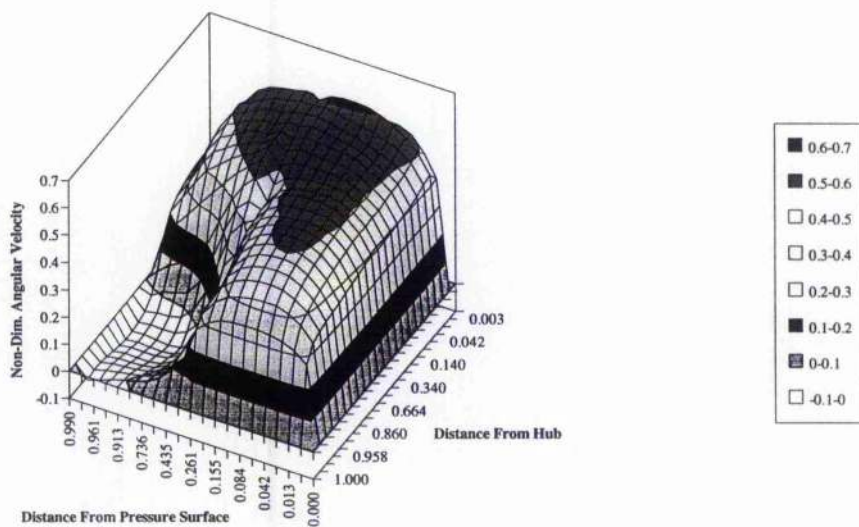


Figure 6.16(b) CFD Predicted Near Discharge Angular Velocity of the ZM1

Near-Discharge Turbulence Comparison

Again these results are marred as Kjörk and Löfdahl [1989] did not investigate the boundary layer flow. No useful deduction can be made.

6.2.3 Comparison between Inviscid and Viscous Computational Runs

Despite the failure of the earlier inviscid 'sparsely meshed' models it was considered interesting to repeat some of the work but this time utilising the current 'viscous mesh'. Slip boundaries and a very low value of viscosity ($\mu = 1 \times 10^{-15} \text{ Pa.S}$) were invoked to simulate the Euler equations. Surprisingly, instead of the premature blade separation and turbine characteristics seen earlier, the flow closely resembled that predicted when using a viscous equation set. This effect of reproducing the Kutta condition by seemingly inviscid means is well documented by Hirsch [1990], where the mechanism of shedding the so-called starting vortex is described. Firstly at $t=0^+$ the flow field is as would be for irrotational flow with a stagnation point on the upper surface. (See Figure 6.17(a)).

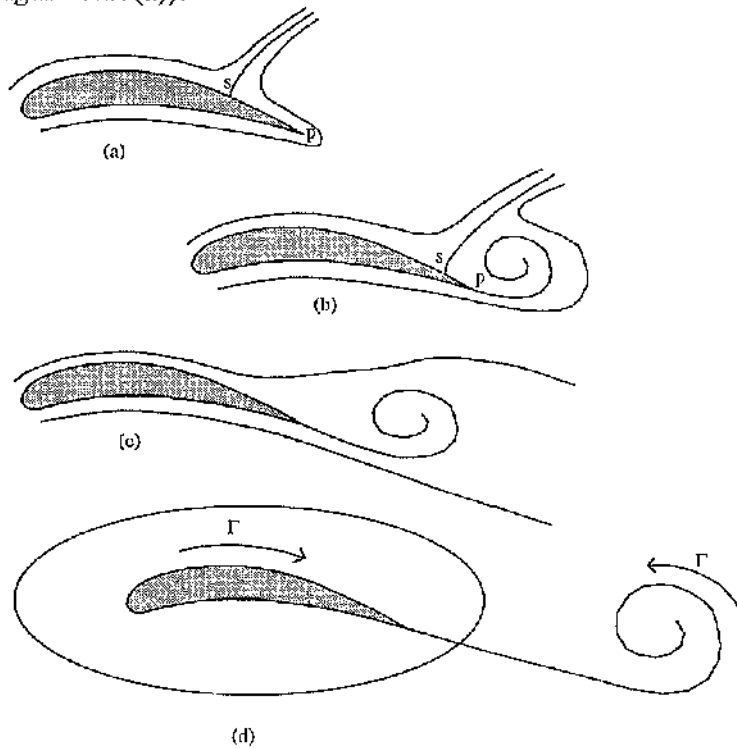


Figure 6.17 Development and Shedding of Starting Vortex (Hirsch [1990])

Then, by viscous action, a vortex is formed (see Figure 6.17(b)) and by inviscid interaction is subsequently shed. Hirsch [1990] indicates that it is only the initial eddy formulation that requires viscous action and that this, for inviscid schemes, could come about due to the inherent numerical dissipation which occurs within all schemes. The small viscosities required are effective due to the high trailing edge velocity gradients. With this phenomena in mind, there are three possible

reasons, or combinations thereof, why the fine grid, as opposed to the earlier coarse grid, was able to predict realistic flows using an inviscid equation formulation.

(a) FLUENT does not solve the Euler equations. Instead the Navier Stokes scheme is 'tricked' using a low value of molecular viscosity. This contribution could have been enough to stimulate a starting vortex.

(b) Hirsch [1990] states that it is only the formulation of the initial trailing edge eddy that requires viscous interaction, with the subsequent vortex shedding purely inviscid. It is the formulation of the viscous eddy, and shedding, that is the engine to create flow circulation, the essential ingredient to achieving flow separation correctly appearing at an aerofoil trailing edge. All of the Euler solutions found here were iterated from an already converged viscous solution. These would inherently contain the correct amount of circulation, having already shed a starting vortex, and therefore it is hypothesised that the circulation created in the earlier viscous runs remained in the solution domain enabling proper trailing edge flow simulation. It should be remembered that inviscid flows can have circulation and it is a parameter which should generally be prescribed to Euler flows in order to gain a unique description.

(c) The early coarse grids were unable to generate the large velocity gradients at the trailing edge due to lack of resolution. Thus the starting vortex could not be formed and the flow kept its irrotational qualities which included an incorrect blade discharge flow angle.

Comparison of Inviscid and Viscous Computational Velocity Fields

Similar velocity fields were predicted using inviscid and viscous formulations for design flow with both showing uniform flow near the blade pressure surface, jet flow at the hub/blade-suction corner and low-speed/reverse flow at the shroud/bladecorner. See Figures 6.18(a) and (b).

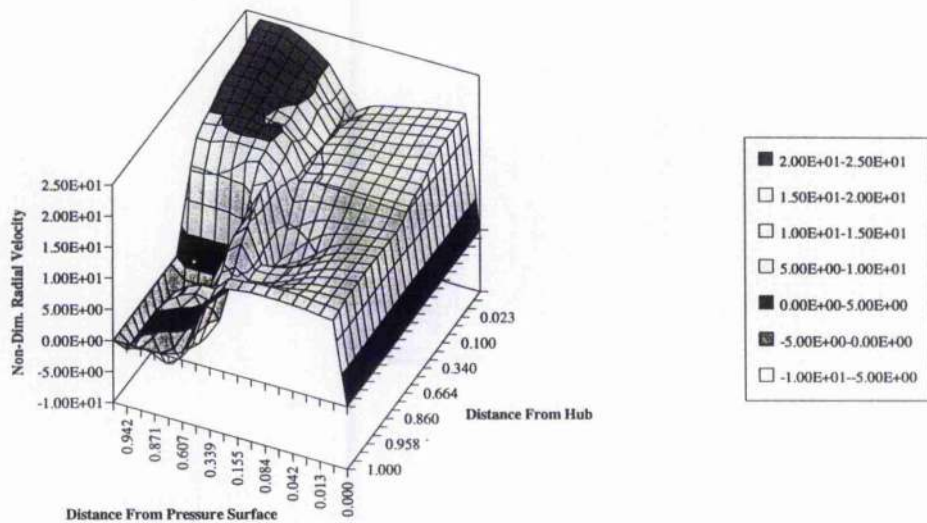


Figure 6.18(a) Inviscid CFD Prediction of Discharge Radial Velocity
(Note: zero blade surface velocity has been introduced on graph for clarity)

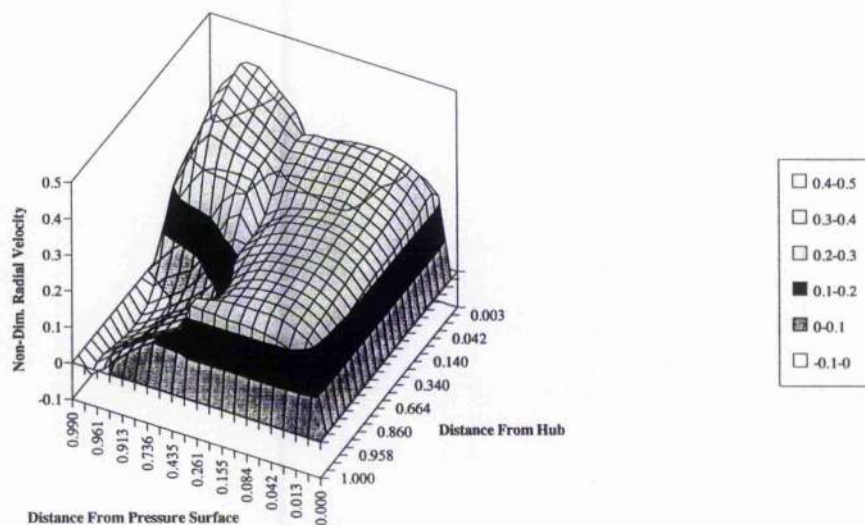


Figure 6.18(b) Viscous (Reynolds Stress Model) Prediction Using CFD

Noticeable is a smaller low-speed/reverse flow zone predicted by the inviscid solution. This discrepancy is also noticed at alternative flow rates, as may be seen in Figure 6.19. For both model types the area of recirculation increases in spanwise length as the flow-rate is reduced, with the blade-blade width of the stalled area remaining constant.

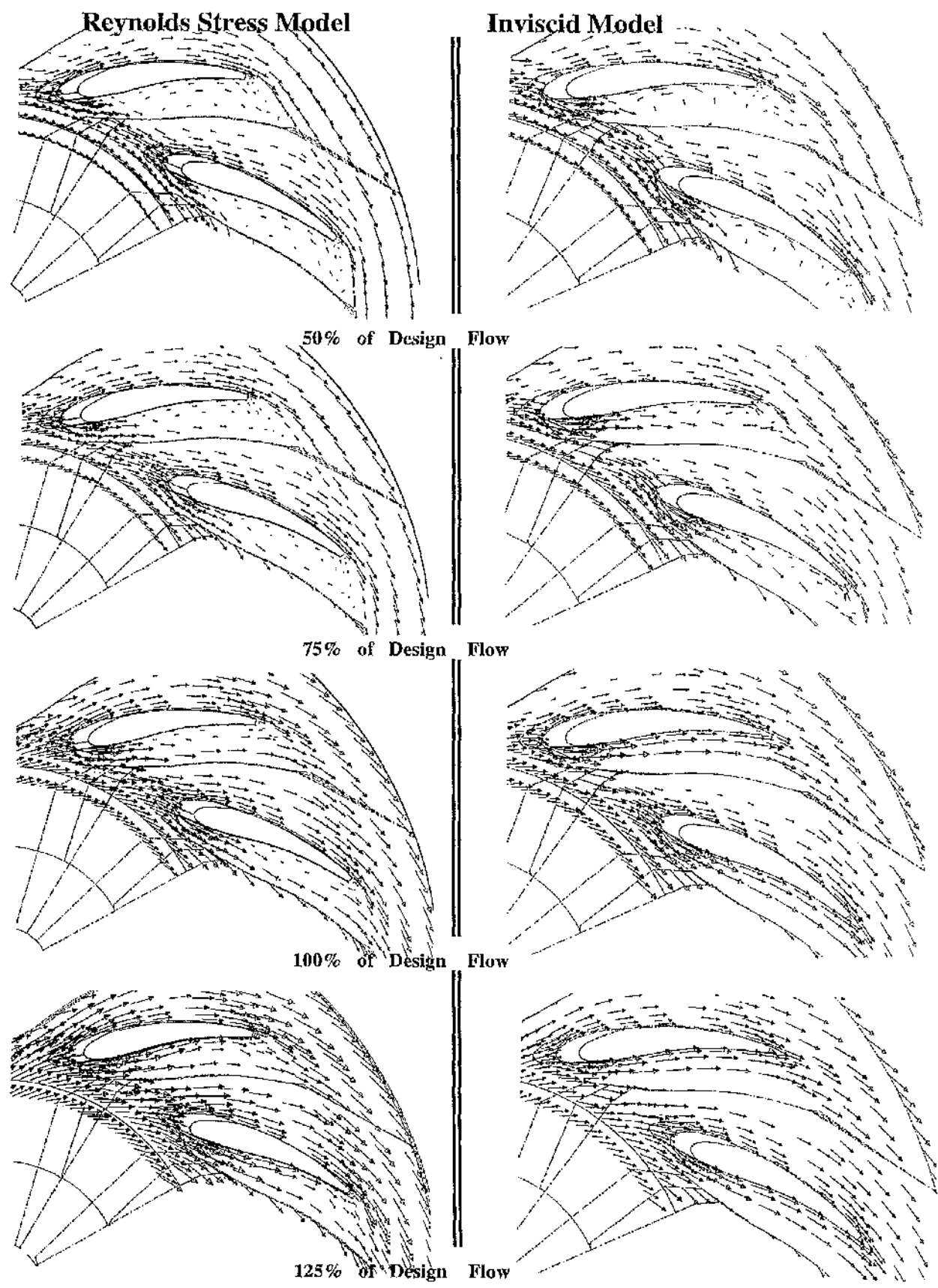


Figure 6.19 Comparison of Mid-Span Flow Rates for RSM and Inviscid Models

6.3 Conclusions

1. The ZM1 centrifugal fan flow predictions have been shown to be sensitive to computational grid. In the extreme, sparsely meshed models have predicted completely different flow patterns with the fan acting like a turbine. The problem area has been identified as the blade trailing edge, where improper modeling has been unable to resolve the high velocity gradients necessary to naturally invoke the Kutta condition. The resulting flow has separated early and consequently spoiled the solution as the modeling of correct blade discharge conditions are necessary to ensure correct fan performance prediction.

2. The internal flow within the ZM1 has been predicted using an inviscid and a viscous formulation. Results only indicate a slight difference in comparative flow predictions for a wide range of operational points. The main discrepancy was shown to be the suction side flow where the viscous model predicts earlier separation. As the RSM model requires the solution of 11 transport equations, with the inviscid requiring the solution of only 4, the extended run times might be debated as being too costly for this minor additional enhancement.

3. Proper discharge flow, with separation near or at the trailing edge, was predicted using an inviscid formulation of the fluid equations of motion. The model did not require the addition of the Kutta condition in order to generate the correct amount of circulation. It did however need a suitably refined mesh that could predict the high velocity gradients at discharge and therefore was only successful when computed using a mesh originally designed for viscous flow.

4. Suitable near wall grid spacing was achieved using theory based on smooth-walled pipe flow.

5. Some solution instabilities were noted caused mainly due to the inherent grid distortion associated with modeling backward curved blades with a structured grid. Given the choice, an investigator should opt for software that allows an unstructured mesh.

CHAPTER SEVEN

Conclusions and further work

The review of the methods used to predict detailed internal centrifugal fan flows in Chapter 3 concluded that centrifugal fans have been neglected by CFD investigators. The objective of this present study was to bridge this gap and utilise, customising if necessary, methods used currently for radial turbomachines and apply them to fans. This objective was achieved through a series of impeller geometries, tackled in order of increasing specific speed. Firstly a radial compressor was modeled using well documented and robust CFD techniques and equation sets. These computer runs were successful and with the author satisfied a new geometry, of higher specific speed, was introduced. This impeller included radial blades like the centrifugal compressor but was designed to operate at pressures much more akin to a fan. The same formulation was applied to this new geometry and the resulting flow-field predicted compared well with experiment. With this success the final geometry, that of an industrial fan, was modeled. Using a similar mesh density the model predicted incorrect flow fields. A much finer grid was required to adequately model the flow, the main discrepancy caused by the inability of the coarse mesh to resolve the flow near the blade trailing edge. After enhancing the mesh, it was shown that an inviscid formulation gave similar results to that of a state-of-the-art viscous model (RSM) with much less computational power needed for convergence due to fewer variables.

Inlet and discharge boundary conditions were also examined. It was experimentally shown, and confirmed in the literature, that the discharge flow boundary has little effect on the minimum unstalled volume flow. The main effect to the flow has been shown to be stall hysteresis, which cannot be modeled using a single blade passage representation and is therefore not pursued here.

Conclusions

1. The SIMPLE Semi-Implicit-Pressure-Linked-Equation algorithm has been used to predict the flow within three centrifugal turbomachines. Good results were gained when care was taken to avoid badly shaped computational cells.

2. It was shown that to model centrifugal fan flow requires a fine mesh in order to resolve the velocity gradients near the blade trailing edge. Without such application totally incorrect results are predicted. The increased number of cells needed makes it impractical at present to model the complete impeller or even a multi-blade channel representation due to the large computational needs. Undoubtedly, this will not be a restriction in years to come. In the meantime, single blade passage runs may still be completed. These are capable of predicting the point of stall; the internal flow near stall, design and maximum flow; and will be of importance in design optimisation.

3. Inviscid and viscous computations yield similar overall flow-fields. However, inviscid formulations over-predict the fan pressure rise as they are unable to account for frictional losses. Despite this deficiency, like Bosman and Ahrabian [1984], the inviscid models completed here were able to predict the recirculatory flow characteristic of impeller stall.

4. Radial Fan/Compressor CFD models only require sparse meshes. This allows the construction and running of full impeller models using existing computational power. These representations could be used to simulate rotating stall for which there is very limited detailed information.

5. Using the guidelines given in Chapter Six, aerodynamicists are able to construct and solve CFD models of centrifugal fans with confidence. Guidelines for the application of boundary conditions are given such that even the unfamiliar user will quickly be able to build and run realistic models. All necessary groundwork has been completed and documented.

Further Work

1. It would be interesting to see results for a multi-blade CFD model radial machine. This is well within the capability of the present software and hardware.

2. Once additional computational power becomes available, a multi channel model of a centrifugal fan should be build. Only then can the unsteady flow measurements taken in the L3R test rig be utilised.

3. It would be useful to investigate the use of simpler turbulence models other than the computationally intensive RSM used in Chapter 6. Although many proprietary CFD packages have RSM capability, a simpler model would reduce run times sufficiently to a level that would enable CFD to be routinely used within a design environment.

References

ADLER D *Status of Centrifugal Impeller Internal Aerodynamics Part 1: Inviscid Flow Prediction Methods* ASME Journal of Engineering for Power Vol. 102 pp. 728 - 737, July 1980

ADLER D, KRIMERMAN Y *On the Relevance of Inviscid Subsonic Flow Calculations to Real Centrifugal Impellers Flow* ASME Journal of Fluids Engineering Vol. 102 pp 79 - 84, March 1980
ASME Paper No. 82-JPGC-GT-16, 1982

BARD H *Turbulence and Stability in Centrifugal Fan Impellers, International Conference on Fan Design and Applications* Paper G3 pp97-310, BHRA Fluid Engineering 1982

BENNETT I, WATSON H *Single Inlet L3R Fan* Report A436 Part 1, James Howden Group Technology, Old Govan Road, Renfrew.

BOLTON A N, *Pressure Pulsations and Rotating Stall in Centrifugal Fans* IMechE C118/75, 1975

BOSMAN C, AHRABIAN D *Calculation of Stalled Flow in a Centrifugal Impeller Computational Methods in Turbomachinery* IMechE Conference Publications 1984, Paper No. C67/84 pp 173 - 182

BOSMAN C, EL SHAARAWI MAI *Quasi - Three - Dimensional Numerical Solution of Flow in Turbomachines* ASME Journal of Fluids Engineering pp. 132 - 140, March 1977

BOSMAN C, MARSH H *An Improved Method for Calculating the Flow in Turbo-Machines, Including a Consistent Loss Model.* Journal of Mechanical Engineering Science Vol. 16 No. 1 pp. 25 - 31, 1974

BS848: Part 1; 1980
British Standards Institute

CASEY MV, DALBERT P, ROTH P *The Use of 3D Viscous Flow Calculations in the Design and Analysis of Industrial Centrifugal Compressors* ASME 90-GT-2, 1990

CHEN, P *Unstable Flows within Centrifugal Fans* PhD Thesis Strathclyde University, 1993

DAVIES WN *Application of Three Dimensional Viscous Compressible Flow Solver to a High Speed Centrifugal Compressor Rotor-Secondary Flow and Loss Generation* Proceedings of the IMechE Turbomachinery- Efficiency Prediction and Improvement Paper No. C261/87, 1987

DAWES WN *Development of a 3d Navier Stokes Solver for Application to All Types of Turbomachinery* ASME Paper 88-GT-70, 1988

DECONICNK H, HIRSH CH *Finite-Element Methods of Transonic Blade to Blade Calculation in Turbomachines* ASME Journal of Engineering for Power Vol. 103 pp 665 - 677, Oct 1981

DENTON JD *The Use of a Distributed Force to Simulate Viscous Effects in 3D Flow Calculations* ASME 86-GT-144

DENTON JD, SINGH UK Cited by PRINCE TC, BRYANS AC 1984 *Time Marching Methods for Turbomachinery Flow Calculations* VKI Lecture Series 7, 1979

ECKARDT D, (Cited in Majumdar Ak, Pratap Vs, Spalding 1977) *Flow Field Analysis of Radial Backswept Centrifugal Compressor Impellers, Performance Prediction of Centrifugal Pumps and Compressors* Edited by GOPALAKRISHNAN ASME New York, 1980 pp 77 - 95

EDWARDS JP, GLYNN DR, TATCHELL DG *Flow and Blade Loading in Centrifugal Impellers* First International Phoenics Users Conference 1985 Concentration Heat and Momentum Limited

FLETCHER CAJ *Computational Techniques for Fluid Dynamics Volume 1* pp36-37
Springer Verlag, Berlin 1988

FLUENT *Fluent Users Manual V4.2* Fluent Inc, Centerra Resource Park, 10
Cavendish Court, Lebanon, NH 0376C

GESSNER FB *An Experimental Study of Centrifugal Fan Inlet Flow and its Influence on Fan Performance* ASME Paper pp. 67-FE-21, 1967

GOULAS A, MEALING B *Flow at the Tip of a Forward Curved Centrifugal Fan*
ASME Paper No. 84-GT-222, 1984

HAFEZ M, LOVELL D *Numerical Solution of the Transonic Stream Function Equation* AIAA Journal Vol. 21, No. 3 pp. 327 - 335, March 1983

HAH C, BRYANS AC, MOUSSA Z TOMSHO ME *Application of Viscous Flow Computations for Aerodynamic Performance of a Backswept Impeller at Various Operating Conditions* ASME Journal of Turbomachinery Vol 110, pp303-311, July 1988

HIRSCH, C *Numerical Computation of Internal and External Flows. Vol 2: Computational Methods for Inviscid and Viscous Flows* Wiley-Interscience Publication, John Wiley and Sons, Chichester, England, 1990

JAPIKSE D *REVIEW - Progress in Numerical Turbomachinery Analysis* ASME Journal of Fluids Engineering 1976 pp. 592 - 606, Dec. 1976

KATSANIS T *Use of Arbitrary Quasi-Orthogonals for Calculating Flow Distribution in the Meridional Plane of a Turbomachine.* NASA TN D-2546, Dec. 1964

KATSANIS T *Use of Arbitrary Quasi-Orthogonals for Calculating Flow Distribution on a Blade-to-Blade Surface in a Turbomachine* NASA TN D-2809, 1965

KATSANIS T *Use of Arbitrary Quasi-Orthogonals for Calculating Flow Distribution in a Turbomachine.* ASME Journal of Engineering for Power pp. 197 - 202 April, 1966

KHALI I, TABAKOFF W HAMED A (Cited in Whitfield and Baines 1990) *Viscous Flow Analysis in Mixed Flow Rotors* ASME Journal of Engineering for Power Vol 102 pp 193 - 201 January, 1980

KHALI I, TABAKOFF W (Cited in Whitfield and Baines 1990) *A Study of the Viscous and Nonadiabatic Flow in Radial Turbomachines* ASME Journal of Engineering for Power Vol 103 pp481-489 July,1981

KJÖRK A, LÖFDAHL L *Hot Wire Measurements Inside a Centrifugal Fan Impeller* ASME Journal of Fluids Engineering Vol. 111 pp. 363 - 368, Dec. 1989

KRIMERMAN Y, ADLER *The Complete Three-Dimensional Calculation of the Compressible Flow Field in Turbo Impellers* Journal Mechanical Engineering Science Vol 20 No. 3 pp. 149 - 158, 1978

KUBO T *Unsteady Flow Phenomenon in Centrifugal Fans (2nd Report), Three Dimensional Unsteady Flow Measurement* Bulletin Of The JSME Vol.23 pp1171-78, 1980

KUBO T, MURATA S *Unsteady Flow Phenomena in Centrifugal Fans* Bulletin of the JSME Vol. 19 No. 135 pp. 1039 - 1046, Sept. 1976

KUETHE A, CHOW C *Foundations of Aerodynamics: Bases of Aerodynamic Design* 4th ed. New York, Wiley, 1986

LAKSHMINARAYANA B *An Assessment of Computational Fluid Dynamic Techniques in the Analysis and Design of Turbomachinery- The 1990 Freeman Scholar Lecture* Journal of Fluids Engineering Vol.113 1991.

LAPWORTH BL, ELDER RL *Computation of the Jet Wake Structure in a Low Speed Centrifugal Impeller* ASME 88-GT-217,1988

LASKARIS TE *Finite Element Analysis of Three Dimensional Potential Flow in Turbomachines* AAIA Journal Vol. 16 pp 717-22, 1978

MADHAVEN S, WRIGHT T *Rotating Stall Caused by Pressure Surface Flow Separation on Centrifugal Fan Blades* ASME Journal of Engineering for Gas Turbines and Power Vol. 107 pp. 775m - 781, July 1985

MAJUMDAR AK, PRATAP VS, SPALDING (Cited in Whitfield and Baines 1990) *Numerical Computation of Flow in Rotating Ducts* ASME Journal of Fluids Engineering Vol. 89 pp 148 - 153, 1977

MANDAS M, MANFRIDA G AND NURZIA F *Measurements of Primary and Secondary Flow in an Industrial Forward Curved Centrifugal Fan* ASME Journal of Fluids Engineering Vol. 109 pp. 353 - 358, Dec 1987

MARSH H A *Digital Computer Program for the Throughflow Fluid Mechanics in an Arbitrary Turbomachine using a Matrix Method* Reports and Memoranda No. 3509, July 1966

MCNALLY WD, SOCKOL PM *Review - Computational Methods for Internal Flows with Emphasis on Turbomachinery* ASME Journal of Fluids Engineering Vol. 107 pp. 6 - 22, March 1985

MIZUKI S, ARIGA I and WATANABE I *Investigation Concerning the Blade Loading of Centrifugal Impellers* ASME Gas Turbine Conference Paper 74-GT-143, 1974

MOORE J, MOORE JG, (Cited in Whitfield and Baines 1990) *Calculation of Three-Dimensional Viscous Flow and Wake Development in a Centrifugal Impeller* ASME Journal of Engineering for Gas Turbines and Power Vol 103 pp. 367- 372 April, 1981

NOVAK RA, HEARSEY RM A *Nearly Three-Dimensional Intrablade Computing System for Turbomachinery* ASME Journal of Fluid Engineering pp. 154 - 166, March 1977

PHELAN JJ, RUSSELL SH, ZEIUFF WC *A Study of the Influence of Reynolds Number in the Performance of Centrifugal Fans* ASME Journal of Engineering for Power Vol 101 pp 671-676, 1979

PRINCE TC, BRYANS AC *Three-Dimensional Inviscid Computation of an Impeller Flow* ASME Journal of Engineering for Gas Turbines and Power Vol. 106 pp 523 - 528, April 1984

RAHMATALLA MAF, BOSMAN C *Flow Field Analysis of Radial Backswept Centrifugal Compressor Impellers Performance Prediction of Centrifugal Pumps and Compressors*. Edited by Gopalakrishnan ASME New York, 1980 pp 77-95.

RAJ D, SWIM WB *Measurements of the Mean Flow Velocities and Velocity Fluctuations at the Exit of an FC Centrifugal Fan Rotor* ASME Journal of Engineering for Power Vol. 103, pp. 393 399, April 1981

STANITZ JD *Two-Dimensional Compressible Flow in Conical Mixed Flow Compressors* NACN TN 1744, 1948

STOW P, NEWMAN SP *Coupled Inviscid - Boundary Layer Methods for Turbomachinery Blading Design* Computational Methods and Aeronautical Fluid Dynamics, Editor P. Stow Institute of Mathematics and its Applications Series No. 25:1990 Clarendon Press

TOURLIDAKIS A, ELDER RL *Computations of Three-Dimensional Viscous Turbulent Flows in Centrifugal Compressors with Tip Leakage* Proceedings of the IMechE Turbomachinery- Efficiency Prediction and Improvement Paper No. C423/050, 1991

WHIRLOW DK, GOLDSCHMIED FR, FARN CLS *Analysis of the Three-Dimensional Potential Flow of Centrifugal Draft Fans* EPRI Symposium on Power Plant Fans (EPRI Publication CS 2206), Oct 1981

WHITEFIELD A, BAINES NC *Design of Radial Turbomachines* London Scientific and Technical 1990 1st Ed. Printed: The Bath Press, Avon

WRIGHT T *Centrifugal Fan Performance with Inlet Clearance* ASME Journal of Engineering for Gas Turbines and Power Vol. 106 pp. 906 - 912, Oct 1984

WRIGHT T, MADHAVEN S AND DIRE J *Centrifugal Fan Performance with Distorted Inflows* ASME Journal of Engineering for Gas Turbines and Power Vol. 106 pp. 895 - 900, Oct 1984

WRIGHT T, TZOU KTS AND MADHAVEN S *Flow in a Centrifugal Fan Impeller at Off-Design Conditions* ASME Journal of Engineering for Gas Turbines and Power Vol. 106 pp. 913 ~ 919, Oct 1984

WRIGHT T, TZOU KTS, GREAVES KW AND MADHAVEN S *The Internal Flow Field and Overall Performance of a Centrifugal Fan Impeller - Experiment and Prediction*

WU CH A *General Theory of Three-Dimensional Flow in Subsonic and Supersonic Turbomachines of Axial -, Radial -, and Mixed Flow Types.* NACA TN 2604, Jan. 1952

APPENDIX A

Mizuki Radial Compressor CFD Model Runs

A.1 Phoenics Mizuki Impeller Run Details

The most significant computational investigations are reported here designated by the file names used for computer storage. Tabulated below are their salient features.

Table A.1 PHOENICS Mizuki impeller computer runs

Model Name	Flow Coeff	Viscosity	Solver	Error	Comments
MizA	0.4	Laminar*	False Time step	$\approx E2$	Standard Library Run
MizB	0.4	Inviscid	False Time step	$\approx E2$	Without viscosity the results were the same as Miz.A
MizC	0.1	Inviscid	False Time step	$\approx E5$	Large areas of recirculating flow
MizD	0.2	Inviscid	False Time step	$\approx E7$	Some small areas of recirculation
MizG	0.4	Inviscid	Linear	$\approx E2$	No difference in convergence time or final residual errors over MizB due to Linear solver
MizI	0.1	Inviscid	Linear	$\approx E6$	Large recirculating flow as shown by MizC.

* A high value of laminar viscosity was used as a crude attempt to simulate turbulence

Observations are noted below:

A.1.1 Effect of viscosity on solution

There is no noticeable difference between the solutions of models MizA and MizB as might be expected with a mesh of this coarseness.

A.1.2 Solution stability and convergence

PHOENICS uses an iterative solution procedure to 'solve' the governing equations for which the user must define the convergence. For the MIZUKI impeller investigation the magnitude of the error residuals, reported by PHOENICS every iteration, were used to gauge when to stop the program. The accepted magnitudes of the error residuals were set by the levels recorded for the standard design flow model test case, MIZA.

Using this approach it quickly became apparent that as the flow coefficient was lowered the problem became less stable and larger numbers of iterations were necessary to gain the convergence quantified by the standard run. As an indication of this, for the design flow cases approximately 150 iterations were required; for the highly stalled flow it became necessary to increase this to 500 iterations. Future iterations beyond this were not effective in reducing the larger residual errors which appeared when modelling low flow rates, and consequently the desired residual levels were not always achieved.

A.2 The FLUENT Mizuki Model

A.2.1 Steady State Fluent Mizuki Runs

Before invoking the time dependent option a series of steady state runs, leading to a fully stalled condition, were completed.

Table A.2 Steady State Fluent Mizuki Runs: Residuals

Filename	Flow Coefficient	Number of Iterations	Pressure Residual	U-Velocity Residual	V-Velocity Residual	W-Velocity Residual
FMIZ2	0.4	250	6×10^{-4}	1×10^{-4}	2×10^{-4}	1×10^{-4}
FMIZ5	0.4	1000	4×10^{-4}	6×10^{-5}	4×10^{-5}	1×10^{-4}
FMIZ11	0.2	500	2×10^{-4}	6×10^{-5}	6×10^{-5}	3×10^{-4}
FMIZ21	0.1	1000	6×10^{-3}	4×10^{-3}	2×10^{-3}	4×10^{-3}

All of the FLUENT Mizuki runs were completed with the following relaxation parameters:

Table A.3 Fluent Mizuki Model Relaxation Parameters

Variable	Relaxation	Number of Sweeps
Pressure	0.1	10
Velocity	0.3	3

The first run completed was FMIZ2. After patching on a velocity field equal to the inlet velocity, throughout the computational domain, the solution converged in 250 iterations. In addition, it should be noted that the run was prematurely halted after 250 of the proposed 500 iteration run by FLUENT. The residuals had reached a summated value of 1×10^{-3} : at this default value FLUENT assumed that the equations had converged. For interest it was decided, after resetting the FLUENT default residual convergence parameter, to continue the run to see if the solution would converge any further. After 1000 iteration no benefits were noted.

With a good approximation to the flow from FMIZ2, it was decided to proceed to the below design flow cases . Two runs were completed with flow coefficients of $\psi=0.2$ and 0.1, the latter representing stalled flow operation. The mid-channel velocity vector plot for the $\psi=0.1$ case is shown in Figure A1.

Appendix A Mizuki Radial Compressor CFD Model Runs

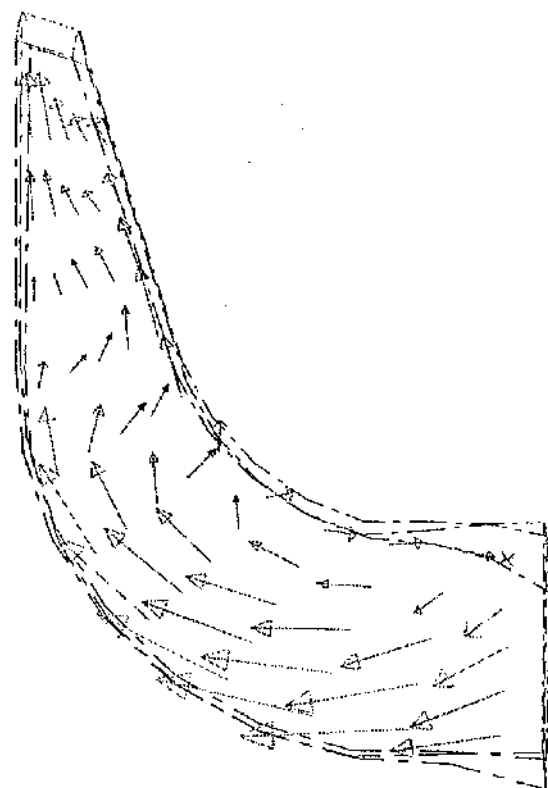


Figure A.1 Fluent Mizuki Highly Stalled Flow Meridional Mid-Channel Velocities

A.2.2 Unsteady Fluent Mizuki Runs

As a first step it was decided to investigate the sensitivity of the model to time step. This analysis could be done interactively due the relatively small number of computational cells and hence reasonable run times. The stalled condition of $\psi=0.1$ modelled by FMIZ21 was used as the starting data set in all time dependent investigations.

These are tabulated below. All runs were completed over one time step as this was all that was required to determine stability (in the earlier L3R runs instability was noted by a divergence within only a few iterations). Each of these time steps were limited to 100 iterations.

Table A.4 Interactive Time Dependent Runs

Time step	Pressure Residual	U-Velocity Residual	V-Velocity Residual	W-Velocity Residual
4×10^{-2}	1×10^{-2}	3×10^{-3}	2×10^{-3}	4×10^{-3}
4×10^{-3}	8×10^{-3}	3×10^{-3}	2×10^{-3}	3×10^{-3}
4×10^{-4}	1×10^{-3}	4×10^{-4}	4×10^{-4}	7×10^{-4}
4×10^{-5}	4×10^{-4}	3×10^{-4}	1×10^{-4}	1×10^{-4}
4×10^{-6}	3×10^{-5}	4×10^{-5}	2×10^{-5}	2×10^{-5}
4×10^{-7}	2×10^{-5}	3×10^{-5}	8×10^{-6}	1×10^{-5}
4×10^{-8}	8×10^{-6}	1×10^{-5}	2×10^{-6}	3×10^{-6}

All runs were therefore stable, with a distinctive trend of decreasing residual with respect to time step duration.

Two batch runs, each incorporating twenty time steps, were subsequently completed. Details are shown in table A.5.

Table A.5 Batch Time Dependent Runs

Filename	Time Step	Pressure Residual	U-Velocity Residual	V-Velocity Residual	W-Velocity Residual	Max. No. of Iters Per Time Step	No. of Time Steps
PMIZ35	0.04	1×10^{-2}	3×10^{-3}	2×10^{-3}	4×10^{-3}	100	20
PMIZ45	2.5×10^{-4}	3×10^{-3}	8×10^{-4}	6×10^{-4}	1×10^{-3}	100	20

No unsteadiness was detected in these solutions.

APPENDIX B

L3R 'Bladed' CFD Model Runs

The pertinent runs completed using the L3R bladed model are shown in Table B.1. The maximum inlet volume flow boundary was applied in all cases apart from the last 3 runs.

B.1 Detailed Description of the bladed L3R model computer runs

In order to fully understand the reasons behind each model run, all of the tabulated examples in Table B.1 are described in turn.

The first of the these, L3RT, followed on from several exploratory computer runs that are not individually documented here. These early runs, although showing numerical stability, were not able to yield fully converged solutions and it became apparent that some tuning of the solution parameters would be required. It was the effect of changing these parameters on the model stability and convergence that was of main concern here. These 'solution parameters' are user defined solution controls called 'relaxation parameters' and 'numbers of sweeps'. These may be independently changed for each variable, namely the three velocities and pressure for the inviscid incompressible runs.

The first three runs, namely L3RT, L3RX and L3RY, were all experiments to investigate reductions in the relaxation parameters. Of these the only positive result came from L3RX, in which the step drop in relaxation parameters triggered a step drop in pressure error residual. However, this positive result was marred due to a trade off in increased velocity residuals. The pressure and velocity residual plots for run L3RX are shown below in Figure B.1.

When reading Table B.1, "600+900" in the 'number of iterations' column means that after 600 of the scheduled 1500 iterations a switch in relaxation parameters was made. The effect of such a step change can be seen in Figure B.1.

Appendix B L3R 'Bladed' CFD Model Runs

Table B.1 Bladed Model L3R Fluent Runs

Run Filename	Relaxation Parameters		No. of Sweeps		No. of iters	Residual Values				Comments
	Pressure	Velocity	Press.	Vel		Press.	U-Vel	V-Vel	W-Vel	
L3RT	0.4/0.2	0.3/0.1	20	10	500 +1000	5x10 ⁻³	4x10 ⁻³	7x10 ⁻³	2x10 ⁻³	Some divergence of the velocity terms after change in relaxation parameters
L3RX	0.3/0.1	0.2/0.05	15	10	600 +900	3x10 ⁻³	3x10 ⁻³	5x10 ⁻³	1x10 ⁻³	Large drop in pressure residuals but some divergence of the v-velocity residuals.
L3RY	0.05/0.02	0.05	15	10	75+75	5x10 ⁻³	3x10 ⁻³	5x10 ⁻³	1x10 ⁻³	Investigating the effect of a change in pressure relaxation. Small increase in pressure residuals. No change in velocities.
L3RZ	0.02	0.05	20	10	30	5x10 ⁻³	3x10 ⁻³	5x10 ⁻³	1x10 ⁻³	Investigation to see if increasing the number of sweeps on pressure made any difference. Results showed no change.
L3RBB	0.4	0.3	30	10	200	7x10 ⁻³	1x10 ⁻³	1x10 ⁻³	1x10 ⁻³	First time that Variable History records were taken during a run. Interesting results showed oscillations in pressure at inlet.
L3RCC	0.4	0.3	30	10	500	6x10 ⁻³	9x10 ⁻⁴	1x10 ⁻³	8x10 ⁻⁴	This run was a continuation of L3RBB
L3REB	0.4	0.3	50	10	300	1x10 ⁻²	2x10 ⁻³	2x10 ⁻³	1x10 ⁻³	Both this run and the one following were investigations into the changes in the number of pressure sweeps.
L3RFF	0.4	0.3	50	10	300	1x10 ⁻²	2x10 ⁻³	3x10 ⁻³	3x10 ⁻³	This run seemed to deviated from the predicted pressure values expected from viewing L3RCC variable History plots.
AL3RB	0.4	0.3	30	10	500	9x10 ⁻³	2x10 ⁻³	2x10 ⁻³	1x10 ⁻³	Continuation of L3RCC
AL3RD	0.4	0.3	30	10	500	1x10 ⁻²	2x10 ⁻³	2x10 ⁻³	1x10 ⁻³	As test , with new boundary
AL3RF	0.075	0.3	30	10	500	2x10 ⁻²	2x10 ⁻³	3x10 ⁻³	1x10 ⁻³	See Figure B.4
AL3RH	0.2	0.15	30	10	500	3x10 ⁻⁵	1x10 ⁻³	1x10 ⁻³	1x10 ⁻³	See Figure B.4
AL3RI	0.4	0.3	30	10	250	1x10 ⁻²	2x10 ⁻³	2x10 ⁻³	2x10 ⁻³	See Figure B.4
AL3RJ	0.2	0.15	30	10	1000	4x10 ⁻³	2x10 ⁻³	2x10 ⁻³	2x10 ⁻³	See Figure B.3
AL3RL	0.1	0.075	30	10	1000	2x10 ⁻³	1x10 ⁻³	2x10 ⁻³	1x10 ⁻³	See Figure B.3
AL3RM	0.4	0.3	30	10	500	3x10 ⁻²	3x10 ⁻³	4x10 ⁻³	2x10 ⁻³	See Figure B.3
L3RBBB	0.4	0.3	30	10	750	4x10 ⁻²	3x10 ⁻³	4x10 ⁻³	1x10 ⁻²	This run had the inlet velocity field reduced from a uniform 43.9ms ⁻¹ to 35ms ⁻¹ . Looking for an improvement in convergence. After about 300 iterations problem started to diverge.
L3RDDD	0.1	0.3	30	10	500	1x10 ⁻¹	3x10 ⁻³	7x10 ⁻³	7x10 ⁻³	The above run was restarted with a smaller pressure relaxation parameter to see if it would prevent the divergence. This first attempt showed some unstable trends. The next run confirmed divergence.
L3REEB	0.1	0.3	30	10	400	5x10 ⁻²	3x10 ⁻³	6x10 ⁻³	6x10 ⁻³	Continuation of the previous run.

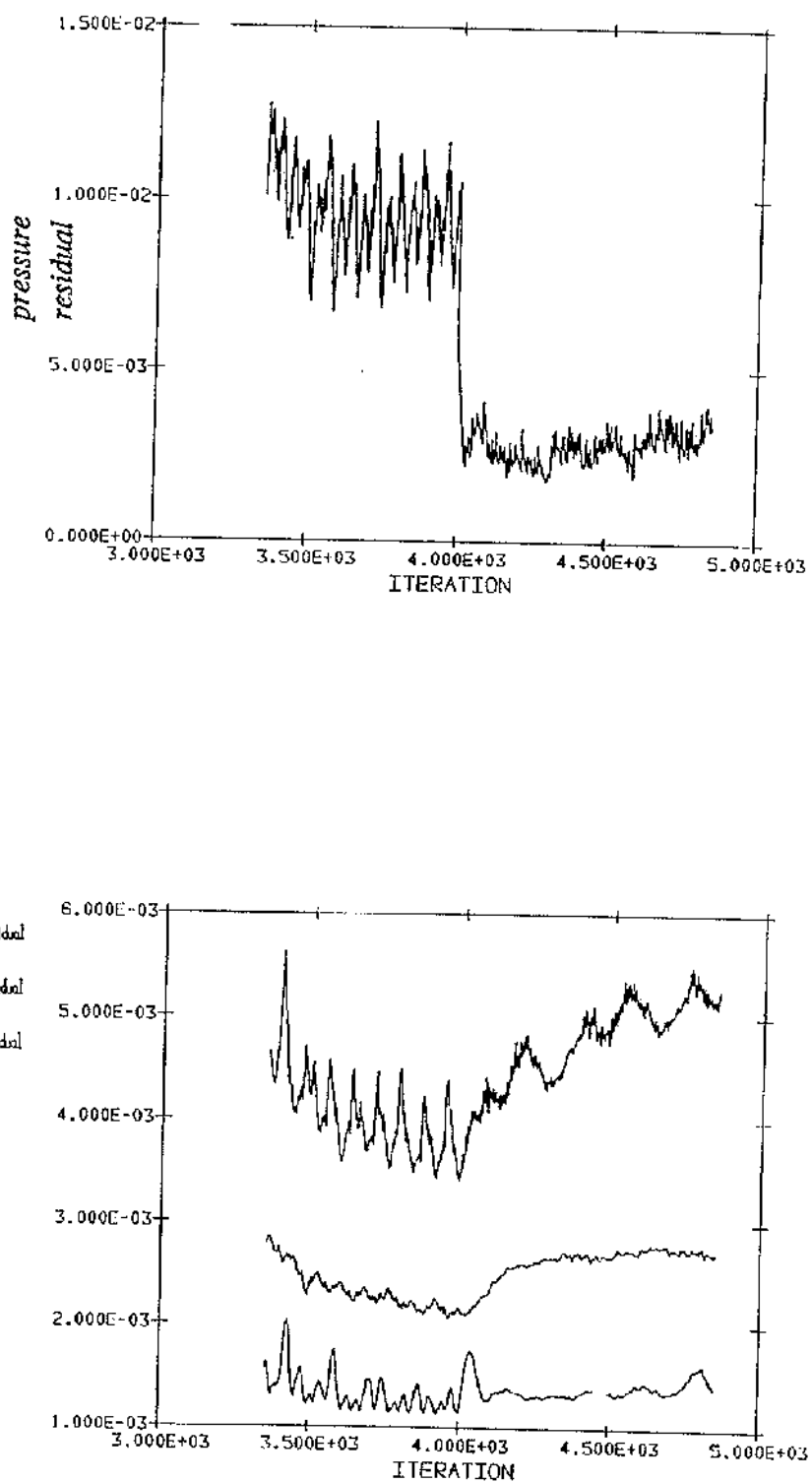


Figure B.1 Plot of pressure and velocity residuals for run L3RX

Run L3RY that followed was an attempt to see if the velocity and pressure values could be uncoupled by changing only the pressure relaxation parameter. This was unsuccessful as there was a marked increase in pressure error residuals.

During the execution and analysis of the preceding runs it became increasingly apparent that the reported residual errors were not sufficient to determine the solver performance i.e. just how quickly, or if at all, the equation set was converging. It became necessary to invoke FLUENT's variable history option. This utility records, after each solution iteration, velocity and pressure magnitudes at any user specified location within the domain. Consequently the solution may be said to have converged, for a steady state run, when these reported variable histories settle to constant values.

For the remaining runs in the section it was decided to record the pressure field at the inlet of the domain, using these values to determine convergence.

Using FLUENT's variable history utility, the model was restarted with the more conventional, that is FLUENT's default, values for pressure and velocity relaxations of 0.4 and 0.3 respectively. This model run was successful and was continued for another 500 iterations finally being stored as L3RCC. A variable history plot which includes run L3RCC is show in Figure B.2.

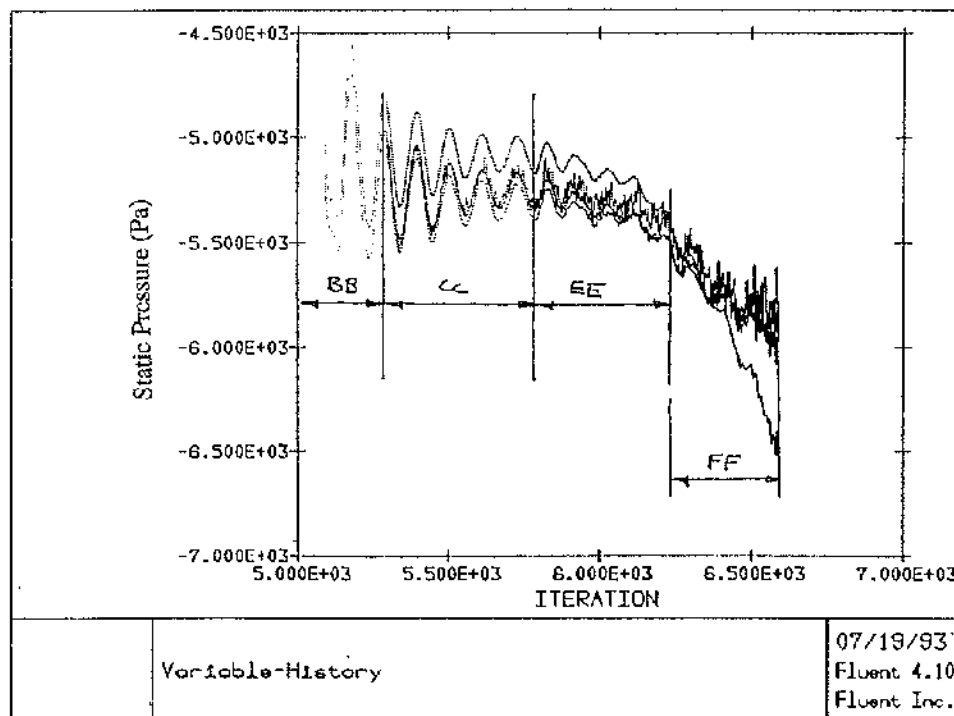


Figure B.2 Variable History Plot of Pressure at Inlet

As can be seen in Figure B.2 the amplitude of oscillation for run L3RCC was decreasing with iteration, suggesting that the problem was approaching convergence. The number of pressure sweeps was further increased from 30 to 50 in order to aid the damping process (runs L3REB and L3RFF). However instead of the problem settling to a constant value, the pressure at inlet drifted away from the projected mean. At this point it was concluded that 30 pressure sweeps should be used for all further runs as it was thought that using 50 sweeps could cause instabilities. However in runs that followed, this was not corroborated by the results obtained.

This method of putting computer runs nose-to-tail produced rapid results but did not clearly show the effect of each individual solution parameter. Indications were clouded by the influence of the initial field data set, which in previous runs had shown, could even effect the overall stability of the solver. It was decided therefore, in order to ensure fair comparisons, that the jobs would be run in parallel. These runs, starting with the same initial data set, and would differ only by a single solution parameter.

Because of the complex relationships connecting each of the runs in this investigation, a tree diagram is drawn below to aid understanding.

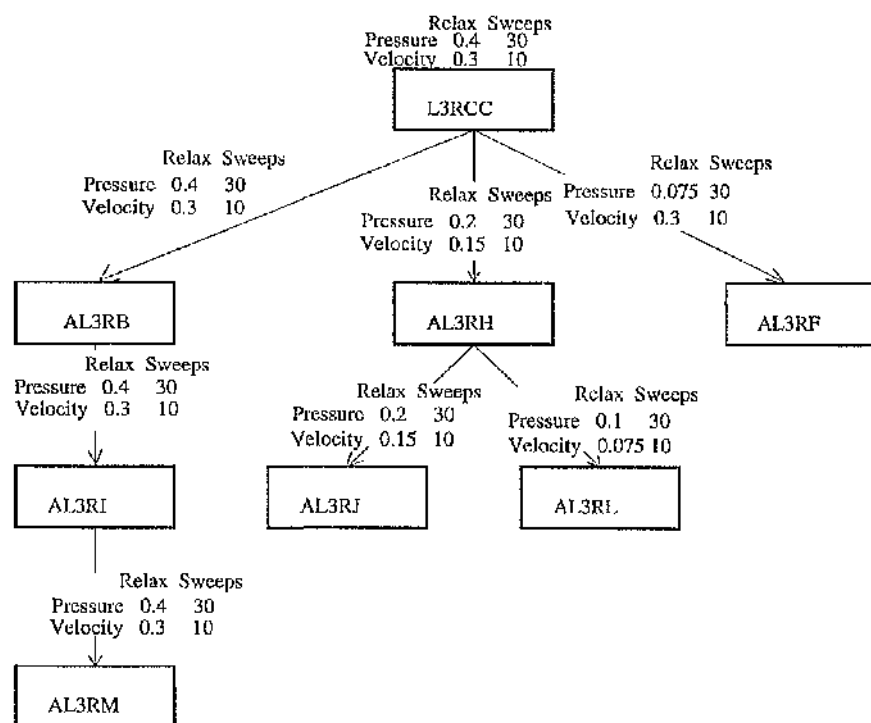


Figure B3 Tree Diagram Showing Relationships between the Relaxation Factor Optimisation Runs

The resultant output from L3RCC was chosen as the initial start variable data set as up to this point the results were promising, only deviating from a converged solution when a change in pressure residual was made. It was therefore decided to continue the run, keeping the same number of sweeps and relaxation factors. These runs were called AL3RB to AL3RI. A drift of inlet pressures, similar to those shown in Figure B.1, were seen. The similarity also extended to the final pressures recorded which were of the order -6 kPa. It was concluded at this point that the large numbers of pressure sweeps were not the cause of the experienced instabilities.

The four remaining runs, shown in Figure B.3, were further relaxation factor investigations. Runs AL3RH and AL3RJ were completed in parallel with AL3RB and AL3RI, together demonstrating that halving both the pressure and velocity relaxation factors made no difference to the solution apart from slowing down convergence. Indeed an examination of recorded pressure histories showed that both solutions oscillated with the same amplitude and mean, but differed only in frequency (where we draw an analogy between time and the number of solver iterations). As the solver dynamics remain unchanged, we may also deduce that there was no change in stability. The only effect was to lengthen computer run times. This phenomena was demonstrated again by runs AL3RL and AL3RJ, in which the relaxation factors of the former were halved. This confirms that there is, in general, no benefit in reducing both relaxation parameters by the same factor.

Runs AL3RF and AL3RB differed only in pressure relaxation factor. The much smaller value used in AL3RF seemed to remove the high frequency fluctuations in the pressure history plots (compare Figure B4 and Figure B5) without over damping the solver.

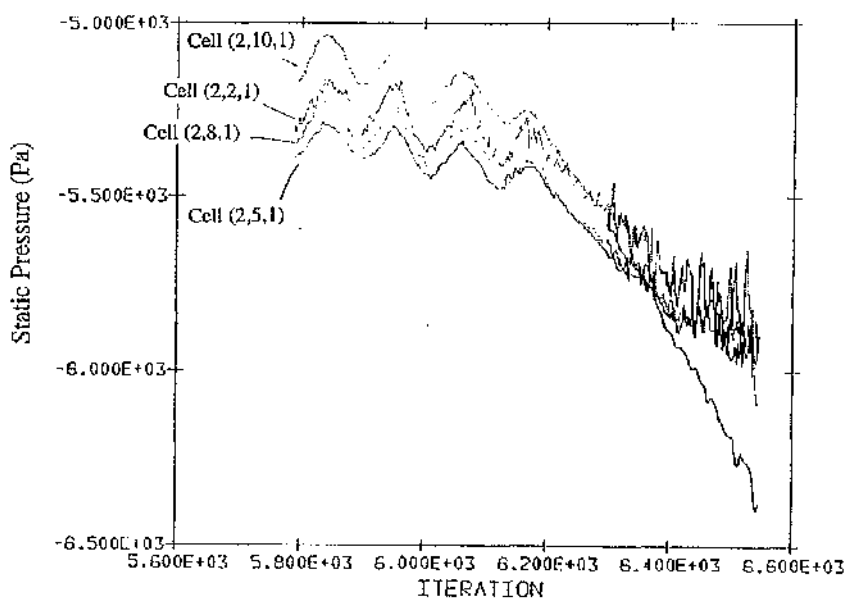


Figure B4 Variation of pressure at inlet: Runs AL3RB and AL3RI

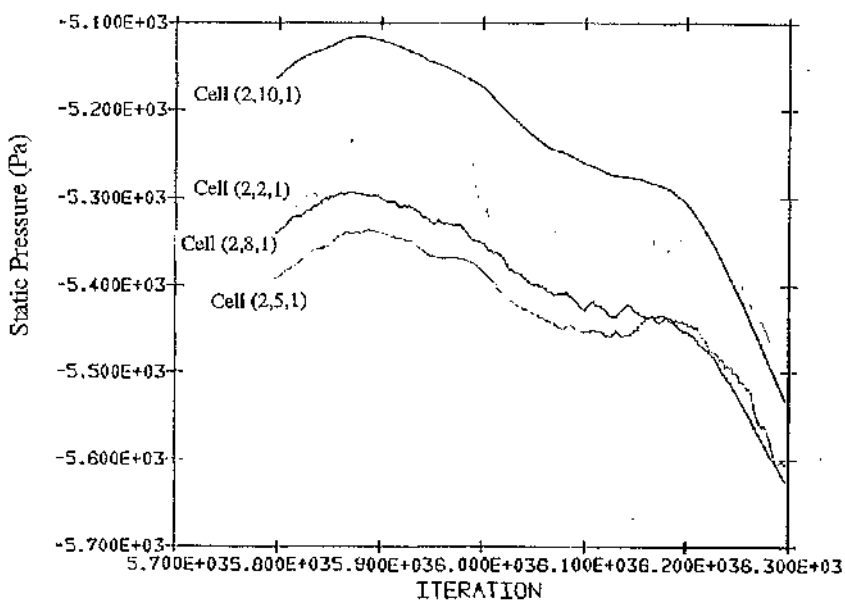


Figure B5 Variation of Pressure at inlet: Run AL3RF

B.2 Reducing the inlet flow rate to help convergence

Runs L3RB3B, L3RD3D and L3RE3E were attempts at trying to solve the system of equations at a different fan duty. Instead of an inlet flow velocity of 43 ms^{-1} a value of 35 ms^{-1} was used. All of these runs were initially very promising; exhibiting stable characteristics. However, in all of the runs the inlet pressure values diverged before becoming constant. This may be seen in Figure B.6. This characteristic behaviour was repeated even when there were corresponding reductions in pressure residual.

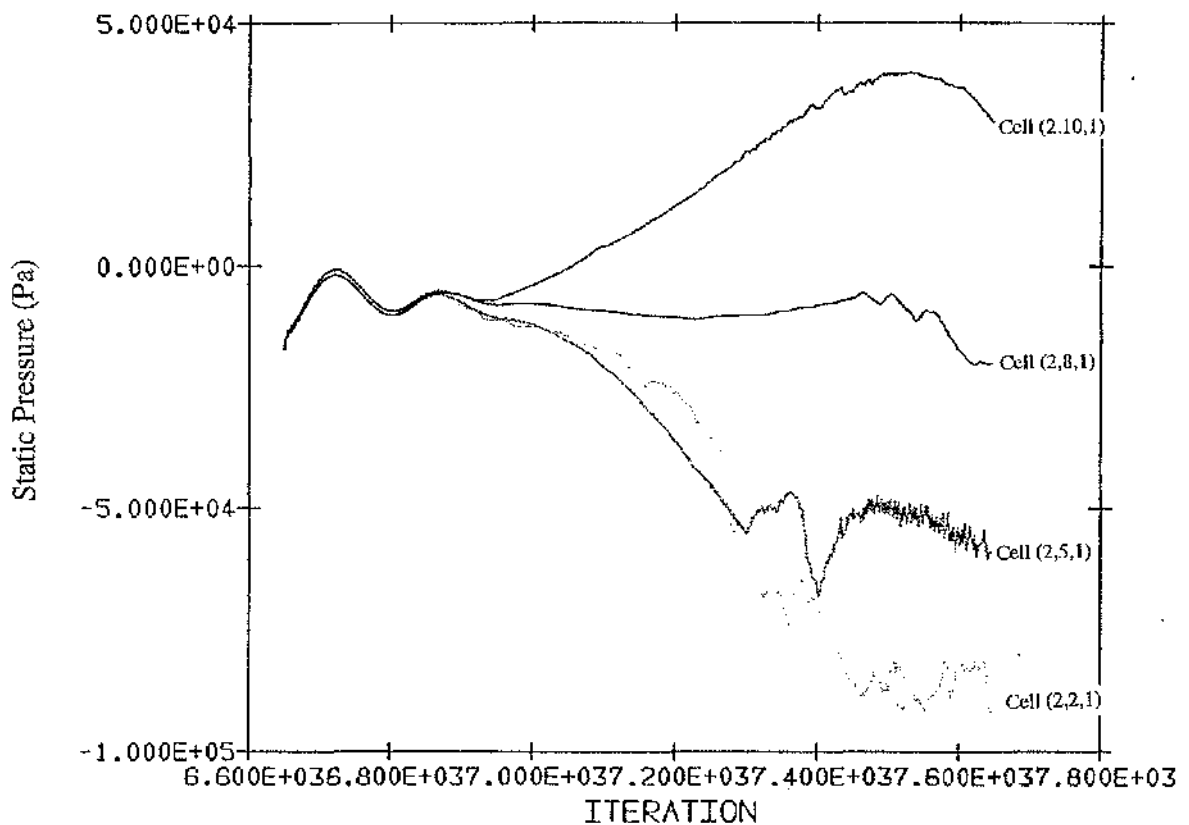


Figure B.6 Run L3RB3B: An example of a divergent solution

APPENDIX C

L3R 'Bladeless' CFD Model Runs

C.1 Incompressible Time-Dependent Runs

Having succeeding in gaining converged solutions for a multitude of flow conditions using the bladeless L3R model, it was decided to invoked the time dependent option available in FLUENT. It was hoped to predict unsteady stall cells as demonstrated by Bosman [1984]. However, there were some reservations as Bosman allowed for compressibility in his finite volume time-marched model whereas here the flow was set as incompressible. In the rest of this section, all runs are tabulated for easy reference.

Table C.1 Incompressible Time Dependent Model Runs

Run	Flow Condition	Pressure Residual	U-Velocity Residual	V-Velocity Residual	W-Velocity Residual	Time Step (secs)	Max No. of iterations	No of time steps
NAB72	100%	6×10^{-2}	5×10^{-4}	1×10^{-3}	5×10^{-4}	0.05	50	20
NAB73	100%	7×10^{-2}	5×10^{-4}	1×10^{-3}	5×10^{-4}	0.05	50	40
NAB75	100%	Diverged	Diverged	Diverged	Diverged	0.005	50	N/A
NAB77	100%	Diverged	Diverged	Diverged	Diverged	0.005	100	N/A
NAB114	40%	1×10^{-1}	1×10^{-3}	2×10^{-3}	1×10^{-3}	0.2	100	20
NAB214	20%	1×10^{-2}	7×10^{-4}	5×10^{-3}	1×10^{-3}	0.5	100	4
NAB219	20%	9×10^{-2}	8×10^{-4}	1×10^{-3}	4×10^{-3}	0.04	200	20

All the above models incorporated the following solution parameters

Table C.2 Solution Parameters

Variable	Number of Sweeps	Relaxation Factor
All Velocities	3	0.3
Pressure	10	0.1

In addition, some investigations into the stability of the models with respect to time step were completed. To ensure good comparison the data set from NAB219 was used as the start data set.

Table C.3 Time Step Investigations at 20% Design Flow- All Runs were UNSTABLE

Time Step (secs)	Number of Sweeps		Relaxation Parameters	
	Pressure	Velocity	Pressure	Velocity
1×10^{-3}	10	3	0.1	0.3
1×10^{-4}	10	3	0.1	0.3
1×10^{-5}	10	3	0.1	0.3
1×10^{-6}	10	3	0.1	0.3
1×10^{-7}	10	3	0.1	0.3
1×10^{-8}	10	3	0.1	0.3
1×10^{-9}	10	3	0.1	0.3
1×10^{-4}	30	3	0.1	0.3
1×10^{-4}	50	3	0.1	0.3
1×10^{-4}	100	10	0.1	0.3

For time dependent runs, the user is able to change other solution parameters which control the time step; the maximum residual sum for ceasing iterations and the maximum number of iterations per time step. The latter is used by FLUENT to trigger a progression onto the next time interval should the current interval solution not sufficiently converge to the level set by the prescribed maximum error residual sum.

However, for the L3R unbladed model runs the pressure residual term dominated the residual sum, and this alone was not considered to be a representative indication of convergence. Therefore the approach taken in the following runs was to set a generous number of 'maximum iterations' that would ensure that the equations

had converged over the prescribed time step. Clearly this was somewhat wasteful in computer time, but it did help to stabilise the solver.

C.1.1 Description of model runs

It was decided that the first time dependent model should be for design flow as this operating condition had been shown to be the easiest to converge. With the same solution parameters as in the previous section, twenty time steps of 0.05 secs were calculated and the run was saved as NAB72. Examination of the reported variable history file showed that all of the recorded variables settled apart from some negligible numerical fluctuations. In addition, for these runs, the variable history measuring stations included the blade passage shroud where recirculation was predicted on the earlier stalled flow model runs. Comparison of meridional velocity distributions showed, as would be expected for the design flow condition, no differences between the time dependent run and the steady state equivalent. To ensure that the model was completely stable, a further 40 time steps were satisfactorily completed and stored under filename NAB73. The time step of 0.05 secs was chosen as this approximately represents the period of one fan wheel rotation and it was thought that this comparably large time step would help yield a stable solution from which to attempt further runs. It would also act as a base from which smaller time step runs, that were necessary to pick up the centrifugal fan unstable flow phenomena, could be started.

To detect rotating stall we must be able to track a stall cell as it crosses a blade passage. This movement takes approximately 0.012 seconds for this particular impeller. Appropriate time steps to capture this phenomena are one or two orders of magnitude less. However further reductions in time step from 0.04 seconds yielded formulations with no stability (see Table C.3); even in conjunction with changes in the number of sweeps which in previous runs had shown to add stability.

Attention was then turned to running a reduced flow model. NAB114 was set to operate in stall with only 40 % of the design flow. A time step of 0.04 seconds was used with the final results identical to the equivalent steady state run, PV4. Reduction of the flow rate further to 20% of design pushed the fan model into deep stall. A time step of 0.04 secs was tried for this condition but the solution became unstable and it became necessary to increase this to 0.5 secs before stability was regained. With this large time-step no unsteady flows were detected. A second and successful attempt at using 0.04 seconds for the highly stalled condition was completed using 200

iterations, rather than 100, per time step. Despite the small time step, no fluctuations in the recorded velocities were noted.

A variation in the frequency of the inlet pressure perturbations was noticed when the variable histories of runs NAB114, NAB214 and NAB219 were compared. These may be seen in Figures C.1-C.3.

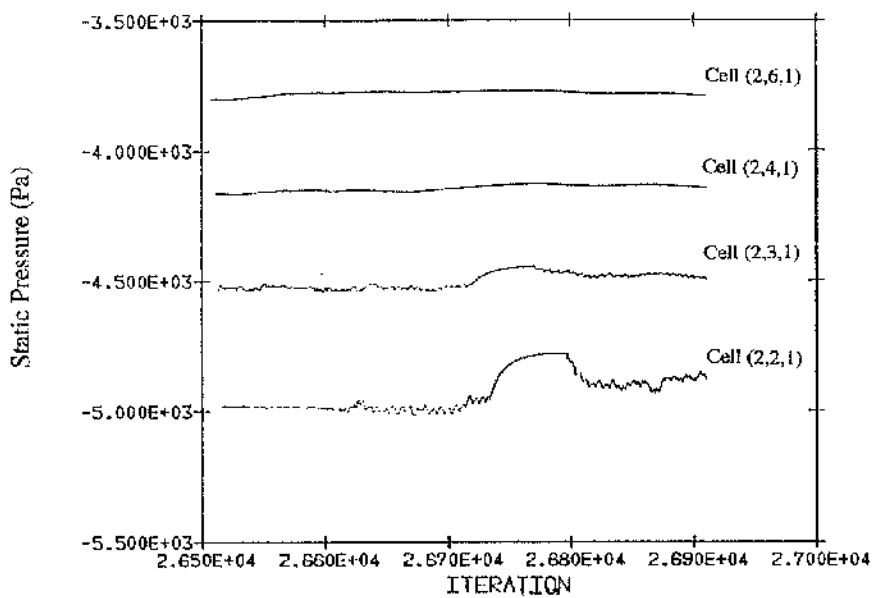


*Figure C.1 Inlet Pressure Variable History, NAB114
(40 % design Flow, Time Step 0.2 secs, 100 iterations per time step)*

Appendix C L3R 'Bladeless' CFD Model Runs

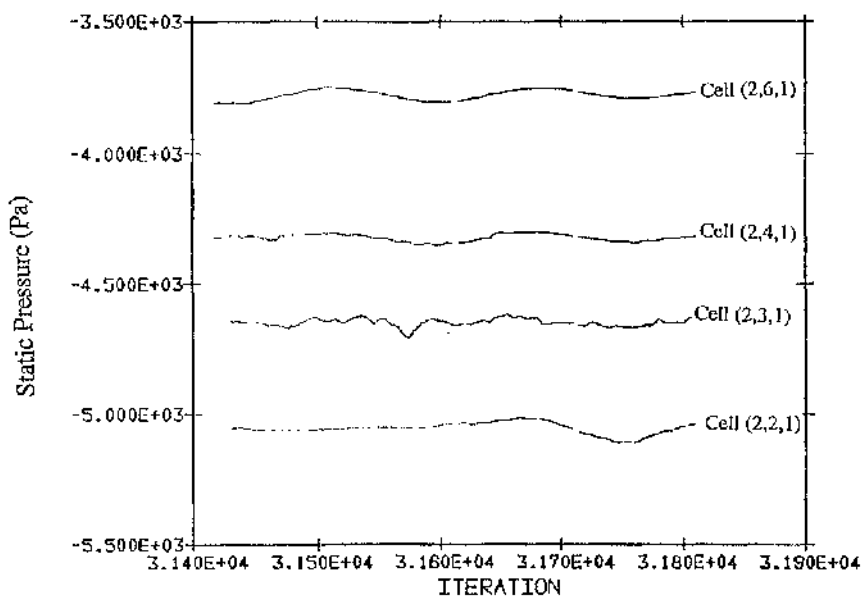


*Figure C.2 Inlet Pressure Variable History, NAB214
(20% design flow, Time Step 0.5 secs, 100 iterations per time step)*

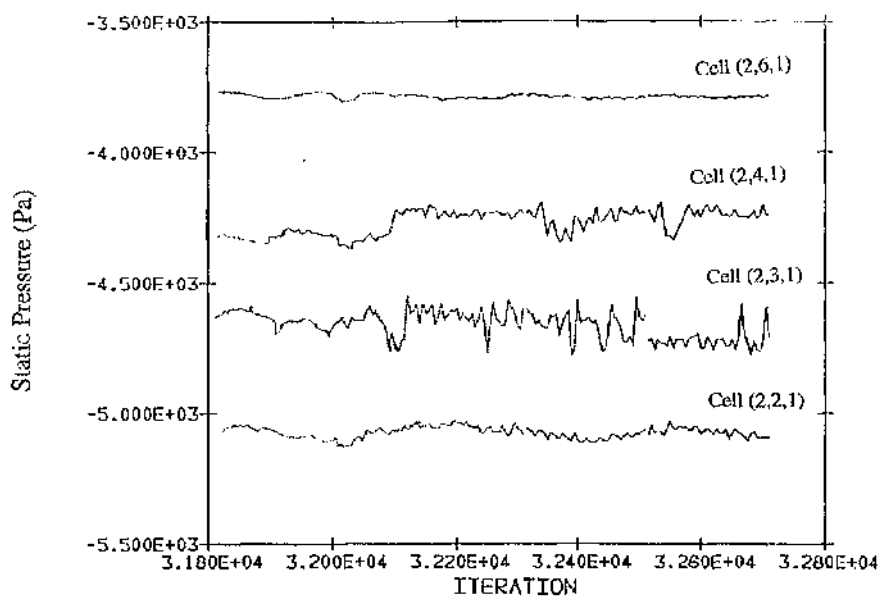


*Figure C.3 Inlet Pressure Variable History, NAB219
(20% design flow, Time Step 0.04 secs, 200 iterations per time step)*

C.2 Full Unsteady Euler Solutions

Having now gained a converged solution at several fan duty points for unsteady incompressible flow it was decided to generalise by allowing compressibility, that is, include the energy equation into the formulation. This complication seemed justified as Bosman and Ahrabian[1984] suggested that energy transfer may be the key to the formulation of the stall cells. Initially a steady state compressible run of 2000 iterations was completed for the highly stalled case. This solution acted as the initial data set for subsequent unsteady model runs. The following residuals were noted:

Table C.4 Steady State Compressible Flow Residuals

Run Name	Number of iterations	Pressure Residual	U-Velocity Residual	V-Velocity Residual	W-Velocity Residual	Enthalpy Residual
NAB305	2000	1.3×10^{-1}	1×10^{-3}	6×10^{-3}	2×10^{-3}	2×10^{-4}

The time dependent runs below followed

Table C.5 Summary of Euler Runs

Run	% of Design Flow	Pressure Residual	U-Velocity Residual	V-Velocity Residual	W-Velocity Residual	Enthalpy Residual	Time Step (secs)	Max No. of iterations	No of time steps
NAB309	20%	1×10^{-1}	6×10^{-4}	5×10^{-3}	2×10^{-3}	2×10^{-4}	0.04	100	8
NAB315	20%	1×10^{-2}	1×10^{-7}	2×10^{-7}	3×10^{-7}	7×10^{-8}	7×10^{-7}	100	8
NAB319	20%	1×10^{-2}	1×10^{-7}	2×10^{-7}	3×10^{-7}	9×10^{-8}	7×10^{-7}	100	8
NAB323	20%	2×10^{-2}	1×10^{-7}	1×10^{-7}	2×10^{-7}	9×10^{-8}	7×10^{-7}	200	4
NAB328C	20%	2×10^{-2}	1×10^{-7}	2×10^{-7}	2×10^{-7}	8×10^{-8}	1×10^{-7}	200	8
NAB333C	20%	3×10^{-2}	1×10^{-7}	2×10^{-7}	2×10^{-7}	8×10^{-8}	1×10^{-7}	200	8
NAB338C	20%	2×10^{-2}	1×10^{-7}	2×10^{-7}	2×10^{-7}	8×10^{-8}	1×10^{-7}	200	20
NAB415C	20%	1×10^{-2}	1×10^{-7}	7×10^{-7}	2×10^{-6}	2×10^{-7}	7×10^{-7}	100	10
NAB505C	20%	8×10^{-2}	6×10^{-8}	1×10^{-7}	2×10^{-7}	4×10^{-8}	1×10^{-8}	100	20
NAB511C	20%	9×10^{-1}	9×10^{-8}	1×10^{-7}	2×10^{-7}	9×10^{-8}	1×10^{-8}	100	20

The first unsteady Euler run, NAB309, was completed with a relatively large time step. This converged, but despite the low flow rate, no unsteadiness was detected. Further reductions in time step to 0.005 sec and 1×10^{-6} sec produced

unstable results although the latter run was stable for a large portion of the time steps after which it suddenly and unexpectedly diverged. It was only when a tiny time step of 7×10^{-7} was used in NAB315, that the formulation became consistently stable. This time step, however, is unpractical as such a large number are required to represent a useful time scale. Whether unsteady effects were present or not, the time of the complete run was just 6 msec which was too small to differentiate between numerical perturbations and real flow phenomena, even when these runs were extended for further time steps. For interest it was decided to continue the trend of reducing the time step to examine stability. A reduction to 1×10^{-8} yielded stable results, but for the reasons mentioned earlier, no stall cell movement could be identified.

APPENDIX D

ZM1 Centrifugal Fan

CFD Model Runs

D.1 Sparsely Meshed Models

As described in Section 6.2, these runs incorporated a mesh which was unable to resolve the flow at the blade trailing edge with sufficient accuracy in order to properly simulate the blade discharge conditions. The resulting predicted performances were correspondingly unrealistic with, in the extreme, predictions indicating that the fan was acting like a turbine. The four variations of computational mesh used were all unsuccessful. The runs are documented here in detail for completeness.

Table D.1 shows the salient features of each computational investigation completed using meshes ZM(a) and ZM(b), i.e. those modelling the full inlet duct, shown in Figure 6.2. The first runs converged rapidly, without the need to start the iterative process at a low rotational speed. Solutions were found for a variety of prescribe inlet flow rates (ZM3 to ZM4C). It became clear on results post-processing however that the predicted fan performances were incorrect apart from operation at the flow rates corresponding stall. To force the model to act as compressor, pressure boundaries were applied with these runs denoted ZM31 to ZM51. Results again were disappointing with corresponding volume flow rates incorrectly predicted. As shown in Figure 6.3, however, there was still some consistency in the results for the CFD performance prediction line, which was independent of whether pressure or velocity boundary conditions were applied. This was subsequently confirmed again by perturbing the inlet pressure boundaries where expected (although incorrect) volume flows were predicted (ZM43, ZM54 and ZM55). Finally the mesh density was doubled to see if the inviscid formulation was sensitive to the grid resolution. Runs ZM61 and ZM71 showed that the solution was not.

In response to these investigations it was decided to reduce the inlet duct length modelled (i.e. using Meshes ZM(b) and ZM(d). See Table D.2. This would prescribe more directly the inlet swirl, in much the same fashion as Inlet Guide Vanes. Runs ZM101 to ZM111 were solutions to the problem for increments in fan speed. Run ZM114 was a continuation of ZM111 to see if the solution would revert to give a

realistic performance. No change was noted and the mesh yielded solutions similar to the earlier runs. Doubling the mesh density (ZM121) again had no effect on the solution and the investigations were finally halted after the pressure predictions at off-design flow rates were also confirmed to be the same as the earlier model runs.

D.2 'Viscous Mesh' Computational Runs

The ZM1 viscous mesh runs are all preceded with 'MEG' and are documented in Table D.3. The reasons behind each of the runs are now given to accompany this Table.

As for several of the other CFD investigations, a series of speed increments were required to gain convergence. These runs were designated MEG20 to MEG31, and included laminar viscosity as they were initially completed as a prelude to including fully turbulent models. It should be noticed that due to the dimensions of the computational mesh, the runs were limited to hundreds rather than thousands of iterations. Next, the Reynolds Stress Model (RSM) was invoked. With convergence at 100% flow after 350 iterations (MEG70 and MEG72), runs MEG75 and MEG76 followed with investigations of 75% and 50% of design flow. However, for 125% of the design flow, the problem diverged. Reasons for the failure are discussed in the main text and are mostly attributed to skew mesh cells.

Using the 100% design flow solution with laminar viscosity (MEG31), inviscid boundary conditions were invoked together with an insignificantly low value of viscosity ($\mu=1\times10^{-15}\text{Pa.S}$) in an attempt to further investigate the need for viscosity in the domain to properly simulate blade discharge flow. The solution was remarkably similar to that for the turbulent flow simulations. Runs at off-design flow were subsequently completed at 75%, 50% and 125% of design flow. These are designated MEG110, MEG112 and MEG117 respectively.

Table D.1 Solution Parameters and Predictions of 'Sparsely Meshed' Models with inlet ducting

Filename	Mesh	Flow (m ³ /sec)	P _{sF} (kPa)	Underrelaxation Parameters		Numbers of Sweeps		Final Residuals			No. of Simple C?
				Used press.	vel.	press.	vel.	u-vel	v-vel	w-vel	
ZM3	ZM(a)	16.5	-11.0	0.1	0.3	10	3	3.5x10 ⁻²	2.2x10 ⁻²	2.2x10 ⁻²	500
ZM4A	ZM(a)	10.0	/	0.1	0.3	10	3	6.2x10 ⁻²	3.8x10 ⁻²	1.6x10 ⁻²	1.2x10 ⁻²
ZM4B	ZM(a)	10.0	-1.3	0.1	0.3	10	3	5.4x10 ⁻²	3.3x10 ⁻²	1.7x10 ⁻²	1.5x10 ⁻²
ZM4C	ZM(a)	4.8	0.6	0.1	0.3	10	3	3.8x10 ⁻¹	8.5x10 ⁻²	6.4x10 ⁻²	8.6x10 ⁻²
ZM4E	ZM(a)	2.4	3.3	0.1	0.3	10	3	1.9x10 ⁻²	8.3x10 ⁻²	4.9x10 ⁻²	6.6x10 ⁻²
ZM3J	ZM(a)	6.0	4.85	0.1	0.3	30	3	1.1x10 ⁻¹	1.8x10 ⁻²	1.4x10 ⁻²	1.4x10 ⁻²
ZM38	ZM(a)	2.9	5.1	0.5	0.3	10	3	5.0x10 ⁻⁵	4.0x10 ⁻⁴	2.1x10 ⁻⁴	3.2x10 ⁻⁴
ZM43	ZM(a)	3.2	4.85	0.5	0.3	10	3	5.5x10 ⁻⁵	3.9x10 ⁻⁴	2.6x10 ⁻⁴	2.9x10 ⁻⁴
ZM45	ZM(a)	3.34	4.85*	0.5	0.3	10	3	4.4x10 ⁻⁵	2.3x10 ⁻⁴	3.0x10 ⁻⁴	4.3x10 ⁻⁴
ZM51	ZM(a)	2.9	5.1	0.5	0.3	10	3	8.9x10 ⁻⁵	3.2x10 ⁻⁴	2.3x10 ⁻⁴	3.6x10 ⁻⁴
ZM54	ZM(a)	2.71	5.7	0.5	0.3	10	3	7.4x10 ⁻⁵	2.2x10 ⁻⁴	2.4x10 ⁻⁴	4.6x10 ⁻⁴
ZM55	ZM(a)	3.71	4.0	0.5	0.3	10	3	3.9x10 ⁻⁵	4.1x10 ⁻⁴	2.9x10 ⁻⁴	2.5x10 ⁻⁴
ZM61	ZM(b)	2.83	4.85	0.5	0.3	10	3	1.9x10 ⁻⁴	1.5x10 ⁻³	1.5x10 ⁻³	1.8x10 ⁻³
ZM71	ZM(b)	2.84	4.85	0.5	0.3	10	3	2.6x10 ⁻⁴	2.9x10 ⁻³	2.7x10 ⁻³	2.2x10 ⁻³

- Note 1: Figures given in italics are those predicted by CFD. Therefore the first series of runs have inlet velocity prescribed; the latter have an inlet static pressure and flow direction cosines applied.
- Note 2: * value has direction cosines for high swirl to correspond with stalled flow

Table D.2 'Sparsely Mesh' ZMI model runs with shortened inlet duct modelled

Filename	Mesh Used	% of Design Rotational Speed		% of Design Flow		Underrelaxation Parameters		Numbers of Sweeps		Final Residuals			No. of Iters	Simple C?
		Psf (kPa)	*1	press.	vel.	press.	vel.	press.	vel.	u-vel	v-vel	w-vel		
ZM101a	ZM(c)	10%	100%	-0.3	0.05	0.2	10	3	2.3x10 ⁻⁴	4.1x10 ⁻⁴	4.2x10 ⁻⁴	1.3x10 ⁻⁴	220	yes
ZM101b	ZM(c)	20%	100%	-0.3	0.05	0.2	10	3	1.0x10 ⁻³	1.7x10 ⁻³	1.1x10 ⁻³	7.5x10 ⁻⁴	200	yes
ZM103	ZM(c)	50%	100%	-1.1	0.05	0.2	10	3	2.4x10 ⁻³	4.2x10 ⁻³	3.5x10 ⁻³	3.8x10 ⁻³	200	yes
ZM103b	ZM(c)	75%	100%	-	0.05	0.2	10	3	2.3x10 ⁻³	2.8x10 ⁻³	1.5x10 ⁻³	2.0x10 ⁻³	200	yes
ZM111	ZM(c)	100%	100%	-11.4	0.05	0.2	10	3	1.8x10 ⁻²	2.1x10 ⁻²	1.3x10 ⁻²	1.6x10 ⁻²	2000	no
ZM114	ZM(c)	100%	100%	-11.0	0.05	0.2	10	3	2.3x10 ⁻³	2.0x10 ⁻³	1.4x10 ⁻³	1.4x10 ⁻³	2000	yes
ZM121	ZM(c)	100%	100%	-16.1	0.05	0.2	10	3	6.7x10 ⁻³	5.4x10 ⁻³	4.1x10 ⁻³	4.3x10 ⁻³	2000	no
ZM131	ZM(d)	100%	50%	-4.8	0.05	0.2	10	3	1.3x10 ⁻²	1.8x10 ⁻²	1.0x10 ⁻²	1.5x10 ⁻²	2000	no
ZM133	ZM(c)	100%	25%	-1.0	0.05	0.2	10	3	3.2x10 ⁻²	4.2x10 ⁻²	2.1x10 ⁻²	5.4x10 ⁻²	1000	no

*1 Conditions are referred to 1910 rpm, 1 kg/m³.

Table D.3 Viscous Mesh' Computational Runs: Solution Parameters

Filename	% of Design Flow	Viscous Model	Undrelaxation Parameters						Numbers of Sweeps			No. of Iters	Simple C?
			press.	vcl.	K.E.	Diss.	press.	vel.	K.E.	Diss.			
MEG21	10%	laminar	0.7	0.2	-	-	5	1	-	-	300	no	
MEG22	10%	laminar	0.7	0.2	-	-	10	3	-	-	500	no	
MEG24	30%	laminar	0.7	0.2	-	-	10	3	-	-	700	no	
MEG26	50%	laminar	0.7	0.2	-	-	10	3	-	-	200	no	
MEG29	75%	laminar	0.7	0.2	-	-	10	3	-	-	300	no	
MEG31	100%	laminar	0.7	0.2	-	-	10	3	-	-	400	no	
MEG108	100%	inviscid	0.7	0.2	-	-	10	3	-	-	200	no	
MEG110	100%	inviscid	0.7	0.2	-	-	10	3	-	-	300	no	
MEG112	100%	inviscid	0.7	0.2	-	-	10	3	-	-	500	no	
MEG117	100%	inviscid	0.7	0.2	-	-	10	3	-	-	200	no	
MEG72	100%	RSM	0.7	0.2	0.2	0.2	10	3	3	3	350	no	
MEG75	100%	RSM	0.7	0.2	0.2	0.2	10	3	3	3	250	no	
MEG76	100%	RSM	0.7	0.2	0.2	0.2	10	3	3	3	150	no	
MEG78	100%	RSM	0.7	0.2	0.2	0.2	10	3	3	3	350	no	
MEG79	100%	RSM	0.7	0.2	0.2	0.2	10	3	3	3	diverged	no	

Table D.4 'Viscous' Mesh Computational Runs: Final Residuals

Filename	% of Design Flow	Viscous Model	Final Residuals			
			press.	u-vel	v-vel	w-vel
MEG21	10%	Laminar	3.7×10^{-7}	2.7×10^{-2}	3.0×10^{-2}	2.3×10^{-2}
MEG22	10%	Laminar	5.1×10^{-8}	2.3×10^{-3}	3.6×10^{-3}	1.8×10^{-3}
MEG24	30%	Laminar	2.5×10^{-8}	2.7×10^{-4}	5.7×10^{-4}	3.1×10^{-4}
MEG26	50%	Laminar	1.5×10^{-7}	1.7×10^{-3}	3.1×10^{-3}	3.4×10^{-3}
MEG29	75%	Laminar	1.6×10^{-7}	9.9×10^{-4}	1.9×10^{-3}	2.1×10^{-3}
MEG31	100%	Laminar	4.5×10^{-5}	6.0×10^{-2}	3.2×10^{-2}	1.0×10^{-2}
MEG108	100%	inviscid	1.4×10^{-6}	1.7×10^{-3}	2.2×10^{-3}	1.2×10^{-3}
MEG110	100%	inviscid	2.2×10^{-6}	4.4×10^{-2}	7.7×10^{-3}	2.8×10^{-3}
MEG112	100%	inviscid	2.8×10^{-6}	1.2×10^{-2}	2.3×10^{-2}	5.8×10^{-3}
MEG117	100%	inviscid	2.0×10^{-6}	2.7×10^{-3}	4.0×10^{-3}	2.3×10^{-3}
MEG72	100%	RSM	3.3×10^{-7}	8.9×10^{-4}	2.1×10^{-3}	7.8×10^{-4}
MEG75	100%	RSM	5.6×10^{-7}	3.0×10^{-3}	4.6×10^{-3}	1.5×10^{-3}
MEG76	100%	RSM	6.1×10^{-7}	6.6×10^{-3}	1.1×10^{-2}	2.7×10^{-3}
MEG78	100%	RSM	2.6×10^{-6}	9.6×10^{-3}	1.1×10^{-2}	5.8×10^{-3}